



National Library  
of Canada

Bibliothèque nationale  
du Canada

Canadian Theses Service

Service des thèses canadiennes

Ottawa, Canada  
K1A 0N4

## NOTICE

The quality of this microform is heavily dependent upon the quality of the original thesis submitted for microfilming. Every effort has been made to ensure the highest quality of reproduction possible.

If pages are missing, contact the university which granted the degree.

Some pages may have indistinct print especially if the original pages were typed with a poor typewriter ribbon or if the university sent us an inferior photocopy.

Reproduction in full or in part of this microform is governed by the Canadian Copyright Act, R.S.C. 1970, c. C-30, and subsequent amendments.

## AVIS

La qualité de cette microforme dépend grandement de la qualité de la thèse soumise au microfilmage. Nous avons tout fait pour assurer une qualité supérieure de reproduction.

S'il manque des pages, veuillez communiquer avec l'université qui a conféré le grade.

La qualité d'impression de certaines pages peut laisser à désirer, surtout si les pages originales ont été dactylographiées à l'aide d'un ruban usé ou si l'université nous a fait parvenir une photocopie de qualité inférieure.

La reproduction, même partielle, de cette microforme est soumise à la Loi canadienne sur le droit d'auteur, SRC 1970, c. C-30, et ses amendements subséquents.

UNIVERSITY OF ALBERTA

PHOTOLUMINESCENCE OF GaAs; DE-TRAPPING MODEL OF  
LUMINESCENCE DECAY

BY  
MARK DAVID SALIK

A THESIS  
SUBMITTED TO THE FACULTY OF GRADUATE STUDIES AND RESEARCH  
IN PARTIAL FULFILMENT OF THE REQUIREMENTS FOR THE DEGREE  
OF

MASTER OF SCIENCE  
IN  
SOLID STATE PHYSICS

DEPARTMENT OF PHYSICS

EDMONTON, ALBERTA  
FALL 1990



**National Library  
of Canada**

**Bibliothèque nationale  
du Canada**

**Canadian Theses Service    Service des thèses canadiennes**

**Ottawa, Canada  
K1A 0N4**

**The author has granted an irrevocable non-exclusive licence allowing the National Library of Canada to reproduce, loan, distribute or sell copies of his/her thesis by any means and in any form or format, making this thesis available to interested persons.**

**The author retains ownership of the copyright in his/her thesis. Neither the thesis nor substantial extracts from it may be printed or otherwise reproduced without his/her permission.**

**L'auteur a accordé une licence irrévocable et non exclusive permettant à la Bibliothèque nationale du Canada de reproduire, prêter, distribuer ou vendre des copies de sa thèse de quelque manière et sous quelque forme que ce soit pour mettre des exemplaires de cette thèse à la disposition des personnes intéressées.**

**L'auteur conserve la propriété du droit d'auteur qui protège sa thèse. Ni la thèse ni des extraits substantiels de celle-ci ne doivent être imprimés ou autrement reproduits sans son autorisation.**

**ISBN 0-315-65073-7**

UNIVERSITY OF ALBERTA  
RELEASE FORM

NAME OF AUTHOR        Mark David Salik


TITLE OF THESIS        Photoluminescence of GaAs;  
De-Trapping Model of Luminescence Decay

DEGREE                Master of Science

YEAR THIS DEGREE GRANTED        1990

Permission is hereby granted to THE UNIVERSITY OF ALBERTA LIBRARY to reproduce single copies of this thesis and to lend or sell such copies for private, scholarly or scientific research purposes only.

The author reserves other publication rights, and neither the thesis nor extensive extracts from it may be printed or otherwise reproduced without the author's written permission.

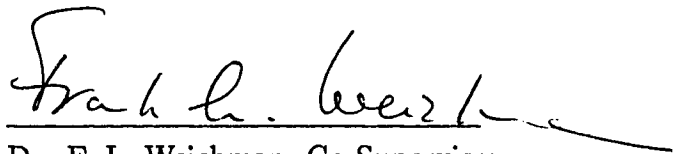
  
\_\_\_\_\_  
Mark David Salik  
6 Sherwood Road  
London  
S.W.19 3QT  
Britain

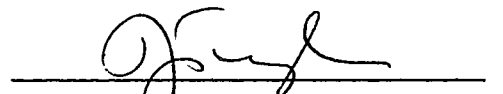
Date: Aug 21, 1990

UNIVERSITY OF ALBERTA


FACULTY OF GRADUATE STUDIES AND RESEARCH

The undersigned certify that they have read, and recommend to the Faculty of Graduate Studies and Research for acceptance, a thesis entitled "Photoluminescence of GaAs; De-Trapping Model of Luminescence Decay" submitted by Mark David Salik in partial fulfilment of the requirements for the degree of Master of Science in Solid State Physics.

  
Dr. F. L. Weichman, Co-Supervisor

  
Dr. J. A. Tuszynski, Co-Supervisor

  
Dr. Z. W. Gortel

  
Dr. I. R. MacDonald

Date: Aug 3, 1990

Dedicated to my family-  
father, mother, and sister-  
to Sally, and to Dr. Jones.

# ABSTRACT

I have reviewed the physics of the semiconductor relating to photoluminescence and with particular reference to the compound semiconductor GaAs. I have described the energy levels of GaAs; these energies determine the spectral lines of photoluminescence. I have also described the various models of energy transfer since the transfer processes determine the time-dependence of the luminescence decay. Energy transfer, either between different energy levels or different ion sites, proceeds by radiative or radiationless transitions. I have described these transition processes and compared the theory with the observations for both luminescence spectra and luminescence time-decay of GaAs. The first part concludes with a study of donor-acceptor pair recombination.

I have studied the luminescence decay curves obtained from a model of de-trapping of energy from a distribution of discrete trap levels. The model is based on equations for carrier dynamics which I derived from general thermodynamic arguments using a statistical description of the occupation of states and the Arrhenius form for the de-trapping rate. Computer simulations show that power-law decays are ubiquitous whenever there is a broad distribution of traps. I verified the critical parameter introduced by Hornyak and Chen to determine whether a distribution is wide enough to give power-law behaviour. I further introduced a parameter to define the minimum energy separation between discrete traps that still gives power-law behaviour. I have compared the results of simulation to the experimental results of Teh. The results show good agreement if an exponential density distribution of traps is used for the simulation. Both the linear temperature dependence of the exponent of the power law and the initial exponential time-decay are verified.

## ACKNOWLEDGEMENTS

I would like to acknowledge the help of my supervisors, Dr. Weichman and Dr. Tuszynski, who planted the seeds; the forbearance of my committee, Dr. Gortel and Dr. MacDonald, who tasted the fruits; the material assistance of the Department of Physics and the Physical Sciences Library; and the encouragement of my fellow office interns, Hugh and Alex, and of other dear friends.

May the favour of the Lord our God be upon us  
to support us in the work we do,  
and support the work we do.

*Psalms 90:17*



# TABLE OF CONTENTS

1	INTRODUCTION	1
<b>I</b>	<b>Photoluminescence of GaAs</b>	<b>6</b>
2	ENERGY LEVELS OF GAAS	7
2.1	Band structure . . . . .	7
a)	Basic Properties of GaAs . . . . .	11
2.2	Excitons . . . . .	15
2.3	Simple Substitutional Impurities . . . . .	18
2.4	Deep levels . . . . .	21
2.5	Phonons . . . . .	22
3	ENERGY TRANSFER AND DECAY	25
3.1	Models of Energy Transfer . . . . .	25
3.2	Continuity Equation . . . . .	27
3.3	Shockley-Read Theory . . . . .	29
3.4	Excitation Transfer Theories . . . . .	32
3.5	Thermal De-Trapping . . . . .	36

<b>4</b>	<b>RADIATIVE AND NON-RADIATIVE TRANSITIONS</b>	<b>38</b>
4.1	Radiative Recombination . . . . .	38
a)	Number of States . . . . .	40
b)	Matrix Element . . . . .	43
c)	Lifetime . . . . .	45
4.2	Non-Radiative Transitions . . . . .	46
a)	Transition Processes . . . . .	47
b)	Theoretical Developments . . . . .	49
<b>5</b>	<b>PHOTOLUMINESCENCE SPECTRA</b>	<b>55</b>
5.1	Comparison with Theory . . . . .	55
5.2	Spectral Lines of GaAs . . . . .	57
<b>6</b>	<b>TIME-DECAY OF PHOTOLUMINESCENCE</b>	<b>67</b>
6.1	Evidence for Non-Radiative Processes . . . . .	67
6.2	Non-Exponential Behaviour . . . . .	67
a)	Decay in GaAs . . . . .	69
<b>7</b>	<b>DONOR-ACCEPTOR PAIR PHOTOLUMINESCENCE</b>	<b>72</b>
7.1	Recombination Spectra . . . . .	72
7.2	Decay Characteristics . . . . .	76

7.3	Observations . . . . .	81
<b>II</b>	<b>De-Trapping Model of Luminescence Decay</b>	<b>86</b>
<b>8</b>	<b>ENERGY DE-TRAPPING</b>	<b>87</b>
8.1	Semiconductor Thermodynamics . . . . .	87
a)	Particle Reactions and Equilibrium Conditions . . . . .	88
b)	Fermi-Dirac Distribution . . . . .	93
c)	Arrhenius Relation . . . . .	93
8.2	Dynamical Equations . . . . .	96
a)	Thermalization . . . . .	97
b)	Radiative Recombination . . . . .	98
c)	De-Trapping . . . . .	98
<b>9</b>	<b>COMPUTER SIMULATION AND RESULTS</b>	<b>101</b>
9.1	Background . . . . .	101
9.2	Simulation . . . . .	102
a)	Parameters and Range . . . . .	103
9.3	De-Trapping Scenarios . . . . .	104
a)	De-trapping from a group of traps to a single energy level . .	104
b)	De-trapping from a single trap to an energy band . . . . .	114

9.4	Critical Parameters . . . . .	118
a)	The critical parameter for power-law decay . . . . .	120
b)	A critical parameter for discrete distributions . . . . .	122
10	DE-TRAPPING IN GAAS	123
10.1	Trap Population in GaAs . . . . .	123
10.2	De-Trapping in GaAs . . . . .	124
	BIBLIOGRAPHY	132
	APPENDICES:	140
A	SIMPLE ENERGY TRANSFER MODEL	140
B	COMPUTER PROGRAM	142

## LIST OF TABLES

2.1	Unit cell size, atomic density and crystal density at $T=300K$ , for stoichiometric GaAs. . . . .	8
2.2	Effective masses for the zone-centre extrema of GaAs. . . . .	15
2.3	Simple acceptor centres in GaAs. . . . .	20
2.4	Simple donor centres in GaAs. . . . .	20
5.1	Energies of photoluminescence transitions. . . . .	66

# LIST OF FIGURES

2.1	Conventional unit cube for GaAs. . . . .	8
2.2	Brillouin zone for fcc crystal. . . . .	9
2.3	Free electron energy levels for fcc crystal. . . . .	11
2.4	Band structure of GaAs. . . . .	12
2.5	Band structure of GaAs near $\Gamma$ . . . . .	13
2.6	Two types of exciton: a) Frenkel b) Wannier . . . . .	16
2.7	Exciton energies. . . . .	18
2.8	Plots of $\log(T_m^2 t)$ vs. reciprocal temperature for all deep levels seen by PITS. . . . .	23
2.9	Dispersion curves for acoustic and optical branch phonons in GaAs. . . . .	24
3.1	Two possible forms of electron distribution function for the same quasi-Fermi level. . . . .	26
3.2	Four fundamental processes involved in recombination through traps . . . . .	29
3.3	Dependence of lifetime upon Fermi energy. . . . .	32
3.4	Luminescence excited by short pulse in the case of energy transfer. . . . .	33
4.1	Radiative transitions . . . . .	41
4.2	Band-band Auger effect. . . . .	48
4.3	Trap Auger effects. . . . .	48

4.4	Other Auger processes. . . . .	49
4.5	Non-radiative capture of an electron . . . . .	52
4.6	Electron and hole capture cross-sections. . . . .	53
5.1	Band-band recombination. . . . .	56
5.2	Band-acceptor recombination . . . . .	57
5.3	Free exciton transitions . . . . .	59
5.4	Exciton transitions. . . . .	60
5.5	Two-electron partial Auger recombinations. . . . .	60
5.6	KP lines. . . . .	61
5.7	Band-acceptor transitions. . . . .	62
5.8	Deep levels. . . . .	63
5.9	Phonon replicas of luminescence lines. . . . .	64
6.1	Immediate time-decay of luminescence from bands. . . . .	71
7.1	Dispersion of the Dunstan and Eggert solutions . . . . .	79
7.2	Photoluminescence spectrum of GaP. . . . .	82
7.3	Energy vs. separation relationship for donor-acceptor pair recombination. . . . .	83
8.1	The particle reactions in a semiconductor . . . . .	89

8.2	Energy diagram of electron-hole system . . . . .	90
8.3	Energy diagram for reaction. . . . .	95
9.1	De-trapping scenarios . . . . .	105
9.2	Trap Distribution . . . . .	106
9.3	Time Decay . . . . .	107
9.4	Trap Distribution . . . . .	108
9.5	Time Decay . . . . .	109
9.6	Time Decay . . . . .	110
9.7	Trap Distribution . . . . .	111
9.8	Time Decay . . . . .	112
9.9	Trap Distribution . . . . .	113
9.10	Trap Distribution . . . . .	114
9.11	Time Decay . . . . .	115
9.12	Trap Distribution . . . . .	116
9.13	Time Decay . . . . .	117
9.14	Trap Distribution . . . . .	118
9.15	Time Decay . . . . .	119
9.16	Trap Distribution . . . . .	120
9.17	Time Decay . . . . .	121



10.1	Luminescence spectrum of $\sim 1.49\text{eV}$ region at different temperatures.	126
10.2	Temperature dependence of the exponent, $p$ , for different carbon concentrations $N$ .	127
10.3	Comparison between theory and experiment for exponent of power-law decay	129
10.4	Trap Distributions	130

# CHAPTER ONE

## INTRODUCTION

Eilhardt Wiedemann defined “luminescenz” in 1888 as “all those phenomena of light which are not solely conditioned by the rise in temperature.”

Ancient man knew of mysterious luminescence phenomena: the aurora borealis, glow-worms and luminous wood.

Modern man has classified many different forms of luminescence according to the method of excitation: photoluminescence, thermoluminescence, electroluminescence, crystalloluminescence, triboluminescence, and chemiluminescence.

Photoluminescence is luminescence that is excited by light itself; it is subdivided into fluorescence and phosphorescence. Fluorescence is the emission of light from substances only during the time that they are exposed to radiation; phosphorescence is that which persists after the exciting radiation is cut off.

Wiedemann used the above definition of luminescence to carefully distinguish it from incandescence—the phenomena whereby objects emit light according to their temperature (“black body” radiation). The distinction is important: luminescence acts to restore equilibrium after excitation has created a non-equilibrium energy distribution while incandescence is itself a thermal equilibrium phenomena.

This thesis is about photoluminescence of semiconductors, in particular about photoluminescence of gallium arsenide (GaAs). The motivation behind writing it has been to understand and possibly to explain the unusual time decays of photoluminescence that were observed by Teh [98] in this laboratory. Teh’s measurements were made on GaAs grown by the liquid encapsulated Czochralski (LEC) tech-

nique.

Photoluminescence has become an important industrial technique for the precise characterization of impurities in semiconductors. Additionally, photoluminescence measurements give data that is rich enough to challenge a detailed understanding of the solid state.

When a semiconductor absorbs light, electron-hole pairs are created. These carry both energy and charge. The distribution of carriers that is set up after excitation is both non-equilibrium—many more electron-hole pairs exist than do under thermal equilibrium conditions—and inhomogeneous—the greatest excitation is near the surface of the crystal. Energy transfer processes act to restore both: radiative and non-radiative recombination restores the equilibrium population and carrier diffusion restores the homogeneity.

The photoluminescence we observe is the product of the radiative recombination of electrons with holes. Measuring the energy spectrum of photoluminescence reveals the energy released from each recombining electron-hole pair—the spectrum is thus totally dependent on the energy level structure of the solid. Measuring the time decay of the photoluminescence reveals nothing directly but, when combined with knowledge from theory or from different observations, does offer insight into the recombination processes.

This thesis is written in two parts. Part I is a review of the physics of the semiconductor which relates to photoluminescence in GaAs. The basic physics is expounded using GaAs as a material example. It is only for certain phenomena, notably donor-acceptor pair recombination, that examples of other materials are needed in order

to illustrate the general principles.

Chapter 2 is a description of the energy levels of GaAs. The basic scheme is the band structure but additional electronic energy levels also arise from excitons, impurities and defects. We also consider the lattice vibration (phonon) energies.

Chapter 3 is a description of various models that have been proposed for energy transfer in crystals. The continuity equation describes the diffusion and recombination of carriers and the Shockley-Read theory is a statistical method of describing carrier populations. The more detailed excitation transfer theories take the microscopic structure into account for transfer of energy between localized sites. De-trapping of energy is neglected by some models of fluorescence because it occurs on a timescale much longer than that of interest. It is recognized, however, as being important for phosphorescence. All of the models show that different mechanisms of energy transfer are associated with different decay forms of luminescence.

Chapter 4 is a description of the radiative and non-radiative transition processes that lead to energy decay. The theory of the transitions is based upon Fermi's golden rule and various approximations are used to make solutions.

Chapter 5 is a comparison of the observed spectral energy dependence of luminescence with the theory of Chapter 4 and is also a summary of the data from photoluminescence spectra for GaAs. For GaAs, different conditions of growth give noticeable differences in spectra.

Chapter 6 begins with a discussion of how measurements of luminescent time decay allow one to infer (using the theory of Chapter 4) knowledge about the non-radiative transitions. Some of the further ideas proposed to explain non-exponential time decays are also described and a summary is made of the time-decay measurements of photoluminescence of GaAs.

Chapter 7 is a description of the photoluminescence from donor-acceptor pairs. This is of particular importance to this theses because the prominent long-lived line observed by Teh ( $\sim 1.49\text{eV}$  line) is associated with donor-acceptor pair photoluminescence. The recombination spectrum can be explained from the structure of energy levels expected for donor-acceptor pairs of different separation. Additionally, the distribution of pairs with separation determines the relative intensities of the different pair lines. The time-decay results from the decay of pairs having a range of different lifetimes.

Part II is a detailed study of one of the physical processes identified in Part I—energy de-trapping. De-trapping is the process by which an electronic carrier receives enough energy through thermal activation to free itself from a trap. The subsequent participation of this carrier in radiative recombination leads to luminescence. De-trapping is important in determining the long-time luminescence because it occurs on a relatively long timescale.

Chapter 8 opens with a discussion of thermodynamics and its importance for describing the semiconductor system. From thermodynamics is derived the statistical description of the semiconductor and the Arrhenius rate of reaction of a thermal process. These are applied to the semiconductor and the equations for carrier dynamics are obtained.

Chapter 9 contains details of the computer simulation which I performed to model the time decay of photoluminescence when thermal de-trapping is taken as the rate-limiting process. The results of Chapter 9 give various trap distributions which can be used to explain the observed time decays.

Chapter 10 is a consideration of the relevance of these trap distributions to

photoluminescence decays in GaAs. The number of carriers existing in GaAs under thermal equilibrium conditions is compared to the number of carriers excited into the bands under photo-excitation. The experimental evidence of  $\tau_{eh}$  for certain time decays is analyzed and an explanation is given of these decays on the basis of the de-trapping model. Suggestions are made for the source of the traps in GaAs.

# **Part I**

## **Photoluminescence of GaAs**

# CHAPTER TWO

## ENERGY LEVELS OF GAAS

### 2.1 Band structure

Gallium arsenide is a III - V compound semiconductor. Its crystal structure is that of the "Zincblende" lattice type and consists of two inter-penetrating face-centered cubic lattices—one containing the Ga atoms, and the other the As atoms. Figure 2.1 shows the basic unit cell of GaAs and Table 2.1 contains basic information about the lattice.

As a starting point for the understanding of the energy band structure, we may calculate the free electron energy bands for this face-centered cubic crystal with a two-atom basis. The energy bands are shown on an  $E - k$  diagram.  $k$  is the wave-vector that characterizes each electron state. The domain of the  $k$ -vector is termed the Brillouin Zone. The shape of the Brillouin Zone is determined by the point symmetry of the atom: eigensolutions of the Schrödinger equation for the crystal must have a functional form that is periodic with the crystal structure—solutions are only allowed to vary in phase between different unit cells.

The lattice basis vectors are

$$a_1 = a/2(011)$$

$$a_2 = a/2(101)$$

$$a_3 = a/2(110)$$

and the reciprocal vectors are

$$b_1 = \pi/2a(\bar{1}11)$$



This Figure has been removed for Copyright reasons.

Figure 2.1: Conventional unit cube for GaAs. (From [114].)

This Table has been removed for Copyright reasons.

Table 2.1: Unit cell size, atomic density and crystal density at  $T=300K$ , for stoichiometric GaAs. (From [114].)

This Figure has been removed for Copyright reasons.

Figure 2.2: Brillouin zone for fcc crystal. (From [10].)

$$b_2 = \pi/2a(1\bar{1}1)$$

$$b_1 = \pi/2a(11\bar{1})$$

The shape of the Brillouin Zone for a face-centered cubic crystal is shown in Figure 2.2. Individual points of the zone are marked with their symmetry representations.

Many advanced techniques have been developed to tackle the problem of finding band structure. Most are based on a “single electron” approximation in which, instead of solving the Schrödinger equation for all of the electrons in the crystal, solve it for a single electron existing within a certain crystal potential. The methods are very successful, as agreement with optical absorption experiments shows. Techniques range from “free electron” models to “nearly free electron” models; to “tight binding” models (particularly the semi-empirical formulation of Harrison [31]); to Green’s function methods; and to Pseudopotential calculations [1].

The most elementary approach to band structure calculation is the “free

electron model". This model solves the Schrödinger equation without a potential but does consider the symmetry of the Brillouin zone,

$$H\Psi = \frac{-\hbar^2}{2m}\nabla^2\Psi = E\Psi \quad (2.1)$$

which gives solutions as plane waves

$$\Psi_{\mathbf{k}}(\mathbf{r}) = e^{i\mathbf{k}\cdot\mathbf{r}} = e^{i\mathbf{K}\cdot\mathbf{r}} e^{i\mathbf{k}\cdot\mathbf{r}} \quad (2.2)$$

where  $\mathbf{K}$  is a reciprocal lattice vector. The energy levels of the free electron model are constructed from the solution,

$$E_{\mathbf{k}-\mathbf{K}} = \frac{\hbar^2}{2m}|\mathbf{k} - \mathbf{K}|^2 \quad (2.3)$$

The energy bands for a face-centred cubic crystal are shown in Figure 2.3. The bands are surprisingly complex; they reveal the basic form of the band structure of GaAs. Most of the curves are highly degenerate; the addition of a weak periodic potential lifts some of this degeneracy. The effect of a potential is also to cause energy gaps to appear at Bragg planes.

The Schrödinger equation,

$$H\Psi = \left( \frac{-\hbar^2}{2m}\nabla^2 + V(\mathbf{r}) \right) \Psi = E\Psi \quad (2.4)$$

has solutions which are the Bloch functions,

$$\Psi_{n\mathbf{k}}(\mathbf{r}) = e^{i\mathbf{k}\cdot\mathbf{r}} U_{n\mathbf{k}}(\mathbf{r}) \quad (2.5)$$

$U_{n\mathbf{k}}(\mathbf{r})$  is periodic with the lattice and  $e^{i\mathbf{k}\cdot\mathbf{r}}$  is a plane wave.

Still more complicated band structure calculations use a sum of plane wave type solutions in an attempt to solve for the rapidly changing crystal potential near to

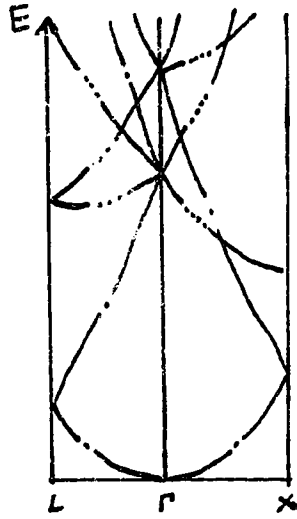


Figure 2.3: Free electron energy levels for fcc crystal. (Adapted from [1].)

the atomic cores. Chelikowsky and Cohen [12,15] used a non-local EPM (elaborated to non-local pseudopotential) approach and calculated the band structure for GaAs shown in Figure 2.4. The same band structure is shown in Figure 2.5 for the top of the valence band and bottom of the conduction band near to the critical point  $\Gamma$ . The similarity of the GaAs band structure to that of the free-electron model, indicates the fundamental role that the symmetry properties, quite apart from the details of the potential, play in determining the energy bands. Knowledge of the symmetry properties is also fundamental to the understanding of the structure of the optical matrix elements which determine the probability of optical transitions between states.

#### a) Basic Properties of GaAs

The most important material properties of GaAs can be understood from the energy diagram, Figure 2.5. It shows that an energy gap exists between the top of the

This Figure has been removed for Copyright reasons.

Figure 2.4: Band structure of GaAs. The valence band maximum is taken to be the zero of energy. (From [15].)

This Figure has been removed for Copyright reasons.

Figure 2.5: Band structure of GaAs near  $\Gamma$ . (Adapted from [15].)

valence band and the bottom of the conduction band. In GaAs, this gap is  $\sim 1.5\text{eV}$  at  $0\text{K}$ . A characteristic property of semiconductors is that, at absolute zero, the valence band is full and the conduction band is empty. The material then acts as an insulator. As the temperature is raised, electrons can cross the energy gap. Electrons in the conduction band and holes in the valence band both contribute to the conductivity,

$$\sigma = \frac{ne^2\tau_e}{m_e^*} + \frac{pe^2\tau_h}{m_h^*} \quad (2.6)$$

where  $n$  and  $p$  are the numbers of electrons and holes respectively.  $\tau_e$  and  $\tau_h$  are the relaxation times for electrons and holes respectively. On a simple model of conductivity the relaxation time is the average time between lattice collisions for a carrier. Lattice collisions occur because the ions of the crystal do not form a perfect, stationary lattice but contain defects and impurities and also vibrate thermally. This perturbation from a perfect lattice causes the electron waves to scatter.

The numbers of  $n$  and  $p$  may be derived from simple statistics. The number of electrons excited from the valence band to the conduction band is given from the Boltzmann probability,

$$n = N_v e^{-\Delta E/kT} \quad (2.7)$$

where  $\Delta E$  is the energy gap and  $N_v$  is the number of states in the valence band. For every electron excited a hole is created. Thus in intrinsic material  $n = p$  and  $np = n_i^2$  where  $n_i$  is the intrinsic number of carriers.

The conductivity also depends on mass, actually the effective masses of holes and electrons. In the free electron model the energy bands are described by parabolae which are characterized by the electron mass,  $m_0$ . A simple way to describe more complicated band structure is to approximate the band structure near to critical points as parabolae and then to characterize each parabola with a single parameter, the effective mass. The effective mass is written in full as a tensor and may be

This Table has been removed for Copyright reasons.

Table 2.2: Effective masses for the zone-centre extrema of GaAs. (Adapted from [114].)

derived as the second derivative, that is the curvature, of the  $E - k$  structure,

$$\left[ \frac{1}{m^*(\mathbf{k})} \right]_{ij} = \pm \frac{\partial^2 E}{\partial k_i \partial k_j} \quad (2.8)$$

where the + or - are used to describe band maxima (holes) or band minima (electrons) respectively. GaAs is extremely useful as a semiconductor device material because its small effective mass gives its carriers a very high mobility. Thus the material responds quickly and can be used in fast electronic circuits. Values of  $m^*$  are shown in Table 2.2 for GaAs at  $0K$  and  $300K$ .

## 2.2 Excitons

In the single-electron model the energy gap is a fundamental limitation: no photon of energy less than the band gap can create an electron-hole pair, neither can photoluminescence occur at energy less than the band gap. However, such energy transitions are very common—in GaAs it is extremely difficult to observe anything other than below-gap recombination. The reason, of course, is that energy levels do exist within the bandgap. The derivation of the band structure has neglected the



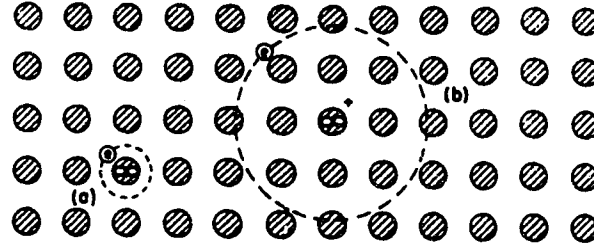


Figure 2.6: Two types of exciton: a) Frenkel b) Wannier

possibility of electron-electron interactions. We assumed that excitation creates a pair of a free electron and a free hole. This is not exactly true. Many-body theory can show with considerable rigour that the lowest allowed electronic excitation is not a free electron-hole pair but rather a bound electron-hole complex, called an exciton.

Two basic types of exciton exist. They are shown in Figure 2.6. The first is the “Frenkel” exciton and is the case for a bound electron-hole pair of zero radius. The electron and hole are tightly bound together but can move in the form of an excitation wave due to the overlap between neighbouring site wavefunctions. The second case is that of the “Wannier” exciton. This involves an excited electron which is spatially separated from its ion. Wannier excitons have been found to exist in covalent crystals with large dielectric constants. They are important for GaAs.

A simple physical picture shows the expected features of the Wannier exciton spectrum remarkably well:

For the electron and hole sufficiently far apart that the medium in between may be treated as homogeneous, the Coulomb interaction between electron and hole is

given by

$$V(r) = -\frac{e^2}{\epsilon r} \quad (2.9)$$

that is, an interaction between a charge  $e$  and a screened charge  $-e/\epsilon$ .

The effect of the band structure is introduced through the effective mass and, for simple spherical bands,

$$E_c(k_e) = E_c(0) + \frac{\hbar^2 k_e^2}{2m_e^*} \quad (2.10)$$

$$E_v(k_h) = E_v(0) + \frac{\hbar^2 k_h^2}{2m_h^*} \quad (2.11)$$

Then the Schrödinger equation for the two-particle system becomes,

$$\left( -\frac{\hbar^2 \nabla_e^2}{2m_e^*} - \frac{\hbar^2 \nabla_h^2}{2m_h^*} - \frac{e^2}{\epsilon r_{eh}} \right) \Psi = (E - E_G) \Psi \quad (2.12)$$

where

$$E_G = E_c(0) - E_v(0) \quad (2.13)$$

$k$  does not represent a good quantum number for excitons. Instead, the exciton is properly characterized by the exciton radius,  $R$ , and the difference between the wave-vectors of electron and hole,  $K$ . The effective mass approximation restricts the solution to a small region of  $K$  space around  $K = 0$  but this is really a minor restriction since the large spatial extent of the exciton necessarily confines it to a narrow portion of  $K$ -space because of the uncertainty relationship,

$$\Delta K \Delta R \sim 1$$

Solving the Schrödinger equation it is easy to find the exciton energy levels [52],

$$E_n(K) = -\frac{\mu e^4}{2\hbar^2 \epsilon^2 n^2} + \frac{\hbar^2 K^2}{2(m_e^* + m_h^*)} + E_G \quad (2.14)$$

where,

$$\frac{1}{\mu} = \frac{1}{m_e^*} + \frac{1}{m_h^*}$$

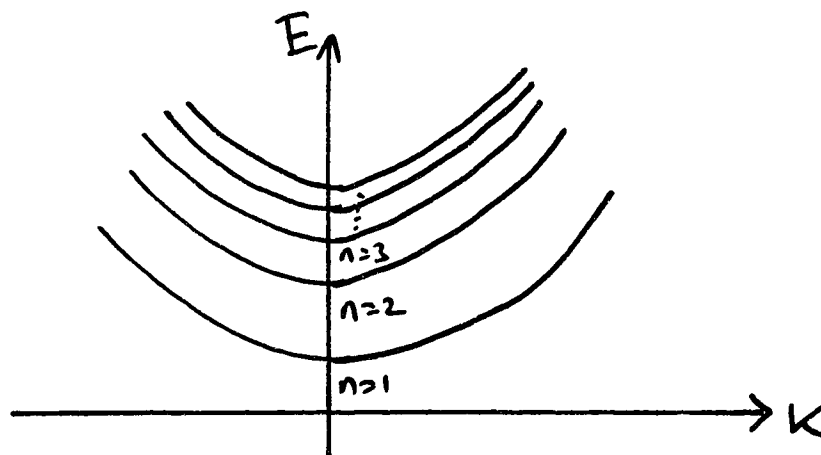


Figure 2.7: Exciton energies.

The solution consists of a hydrogenic type spectra plus a kinetic energy term. Figure 2.7 shows the expected spectrum of exciton levels below the band gap.

Excitons also bind to impurities in the crystal. Transitions involving bound excitons tend to dominate the optical emission spectra at low temperatures. From Haynes' rule [33] the exciton binding energy is roughly 10% of the impurity ionization energy. The linewidth of the bound exciton is very small since binding prevents the exciton from keeping its kinetic energy component. This makes possible an identification of impurity content from the bound exciton lines. Thewalt [94] has reviewed recent progress in exciton photoluminescence.

## 2.3 Simple Substitutional Impurities

Simple substitutional impurities are of most importance for the properties of semiconductors. They occupy the site of an original lattice atom and attempt to bind

in the same way. However, if the valence of the impurity atom is different from the original atom then the binding of electrons is not complete. An impurity is characterized as either a donor or acceptor depending on whether it contributes to or depletes the electron carrier density. Simple donors have an extra electron which is not needed for binding to nearby impurities. This electron is easily ionized from its ion and jumps to the conduction band of the crystal, thereby increasing the density of charge carriers. An estimate of this energy for the extra electron to jump to the conduction band can be obtained within the effective mass approximation [89]

$$E_n = E_G - \left( \frac{m^*}{m_0} \right) \frac{13.6}{\epsilon^2} \text{ eV} \quad (2.15)$$

Thus the value of  $(m^*/m_0)$  determines the ionization energy of the impurity. For GaAs the effective mass is very small and so the impurity state is very close to the band and the ionization energy is very small. For donors, the effective mass theory gives an energy of  $5.2\text{meV}$ . The same calculation holds for simple acceptor impurities and the ionization energy of the extra hole is found to be  $34\text{meV}$  [5]. In GaAs the same impurity may act as either a donor or an acceptor depending on whether it occupies a Ga or an As site. Tables 2.3 and 2.4 list the simple centres in GaAs together with the values of the ionization energy. Differences from the effective mass (hydrogenic) theory arise because this simple theory does not account for the rapid fluctuations in potential near to the atoms.

Impurities are localized in the crystal and thus so are the impurity energy states at low concentrations. If, however, the impurity concentration is high enough, interactions between neighbouring impurities form impurity bands. The threshold concentration for a Mott transition to a metallic conduction of the donor electrons is

$$n^{1/3}a = 0.25 \quad (2.16)$$

*This Table has been removed for Copyright reasons.*

**Table 2.3: Simple acceptor centres in GaAs. (Adapted from [110].)**

*This Table has been removed for Copyright reasons.*

**Table 2.4: Simple donor centres in GaAs. (Adapted from [110].)**

where  $a$  is the Bohr radius of the donor [17]. For GaAs,  $a = a_0 \epsilon \left( \frac{m_0}{m_*} \right) \sim 105 \text{\AA}$  and so  $n \sim 1.3 \times 10^{22} \text{cm}^{-3}$ . This concentration would be roughly equivalent to one impurity ion for every four lattice ions. The purest form of GaAs currently available is SI LEC-grown. Residual concentrations of electrically active impurities have been determined as low as  $1 \times 10^{16} \text{cm}^{-3}$  and concentrations of shallow acceptors of  $1 \times 10^{16} \text{cm}^{-3}$ .

The control and characterization of impurity properties in semiconductors is crucial to their practical application. Because the ionization energy of donors and acceptors is small, the probability of their excitation into a band at room temperature is high. Conduction is greatly enhanced in materials with high impurity content. The conduction may proceed by electrons or by holes in different materials, dependent on whether donors or acceptors predominate. The materials are called “n-type” and “p-type” respectively. The Fermi level of the material actually determines whether a material is n or p-type. If the Fermi level lies midway between conduction and valence bands then the material is said to be “compensated”.

## 2.4 Deep levels

The simple substitutional impurities are termed “shallow centres” because their energies are near to the band energies. “Deep levels” are those that exist far from the band edges, and are thus associated with very large binding energies. Large binding energies can exist for certain substitutional impurities, and also for crystal defects.

Very simple models of defects can be built up from a “tight-binding” theoretical approach. The defect states have eigenfunctions which decrease exponentially away from the defect and have very small extension. Lannoo has shown simple models

for a vacancy, interstitial, and substitutional impurity [59]. One conclusion from the simple theory of deep substitutional impurities is that if the potentials are strong enough all impurity levels become pinned to energies corresponding to the energy of a vacancy.

In LEC-grown GaAs, understanding of the deep levels is particularly important because it is one of the deep levels, identified as “EL2”, that controls the electrical and optical properties of the crystal to a great extent. EL2 provides the electrical compensation of the whole crystal by acting as compensation centres for residual shallow acceptor impurities [97]. It is important to obtain compensated GaAs for the production of thermally stable semi-insulating crystals—the key material for integrated circuits technology. It is becoming accepted that EL2 is a complex involving an As-on-Ga-site antisite defect,  $\text{As}_{\text{Ga}}$  as one of its constituents although its exact atomic identity is still controversial [104].

Burd and Braunstein [9] performed photo-induced transient spectroscopy on LEC-grown Cz-GaAs and observed seven deep levels, see Figure 2.8.

## 2.5 Phonons

Phonon co-operation is an important interaction in the semiconductor. Phonon exchange leads to “thermalization”—the process by which non-equilibrium distributions of electrons and holes in the bands acquire the same temperature as the lattice. Phonons also co-operate in photoluminescence when a change of crystal momentum is required to effect an energy transition.

The phonon spectrum for GaAs can be measured by the inelastic scattering of slow neutrons. Figure 2.9 shows the  $\omega - k$  phonon dispersion curves at room

This Figure has been removed for Copyright reasons.

Figure 2.8: Plots of  $\log(T_m^2 t)$  vs. reciprocal temperature for all deep levels seen by PITS. (From [9].)

temperature obtained in this way by Waugh and Dolling [106]. Also shown are the theoretical attempts to fit data with a dipole approximation force constant model.



This Figure has been removed for Copyright reasons.

Figure 2.9: Dispersion curves for acoustic and optical branch phonons in GaAs.  
(From [106].)

# CHAPTER THREE

## ENERGY TRANSFER AND DECAY

### 3.1 Models of Energy Transfer

Photoluminescence experiments typically excite the crystal with radiation of energy greater than the band gap. Electron-hole pairs are created and these recombine to give a spectrum of energies lower than the excitation energy. Luminescence does not always occur as an immediate decay of excitation but can be delayed. In phosphorescent materials the luminescence lifetime can be as long as several hours and is strongly temperature dependent. For GaAs, luminescence lifetimes vary between  $1ns$  and  $1000ns$  [69] with the slower decays corresponding to very pure samples for which the quick decay through intermediary impurity states is not possible. The decay of the band-band recombination, however, is seen to be much faster—  $100-1200ps$  [107]. This indicates that excited carriers are transferred away from their initial states before decaying.

When the crystal is excited, electrons and holes are created in the bands. The energy at which they are created depends on the energy of the incident excitation. Generally, the distribution of excitation energy is highly non-equilibrium. Curve b) of Figure 3.1 shows a typical distribution immediately after excitation.

What happens after excitation? We presume that the excess population decays, but how?

There are several different processes that transfer the excitation energy to different states. Each process is associated with a particular mechanism and has a different rate of decay of carriers.

This Figure has been removed for Copyright reasons.

Figure 3.1: Two possible forms of electron distribution function for the same quasi-Fermi level. (From [113].)

The immediate effect following excitation is for thermalization to take place within each band. Carrier energy is re-distributed through interaction with the lattice: phonons are exchanged. After thermalization the carrier distributions in the bands are described by the Fermi probability distribution. However, there is still an over-population of carriers compared to the thermal equilibrium population so a “quasi-Fermi” energy-level is used to characterize each band rather than the single Fermi level of the crystal. Figure 3.1, curve a), shows the thermalized distribution of carriers.

Most electron-hole pairs do not recombine directly from the energy bands. Instead, one or both of the carriers is usually captured by an energy level within the band gap. It is very easy for carriers to jump to shallow impurity levels through the emission of a phonon or two. An ionized donor, for example, has a very large capture cross-section for the capture of an electron. Exciton states and deep levels also capture carriers.

Transfer of excitation takes place between the crystal's energy states until the thermal equilibrium distribution is re-established.

### 3.2 Continuity Equation

The continuity equation provides an important way of describing the behaviour of a carrier population. It includes the effects of carrier generation, recombination and diffusion. Several authors have solved the continuity equation in detail in order to investigate the time dependence of luminescence decay under specific excitation conditions [48,101,67]. Others use the equation to interpret experimentally observed carrier decays [69,107].

The continuity equation is

$$\nabla \cdot \mathbf{J} + \frac{\partial[qn(\mathbf{x})]}{\partial t} = 0 \quad (3.1)$$

where  $n(\mathbf{x})$  represents a carrier distribution and the current,  $\mathbf{J}$ , is due to diffusion of carriers,

$$\mathbf{J} = -D\nabla [qn(\mathbf{x})] \quad (3.2)$$

Weiner and Yu [107] modelled their experimental conditions by assuming that the medium was semi-infinite with the sample surface located at the  $z = 0$  plane. The carrier concentration was assumed to depend only on time,  $t$ , and depth,  $z$ . Then from 3.1, the concentration of electron-hole pairs  $N(z, t)$  obeys,

$$\frac{\partial N}{\partial t} = G(z, t) + D \frac{\partial^2 N}{\partial z^2} - \frac{N}{\tau} \quad (3.3)$$

where  $G(z, t)$  is the generation rate due to an incident laser,  $D$  the diffusion coefficient and  $\tau$  the bulk recombination time due to carrier capture at impurities and defects.

This equation has to be solved subject to the boundary conditions that

$$D \frac{\partial N}{\partial z} \Big|_{z=0} = N(0, t)S$$

and

$$N(\infty, t) = 0$$

where  $S$  is the surface recombination velocity. It is assumed that the incident laser pulse is a delta function in time so that  $G(z, t)$  is given by

$$G(z, t) = N_0 \delta(t) e^{-\alpha_i z} \quad (3.4)$$

where  $\alpha_i$  is the absorption co-efficient of GaAs at the incident laser frequency.

The solution for the time-dependent emission intensity is [102],

$$I(t) \propto e^{-t/\tau} [A_1 W(\alpha_i \sqrt{Dt}) + A_2 W\left(\frac{S}{D} \sqrt{Dt}\right) + A_3 W(\alpha_e \sqrt{Dt})] \quad (3.5)$$

where

$$\begin{aligned} A_1 &= \frac{\alpha_e}{\alpha_e^2 - \alpha_i^2} + \left(\frac{2S}{D}\right) \left(\frac{S}{D} - \alpha_i\right)^{-1} (\alpha_e - \alpha_i)^{-1} \\ A_2 &= \left(\frac{2S}{D}\right) \left(\frac{S}{D} - \alpha_i\right)^{-1} \left(\alpha_e - \frac{S}{D}\right)^{-1} \\ A_3 &= \frac{2}{\alpha_e + \alpha_i} - (A_1 + A_2) \end{aligned}$$

and

$$W(x) = e^{(x^2)} \operatorname{erfc}(x)$$

$\alpha_e$  is the absorption co-efficient at the emission frequency and  $\operatorname{erfc}$  is the complementary error function.

In 3.5 the term outside the bracket is a simple exponential decay with decay time  $\tau$ . The terms inside the bracket are significant only when  $S$  and  $D$  are both large. Since these terms lead to non-exponential decays, the surface recombination and diffusion terms can be readily distinguished from the bulk recombination term.

This Figure has been removed for Copyright reasons.

Figure 3.2: Four fundamental processes involved in recombination through traps  
 a) the capture of a conduction electron by an empty trap b) the emission of an electron from the trap to the conduction band c) the capture of a hole from the valence band by a trap containing an electron d) the promotion of a valence electron into an initially empty trap. (From [66].)

Typically quoted values of  $D$  and  $S$  are [37]

$$D = 10\text{cm}^2/\text{s}$$

$$S = 10^6\text{cm}/\text{s}$$

Weiner and Yu [107], however, found that the best fits to their observations of band-band luminescence came from assuming  $S = D = 0$ .

### 3.3 Shockley-Read Theory

Shockley and Read [88] analyzed the statistics of recombination of holes and electrons for a model in which the recombination occurs through the mechanism of trapping. Figure 3.2 shows the four basic processes of carrier capture and emission that they considered [66]. Shockley and Read derived statistical rates for capture and emission of electrons and holes by traps. These can be used to find the time-decay of the carrier population. For a population  $n$  of electrons, the capture and

emission rates by traps are  $R_{cn}$  and  $R_{en}$

$$R_{cn} = C_n N_t (1 - f(E_t)) n \quad (3.6)$$

$$R_{en} = E_n N_t f(E_t) \quad (3.7)$$

where  $C_n$  and  $E_n$  are constants representing capture and emission probabilities for electrons,  $N_t$  represents the total concentration of trapping centres and  $E_t$  is the trap energy. In equilibrium, the detailed balance condition  $R_{en} = R_{cn}$  gives,

$$E_n = n_o C_n \left( \frac{1 - f_o(E_t)}{f_o(E_t)} \right) \quad (3.8)$$

with  $f_o$  being the equilibrium distribution, the Fermi function.

Off-equilibrium, consider the net recombination rate

$$R_n = R_{cn} - R_{en} \quad (3.9)$$

Define

$$E_n = n_1 C_n \quad (3.10)$$

where

$$n_1 = N_c e^{-(E_c - E_t)/kT} \quad (3.11)$$

and get a net rate,

$$R_n = C_n N_t [n(1 - f(E_t)) - n_1 f(E_t)] \quad (3.12)$$

$n_1$  is the electron concentration which would be present in the conduction band if the Fermi level were to coincide with the trap level  $E_t$ .

Similarly for holes, obtain

$$R_p = C_p N_t [p f(E_t) - p_1 (1 - f(E_t))] \quad (3.13)$$

where

$$p_1 = N_v e^{-(E_t - E_v)/kT} \quad (3.14)$$

We may set  $R_n = R_p$  since every recombination requires an electron and a hole. Then solving for  $f(E_t)$ ,

$$f(E_t) = \frac{C_p p_1 + C_n n}{C_n(n + n_1) + C_p(p + p_1)} \quad (3.15)$$

and substituting back into 3.12 and 3.13,

$$R_n = R_p = \frac{N_t C_n C_p (np - n_1 p_1)}{C_n(n + n_1) + C_p(p + p_1)} \quad (3.16)$$

If we define a common lifetime  $\tau$  for the recombination

$$R_n = R_p = -\frac{d(\delta p)}{dt} = \frac{\delta p}{\tau} \quad (3.17)$$

then substituting  $n = n_0 + \delta p$ ,  $p = p_0 + \delta p$  and  $n_1 p_1 = n_0 p_0$ , assuming that the number of excited carriers  $\delta p$  is very small compared to  $n_0$  or  $p_0$ .

$$\frac{1}{\tau} = \frac{N_t(p_0 + n_0 + \delta p)}{1/C_p(n_0 + n_1 + \delta p) + 1/C_n(p_0 + n_0 + \delta p)} \quad (3.18)$$

The lifetime depends on the position of the Fermi level, since this determines the carrier populations  $n$ ,  $n_1$ ,  $p$ ,  $p_1$ . The lifetime varies from

$$\tau = \tau_{po} = \frac{1}{C_p N_t} \quad (3.19)$$

in strongly extrinsic n-type material to

$$\tau = \tau_{no} = \frac{1}{C_n N_t} \quad (3.20)$$

in p-type material. A maximum occurs between the two extremes. Figure 3.3 shows the lifetime as a function of the Fermi level.

The Shockley-Read theory contains a number of unknown parameters whose value must be adjusted to fit experimental data. This makes it difficult to make precise comparisons between the theory and experiment.



This Figure has been removed for Copyright reasons.

Figure 3.3: Dependence of lifetime upon Fermi energy. (From [66])

### 3.4 Excitation Transfer Theories

The continuity equation and the Shockley-Read statistical description consider energy transfer on a large scale—their descriptions are for the total numbers of carriers. In contrast, the more detailed excitation transfer theories are based upon microscopic models. Their approach is to solve sets of coupled rate equations for the probability of carriers existing on certain sites.

A very simple model of energy transfer between two monomolecular centres was considered by Chimzak [14]. A first type of centre is excited and decays according to,

$$\frac{dN_1}{dt} = -\alpha_1 N_1 \quad (3.21)$$

Assuming that all of the excitation is transferred to emitting centres,  $N_2$ , then the decay of the second centres is,

$$\frac{dN_2}{dt} = -\frac{dN_1}{dt} - \alpha_2 N_2 \quad (3.22)$$

Equations 3.21 and 3.22 can be solved by Laplace transform (see Appendix A).

This Figure has been removed for Copyright reasons.

Figure 3.4: Luminescence excited by short pulse in the case of energy transfer. (From [14].)

Following the excitation the luminescence decays as

$$I = -\frac{dN_2}{dt} = \frac{N_{o1}}{\tau_2 - \tau_1} \left[ e^{-t/\tau_2} - \frac{\tau_2}{\tau_1} e^{-t/\tau_1} \right] \quad (3.23)$$

where  $N_1(0)$  is the initial number of excited transferring centres and  $\tau_1$  and  $\tau_2$  are the lifetimes of transfer and emission centres, respectively. This describes the curve of Figure 3.4. The transfer process actually causes the luminescence to increase after the excitation has ended. There is a delay time of

$$\tau_{max} = \frac{\tau_1 \tau_2}{\tau_2 - \tau_1} 2 \ln \frac{\tau_2}{\tau_1} \quad (3.24)$$

before the luminescence begins to decrease. This simple model demonstrates a very interesting luminescence profile.

Huber et. al. [44] proposed a model for energy transfer which relates the luminescent decay curves to the microscopic transfer processes. The starting point is a set of

coupled rate equations for the luminescence centres,

$$\frac{dP_n(t)}{dt} = - \left[ \gamma_R + \sum_{n''} W_{nn''} \right] P_n(t) + \sum_{n'} W_{n'n} P_{n'}(t) \quad (3.25)$$

$P_n(t)$  is the probability that the  $n$ 'th ion is excited at time  $t$ . The parameter  $\gamma_R$  denotes the radiative decay term and  $W_{nn'}$  is the transfer rate from ion  $n$  to ion  $n'$ . The second term on the right hand side characterizes the transfer away from excited ions and the third term describes a "back transfer" process where energy is transferred from neighbouring ions.

The luminescent intensity is identified with the function  $P_0(t)$  which is the solution to 3.25 with the initial conditions  $P_0(0) = 1$ ,  $P_n(0) = 0$  and  $n \neq 0$ . The radiative decay term can be factored out of  $P_n(t)$ ,

$$P_n(t) = e^{-\gamma_R t} P'_n(t) \quad (3.26)$$

so 3.25 becomes,

$$\frac{dP'_n(t)}{dt} = - \sum_{n''} W_{nn''} P'_n(t) + \sum_{n'} W_{n'n} P'_{n'}(t) \quad (3.27)$$

Considering the short-time behaviour for  $n = 0$ , the back transfer term may be neglected. Then the solution is

$$P'_0(t) = e^{-\sum_n W_{0n} t} \quad (3.28)$$

Including the back transfer, equation 3.27 may be solved with the initial conditions  $P'_0(0) = 1$  and  $P'_n(0) = 0$  for  $n \neq 0$  and for a spatially ordered array of optically active ions. Introduce the Fourier transform of  $P'_n(t)$ ,

$$P'(k, t) = \sum_n e^{-i\mathbf{k} \cdot \mathbf{r}_n} P'_n(t) \quad (3.29)$$

$$P'_n(t) = \frac{1}{N} \sum_k e^{i\mathbf{k} \cdot \mathbf{r}} P'(k, t) \quad (3.30)$$

where the sum on  $n$  is over the  $N$  ions located at sites  $R_n$  while sum on  $k$  is over Brillouin Zone associated with ionic lattice.  $P'_0(t)$  is then expressed as

$$P'_0(t) = \frac{e^{-\Gamma_0 t}}{N} \sum_k e^{\Gamma_k t} \quad (3.31)$$

where

$$\Gamma_0 = \sum_n W_{0n} \quad (3.32)$$

$$\Gamma_k = \sum_n \cos(\mathbf{k} \cdot \mathbf{r}_{n0}) W_{0n} \quad (3.33)$$

in which  $\mathbf{r}_{n0} = \mathbf{r}_n - \mathbf{r}_0$  and the lattice has inversion symmetry.

The solution 3.31 is exact for a lattice with all sites occupied. The short-time behaviour of 3.31 is

$$P'_0(t) = e^{-\Gamma_0 t} \left( 1 + \frac{t^2}{2N} \sum_k \Gamma_k^2 + \dots \right) \quad (3.34)$$

so that the correction for back-transfer is of the form  $1 + at^2$  for small  $t$ .

The long time behaviour of 3.31 is

$$P'_0(t) \sim t^{-3/2} \quad (3.35)$$

which is indicative of diffusive decay at long times, in contrast to near-exponential decay at short times.

The time evolution of  $P'_n(t)$  is determined by the symmetry of the ionic lattice, and the functional dependence of  $W_{nn'}$  on the inter-ionic separation. A frequently used approximation is to take  $W_{nn'}$  to be of the form [46]

$$W_{nn'} = \left( \frac{R_{min}}{r_{nn'}} \right)^s W_0 \quad (3.36)$$

This relationship includes the symmetry  $W_{nn'} = W_{n'n}$ .  $R_{nn'}$  is the distance between the sites  $n$  and  $n'$ .  $R_{min}$  is the distance between nearest-neighbours and  $W_0$  and

$s$  are parameters.  $s$  in particular characterizes the decrease in transition rate with increasing separation and thus reflects the interaction mechanism involved in the transfer—for instance, dipole-dipole or quadrupole-quadrupole interactions. Other physical transfer mechanisms may be modelled with different forms of  $W_{nn'}$ —hopping or tunneling transitions.

Finding a general solution to this transfer model without the special initial conditions and with a set of luminescent centres that does not fill every site of the lattice is considerably difficult. Huber et. al. [44] put forward several approximate solutions, especially for the short-term behaviour to model fluorescence.

### 3.5 Thermal De-Trapping

The microscopic transfer theories of Huber are complete in the sense that they allow for all possible microscopic processes between atoms or states. If we were only able to solve the set of coupled equations 3.25 for every atom in the crystal then we would not need to worry about the details of the transfer rate  $W_{nn'}$ , which determines that some atoms transfer excitation quickly, others slowly, and some have a certain temperature dependence, others do not. In order to be able to solve the Huber equations it is necessary to make certain approximations. The nature of these approximations is determined by what is known about the physical system.

Huber's approximate solutions ignored the possibility of "trapping" of excitation. Trapping occurs if energy becomes caught at a site from which it escapes only very slowly, as an equilibrium restoring process. This can occur, for example, if the matrix element determining optical transitions is zero and the de-trapping process is a slow thermal excitation.

Trapping is considered to be an important process in luminescence. Randall and Wilkins [78] proposed that excitation from traps could account for the time decays and temperature variations that were observed for phosphorescence. Theories of thermo-luminescence (luminescence that is excited by thermal effects) are based upon the thermal release of trapped carriers into a band [13] and consideration is given to the detailed distributions of traps that lead to particular time decays.

Huber did extend his transfer theories to include the effects of traps [42,43] but in a very limited way: in modelling the short-time fluorescence behaviour he assumed that the rate of energy transfer from traps was time-independent and he did not consider the effects of temperature on the de-trapping rate.

Teh [98], in experiments with LEC-grown SI GaAs doped with carbon impurities, discovered a temperature dependence in the time decay of luminescence. The luminescence of  $\sim 1.49\text{eV}$  was observed to decay as a power law in time and the exponent of the power law varied linearly with temperature. This led Teh to propose as a possible explanation the thermal de-trapping of carriers from traps.

The excitation transfer process of thermal de-trapping thus has an important effect on the luminescent time decay. The effect is investigated in detail in the second part of this thesis, where the results of computer simulations of luminescence decay from various distributions of traps are presented.

## CHAPTER FOUR

# RADIATIVE AND NON-RADIATIVE TRANSITIONS

### 4.1 Radiative Recombination

Energy decay processes involving the emission of light result from the recombination of an electron with a hole. The processes are readily observable as luminescence.

In order to use Fermi's golden rule to describe the transitions we must know some details of the quantum system. The interaction energy between the radiation field and the atomic system is,

$$\mathcal{H}_{Int} = \sum_j - \left( \frac{e}{mc} \right) \mathbf{A}_j \cdot \mathbf{p} + \left( \frac{e^2}{2mc^2} \right) A_j^2 \quad (4.1)$$

where  $A$  is the vector potential,  $p$  is the momentum and the sum is over all the electrons of the system.

The one-electron approximation is assumed in order to find approximate wavefunctions and the contribution from the  $A_j^2$  term is neglected. Once the vector potential is expanded, the interaction Hamiltonian can be split into two terms—one for photon absorption the other for photon emission.

Fermi's golden rule for the total emission rate,  $\mathcal{W}_{em}$ , due to transition between an upper  $|u\rangle$  and lower  $|l\rangle$  state gives,

$$\mathcal{W}_{em} = \frac{2\pi}{\hbar} \sum_{\lambda} \sum_{u,l} | \langle l | \mathcal{H}_{Int}^{em} | u \rangle |^2 \delta(E_l - E_u + \hbar\omega_{\lambda}) \quad (4.2)$$

where the sums are over all radiation modes,  $\lambda$ , and all states,  $u$  and  $l$ . The momentum matrix element  $|P_{lu}^{em}|$  may be separated out of the above expression and

the transition rate written as,

$$\mathcal{W}_{em} = \frac{2\pi}{\hbar} \sum_{\lambda} \sum_{u,l} |\mathcal{H}_{lu}^{em}|^2 (N_{\lambda} + 1) \delta(E_{lu} - \hbar\omega_{\lambda}) \quad (4.3)$$

where

$$|\mathcal{H}_{lu}^{em}|^2 = \left( \frac{2\pi\hbar^2 e^2}{\epsilon_r m^2 \omega_{\lambda}} \right) |P_{lu}^{em}|^2 \quad (4.4)$$

and the momentum matrix element is,

$$|P_{lu}^{em}| = | \langle l | e^{-ik_{\lambda} \cdot r} \hat{\mathbf{e}}_{\lambda} \cdot \mathbf{p} | u \rangle | \quad (4.5)$$

This emission rate 4.3 includes the effects of both stimulated and spontaneous emission. The portion due to spontaneous emission does not depend on the occupation numbers of the radiation modes,  $N_{\lambda}$ , and we may replace the sum over radiation modes  $\lambda$  by a sum over photon frequencies,  $\omega$ , by introducing a spectral density of states  $G(\hbar\omega)$ ,

$$\begin{aligned} \mathcal{W}_{sp} &= \frac{2\pi}{\hbar} \sum_{\lambda} \sum_{u,l} |\mathcal{H}_{lu}^{em}|^2 \delta(E_{lu} - \hbar\omega_{\lambda}) \\ &= \frac{2\pi}{\hbar} \sum_{\omega} \sum_{u,l} |\mathcal{H}_{lu}^{em}|^2 G(\hbar\omega) \delta(E_{lu} - \hbar\omega) \end{aligned} \quad (4.6)$$

This formula for the transition rate is valid if every initial state is occupied and every final state is empty. In most cases some of the initial states will be empty and some of the final states filled. We introduce probabilities  $P_j$  and  $P'_j$  that the state  $|j\rangle$  is filled or empty, respectively. The emission rate involving photons within a narrow spectral region is then,

$$\begin{aligned} R_{sp}(\hbar\omega) d\hbar\omega &= -d\mathcal{W}_{sp} P_u P'_l \\ &= \frac{2\pi}{\hbar} \sum_{u,l} |\mathcal{H}_{lu}^{em}|^2 G(\hbar\omega) P_u P'_l \delta(E_{lu} - \hbar\omega) d\hbar\omega \\ &= \frac{2\pi}{\hbar} \sum_{E_u, E_l} | \langle \mathcal{H}_{lu}^{em} \rangle |_{av}^2 G(\hbar\omega) n(E_u) n'(E_l) \delta(E_{lu} - \hbar\omega) d\hbar\omega \end{aligned} \quad (4.7)$$



where the sum over states has been replaced by a sum over energies and the degenerate components have been included in  $|\langle \mathcal{H}_{lu}^{em} \rangle|^2$  and  $n$ .

For each distinct line in the photoluminescence spectrum— whether band-impurity, exciton-band, impurity-impurity or band-band— we can now work out the characteristics of the emission profile. The recombination of an electron and a hole is proportional to the occupation number of electrons in the upper state, to the number of empty electron sites (holes) in the lower state, and to the square of the optical matrix element.

The definition 4.7 is valid for both discrete and continuous states. Three situations are of particular interest:

- the upper and lower energy levels are both discrete
- one level is discrete and the other is continuous
- both levels are continuous

*a) Number of States*

For discrete-discrete transitions (see Figure 4.1c), the number of states at energies other than  $E_u$  and  $E_l$  is zero. Hence,

$$n_u(E'_u) = n_u \delta(E'_u - E_u) \quad (4.8)$$

$$n'_l(E'_l) = n'_l \delta(E'_l - E_l) \quad (4.9)$$

and the sums over energies in 4.7 are reduced to a single term,

$$R_{sp}(\hbar\omega) = \frac{2\pi}{\hbar} |\langle \mathcal{H}_{lu}^{em} \rangle|^2 G(\hbar\omega) n_u n'_l \delta(E_{lu} - \hbar\omega) \quad (4.10)$$

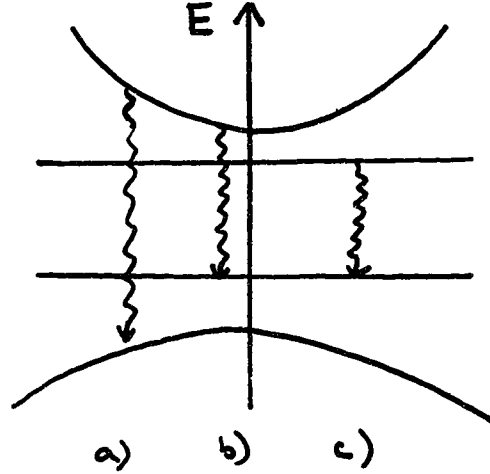


Figure 4.1: Radiative transitions: a) band-band b) band-impurity c) impurity-impurity

If the number of states  $n_u$  and  $n'_l$  refers to  $N_u$  and  $N_l$  impurity atoms with degeneracies of  $g_u$  and  $g_l$  then  $n_u = g_u N_u P_u$  and  $n'_l = g_l N_l P'_l$ . Then the total spontaneous emission rate is,

$$\begin{aligned} R_{sp} &= \int R_{sp}(\hbar\omega) d(\hbar\omega) \\ &= \frac{2\pi}{\hbar} | \langle \mathcal{H}_{lu}^{em} \rangle |^2_{av} G(\hbar\omega) g_u g_l N_u N_l P_u P'_l \end{aligned} \quad (4.11)$$

In general, even discrete lines possess a finite width so that all of the photons are not emitted at  $\hbar\omega = E_{lu}$ . Let  $A(E_{lu} - \hbar\omega)$  represent the line shape normalized to unity,

$$\int_0^\infty A(E_{lu} - \hbar\omega) d\hbar\omega = 1 \quad (4.12)$$

then

$$R_{sp}(\hbar\omega) = R_{sp} A(E_{lu} - \hbar\omega) \quad (4.13)$$

The line-shape function  $A(E_{lu} - \hbar\omega)$  is often adequately approximated by a Lorentian or Gaussian curve.

Consider discrete-continuum transitions from a continuous set of upper levels to a discrete lower level, Figure 4.1b). The number of occupied states in the continuum is given by the density of energy states  $\rho(E_u)$  times the probability that they are occupied  $P(E_u)$ ,

$$n(E_u) = \rho(E_u)P(E_u) \quad (4.14)$$

where  $P(E_u)$  is the Fermi-Dirac distribution for a thermalized non-equilibrium population. The number of states in the lower level (as before) is,

$$n'_l(E'_l) = n'_l \delta(E'_l - E_l)$$

For a parabolic band the energy surface is defined by

$$E_c(\mathbf{k}) = \left( \frac{\hbar^2 \mathbf{k}^2}{2m_c} \right) + \epsilon_G \quad (4.15)$$

where  $\epsilon_G$  is the band gap energy. So the density of states is

$$\rho(E_u) = \rho(E_c) = \frac{1}{(2\pi)^2} \left( \frac{2m_c}{\hbar^2} \right)^{3/2} E_c(\mathbf{k})^{1/2} \quad (4.16)$$

Then the recombination rate is,

$$\begin{aligned} R_{sp}(\hbar\omega) &= \frac{2\pi}{\hbar} | \langle \mathcal{H}_{lu}^{em} \rangle |^2 G(\hbar\omega) n(E_u) n'_l \delta(E_{lu} - \hbar\omega) \\ &= \frac{2\pi}{\hbar} | \langle \mathcal{H}_{lu}^{em} \rangle |^2 G(\hbar\omega) \rho(E_u) g_l N_l P(E_u) P'(E_l) \delta(E_{lu} - \hbar\omega) \end{aligned} \quad (4.17)$$

The principal spectral variation of  $R_{sp}(\hbar\omega)$  is contained in the product  $\rho(E)P(E)$ . Since for parabolic bands,  $\rho(E) \sim E^{1/2}$  and normally  $P(E) \sim e^{-E/kT}$ ,

$$R_{sp}(\hbar\omega) \sim E^{1/2} e^{-E/kT} \quad (4.18)$$

where  $E = \hbar\omega - \epsilon_G - \epsilon_l$  and  $\epsilon_l$  is the impurity binding energy.

The energy dependence of  $\mathcal{H}_{lu}^{em}$  can be neglected to a good level of approximation.

The case of continuum-continuum transitions (Figure 4.1a)) is somewhat more involved than the previous two cases because of the appearance of  $k$  selection rules. Conservation of momentum in optical transitions requires that

$$\mathbf{k}_u = \mathbf{k}_l \quad (4.19)$$

since the photon wave vector is negligible. If the relation between  $E(k)$  and  $k$  is known for each band then 4.7 becomes

$$\begin{aligned} R_{sp}(\hbar\omega) &= \frac{2\pi}{\hbar} \sum_{E_u, E_l} | \langle \mathcal{H}_{lu}^{em} \rangle |^2 G(\hbar\omega) n(E_u) n'(E_l) \delta(E_{lu} - \hbar\omega) d\hbar\omega \\ &= \frac{2\pi}{\hbar} \sum_{k_u, k_l} | \langle \mathcal{H}_{lu}^{em} \rangle |^2 G(\hbar\omega) n_u(k_u) n'_l(k_l) \delta_{k_u, k_l} \delta(E_u(k_u) - E_l(k_l) - \hbar\omega) \\ &= \frac{2\pi}{\hbar} | \langle \mathcal{H}_{lu}^{em} \rangle |^2 G(\hbar\omega) \rho_{red}(E) P_u(E_u) P'_l(E_l) \delta_{k_u, k_l} \delta(E_u - E_l - \hbar\omega) \end{aligned} \quad (4.20)$$

The reduced density of states is given by,

$$\rho_{red}(E) = \frac{1}{2\pi^2} \frac{k^2}{(d/dk)[E_u(\mathbf{k}_u) - E_l(\mathbf{k}_l)]|_{E_u=E_l+\hbar\omega}} \quad (4.21)$$

and  $E = \hbar\omega - \epsilon_G$ . For parabolic bands  $\rho(E) \sim E^{1/2}$  and  $P(E) \sim e^{-E/kT}$ . Again assuming that  $\mathcal{H}_{lu}^{em}$  is independent of energy,

$$R_{sp}(\hbar\omega) \sim E^{1/2} e^{-E/kT} \quad (4.22)$$

#### b) Matrix Element

The momentum matrix element determines the value of  $R_{sp}(\hbar\omega)$  which in turn determines the strength of the luminescent intensity. We mentioned in connection with continuum-continuum transitions that the wave-vectors of the recombining

electron and hole need to be practically the same in order for the transition to be momentum-conserving. This is an example of a selection rule that arises from a calculation of the matrix element 4.5. Just as in atomic physics, when the matrix element becomes zero the transitions are forbidden.

The vanishing matrix elements can be determined if the symmetry properties of the initial and final states are known.

Each type of point impurity or defect is associated with a particular symmetry arrangement, as is every point in the Brillouin zone and so can be represented by an irreducible symmetry representation. In general, when calculating matrix elements,

$$\langle \phi_m / V_i / \psi_n \rangle \quad (4.23)$$

each component may be represented by its irreducible symmetry representation, so for instance write the above as,

$$\langle \phi_m^\mu / V_i^\alpha / \psi_n^\nu \rangle \quad (4.24)$$

where the  $\mu, \alpha$  and  $\nu$  are indicative of the representations. Now, if the representation  $D^\mu$  does not appear in the decomposition of the product representation  $D^\alpha \times D^\nu$  then the matrix elements are zero because of the orthogonality theorem in group theory.

For band-band transitions  $\mathcal{H}_{cv}(k)$  vanishes at  $k = 0$  if the periodic portions of the Bloch functions  $U_{n,k}(r)$  possess similar symmetries for both the conduction and valence bands. If the symmetry at  $k = 0$  is  $s$ -like then away from  $k = 0$  the symmetry is usually lowered by admixture with  $p$ -like symmetry; then  $\mathcal{H}_{cv}(k)$  for  $k \neq 0$  is non-vanishing.

## c) Lifetime

It is useful to be able to calculate a radiative lifetime and to understand the form of the time-decay predicted by  $R_{sp}(\hbar\omega)$  even though the radiative decay is not necessarily the only process affecting the carrier lifetime. In the discussion of energy transfer we showed that thermalization, radiative recombination and non-radiative transfer between ions were all important to the total decay. An independent estimate of the radiative lifetime is obtainable from the theory. In the simplest case, the spontaneous emission rate can be written

$$\begin{aligned} R_{sp} = -\frac{dn}{dt} &= \left( \frac{R_{sp}^0}{n_0 p_0} \right) np \\ &= B np \end{aligned} \quad (4.25)$$

where  $n_0$ ,  $p_0$ ,  $R_{sp}^0$  are the equilibrium values of  $n$ ,  $p$  and  $R_{sp}$ , respectively.

In intrinsic materials,  $np = n^2$ , and integration of 4.25 gives

$$n(t) = \frac{n(0)}{1 + Bn(0)t} \quad (4.26)$$

This shows non-exponential recombination behaviour.

For strongly extrinsic materials, say  $p$ -type, there exist  $p_0$  holes before excitation. Excitation creates equal numbers of electrons and holes,  $\delta p$ , and the total populations are:

for electrons,

$$n = \delta p \quad (4.27)$$

and for holes,

$$p = p_0 + \delta p \quad (4.28)$$

Assuming  $\delta p \ll p_0$  the solution to 4.25 is now

$$n(t) = n(0)e^{-t/\tau} \quad (4.29)$$

where

$$\frac{1}{\tau} = - \left( \frac{1}{n} \right) \frac{dn}{dt} = Bp_0 \quad (4.30)$$

This is familiar exponential behaviour. The radiative lifetime is not determined by the optical transition rate alone but also depends on the equilibrium carrier densities.

## 4.2 Non-Radiative Transitions

Non-radiative transitions are extremely important to the energy decay process. A rough idea of their importance can be obtained from the internal quantum efficiency of a material,

$$\eta = \frac{\tau_{nr}}{\tau_{nr} + \tau_r} \quad (4.31)$$

where  $\tau_{nr}$  and  $\tau_r$  are the decay times for non-radiative and radiative processes respectively. A good efficiency is achieved when radiationless transitions are minimized— $\tau_{nr}$  is large and  $\tau_r$  small. However, even for the best semiconductor materials used for light-emitting diodes,  $\eta \sim 0.3\%$  [71].

It is further apparent that radiationless processes are of utmost importance for a material such as GaAs because of the effect of quenching of luminescence as the temperature is raised.

A theoretical understanding of non-radiative transitions should enable us to calculate the probability of occurrence of the various types of transition. If the probability sufficiently exceeds that of the corresponding radiative processes then the transition is radiationless and not radiative. Theory will need to explain why the non-radiative rate grows faster than the radiative rate with temperature, and with carrier concentration. Such a comprehensive understanding has not been achieved.

In the remainder of this chapter I describe the main transition processes that result in non-radiative transitions and also outline the theoretical developments.

### a) Transition Processes

Landsberg [57] has reviewed the non-radiative transition processes in semiconductors. The only known non-radiative capture processes are the Auger effect, lattice-relaxation multi-phonon emission and, under certain circumstances, phonon cascade capture:

- The band-band Auger effect is illustrated in Figure 4.2. Electrons in states 1' and 2' collide and the first electron loses energy while the second gains. A recombination is achieved because one electron and a heavy hole both disappear. Competing with this is the collision between an electron in state 1' and an electron in the light hole band in state 3'. Again a recombination ensues.

The laws governing these Auger effects can be understood in terms of classical collisions. Once an electron has been noticeably deflected by the Coulomb forces due to another electron, the collision can be said to have started. The effective potential is just the electron-electron interaction. Just as in classical theory, both energy and momentum have to be conserved, this leads to a threshold energy which state 1' must have before the process can proceed at all.

Impact ionization is a process in which an electron-hole pair is created due to a collision between electrons. It may be considered as identical to Auger recombination in Figure 4.2 if the arrows are reversed.



*This Figure has been removed for Copyright reasons.*

Figure 4.2: Band-band Auger effect. (From [57].)

*This Figure has been removed for Copyright reasons.*

Figure 4.3: Trap Auger effects. (From [57].)

Auger transitions can take place through intermediary traps— one carrier is trapped at a centre and the energy released or absorbed by another carrier, see Figure 4.3.

A variety of more complicated Auger processes involving recombination centres can also be conceived. For instance, a centre can lose two electrons with the result that a hole is replaced by an electron, see Figure 4.4a).

Electrons may recombine with a centre and the energy may be used up to create a hole by promoting an electron to a neighbouring centre. This has the effect of changing the electron into a hole, see Figure 4.4b). The reverse

This Figure has been removed for Copyright reasons.

Figure 4.4: Other Auger processes. (From [57].)

process changes a hole into an electron, see Figure 4.4c).

- Lattice-relaxation multi-phonon emission is a process whereby large amounts of energy can be efficiently dissipated by emission of many single phonons.
- Cascade capture occurs when an electron loses energy by dropping through a series of closely spaced levels, emitting one phonon during each transition. Lax [60] devised the theory for this process. However, it is only applicable to relatively shallow centres with closely spaced excited states.

#### *b) Theoretical Developments*

There is general agreement in recent literature that multi-phonon capture and emission processes are consistent with observed material behaviour [63].

The theory of many-quantum processes is very much more complicated than that of Section 4.1 for radiative recombination. Instead of considering the transitions of the electronic states caused by the effect of the radiation field, we now have to consider the quantum system consisting of interacting electron and lattice particles. Haug [32] writes the eigenfunctions for the unperturbed problem of an

uncoupled system of electron and lattice particles as,

$$\Psi_{r,s}(\mathbf{r}, Q) = \phi_r(\mathbf{r}) X_{r,s}(Q_r) \quad (4.32)$$

$Q$  is the lattice co-ordinate,  $\phi_r(\mathbf{r})$  is the electronic function ( $r$  is its quantum number) and  $X_{r,s}(Q_r)$  is the lattice function ( $r$  and  $s$  are its quantum numbers). the lattice states have the suffix  $r$  because they also depend on the electron state when dealing with transition processes of the order of magnitude of many vibrational quanta. The electron-lattice interaction energy is,

$$\mathcal{H}_{Int} = \sum_i U_i \left( \frac{\partial V}{\partial U_i} \right)_U = 0 \quad (4.33)$$

where the sum is over the lattice particles  $i$  and  $U$  is a potential energy representing the interaction term. Fermi's golden rule gives as the transition rate of an electron from state  $r$  to  $r'$ ,

$$\mathcal{W}_{r,r'} = \frac{2\pi}{\hbar} \sum_{s',s} | \langle \Psi_{r',s'} | \mathcal{H}_{Int}^{em} | \Psi_{r,s} \rangle |^2 p_s \delta(E_{r',s'} - E_{r,s}) \quad (4.34)$$

A sum is taken over all initial and final states of the lattice since all possible lattice transitions must be permitted. Also the probability of the occupation of the initial lattice states is taken into account by the factor  $p_s$ .

The multi-phonon decay rate was first calculated by Huang and Rhys [41]; their theory was restricted to interaction with longitudinal-optical phonons of constant frequency. It was later extended to take into account the interaction with phonons having an arbitrary frequency distribution [30,55,81]. All of the calculations were simplified by making the "Condon" approximation in which the electronic matrix element is taken to be independent of the lattice co-ordinate. The resulting non-radiative recombination rate was found to increase exponentially with temperature but to decrease exponentially with transition energy. In comparison,

the radiative rate is independent of temperature and depends only weakly on the transition energy. This basically explains why the radiationless processes dominate at high temperatures. Detailed calculations of the absolute values of the two rates, however, showed that radiationless processes at room temperature can only dominate when the energy difference of the electron states amounts to nothing more than a few vibrational quanta ( $\sim 0.05\text{eV}$ ) [32]. This does not explain the observed predominance of radiationless processes in a material such as GaAs with an energy gap of  $1.5\text{eV}$ .

Kovarskii and Sinyavskii [53,54] attempted a calculation without the Condon approximation. Their non-radiative rates were two to three orders of magnitude larger than those calculated in the Condon approximation.

Henry and Lang [36,58] developed a theory of capture at deep levels by multi-phonon emission without the Condon approximation. The capture takes place because the energy of the deep level depends on the positions of the atoms comprising the defect and on the position of the lattice and, as the lattice vibrates, the level moves up and down in the energy gap. The configuration co-ordinate model can be applied to the behaviour of the deep levels to describe the capture process. Figure 4.5 illustrates a simple model of the electron-lattice interaction in which the lattice is represented by a single co-ordinate. The figure shows that the vibrations of the single lattice co-ordinate linearly modulate the depth of the potential well binding the carrier. For sufficiently large vibrations the level can cross into the conduction band and capture an electron. Prior to capture, the equilibrium position of the level is in the upper half of the gap. After capture of the electron the lattice near the defect relaxes in such a way as to lower the equilibrium position of the level in the energy gap. It is clear from Figure 4.5 that immediately after capture of the electron the lattice is displaced far from the new equilibrium

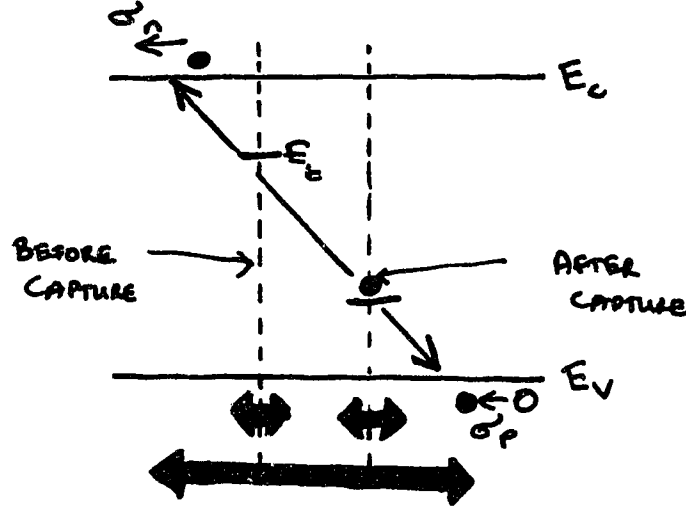


Figure 4.5: Non-radiative capture of an electron due to variation of trap depth with lattice vibration. (Adapted from [36,58].)

position and there will be a violent lattice vibration at the defect. The vibration will rapidly damp down to the amplitude of thermal vibrations after a small number of vibrational periods. During the damping, the localized energy propagates away from the defect as lattice phonons. This justifies calling the process nonradiative capture by multi-phonon emission.

Lang and Henry [36,58] found the limiting semi-classical behaviour of the theory at high temperatures to give a capture cross-section,

$$\sigma \rightarrow \sigma_{\infty} e^{-E_{\infty}/kT} \quad (4.35)$$

where  $\sigma_{\infty} = (0.5 - 4) \times 10^{-15} \text{cm}^2$  for a neutral centre. Considering the fact that Coulomb enhancement tends to decrease with temperature they predicted that the cross-sections should extrapolate to  $\sigma_{\infty} = 10^{-14} - 10^{-15} \text{cm}^2$  at  $T \rightarrow \infty$ . The values

This Figure has been removed for Copyright reasons.

Figure 4.6: Electron and hole capture cross-sections. (From [36].)

of  $\sigma_\infty$  calculated from experiment show excellent agreement with this prediction, see Figure 4.6.

Ridley [82] made a quantum-mechanical calculation of the multi-phonon emission using infinite order perturbation theory. His capture cross-section agreed exactly with the result of Lang and Henry for the high temperature limit but additionally he was able to obtain a low-temperature limit.

Passler [74] developed a semi-empirical theory of Shockley and Read processes in semiconductors and was successful in deriving explicit expressions for the non-radiative capture and emission in semiconductors. However, the static Condon approximation he used has been shown to breakdown near the crossing point of the trap state and respective lattice band edge potential curves.

Mandelis [63] provided a self-consistent semi-classical dynamic theory of non-radiative capture. He claims that it bridges the gap between rigorous but complex

## ***4.2 Non-Radiative Transitions***     **54**

quantum-mechanical theories and rough but experimentally useful semi-classical calculations. The theory takes into account the dynamic response of the lattice after optical excitation.

# CHAPTER FIVE

## PHOTOLUMINESCENCE SPECTRA

### 5.1 Comparison with Theory

Lucovsky, Varga and Schwarz [62] were among the first to make extensive measurements of edge absorption and photoluminescence in Zn-doped GaAs. The two effects could be correlated using the relationship which was derived theoretically by Van-Roosebroeck and Shockley [83] from a consideration of the detailed balance between absorption and recombination at thermal equilibrium,

$$S(h\nu) \propto (h\nu)^2 \alpha(h\nu) \quad \text{for } h\nu \gg kT$$

or,

$$\alpha(h\nu) \propto \frac{S(h\nu)}{(h\nu)^2 e^{-h\nu/kT}} \quad (5.1)$$

Photoluminescence measurements were thus able to be used as complimentary to absorption measurements for photon energies at which absorption was either very strong or very weak. They also correlated the behaviour of absorption and photoluminescence with the level of doping of their samples.

Direct comparison between the theory of Section 4.1 and observations could only be made as the quality of GaAs samples improved significantly to be able to resolve the fine spectral structure.

Weiner and Yu [107] observed the band-band recombination. This decays extremely rapidly. Figure 5.1 shows the lineshape they observed and may be compared with that predicted from 4.22.



This Figure has been removed for Copyright reasons.

Figure 5.1: Band-band recombination. (From [107].)

Eagles [48] was the first to make a direct calculation of the spectral line-shape for conduction to simple acceptor recombination. He assumed that the impurity wave functions were adequately described by the hydrogenic envelope functions and that only the ground state of the impurity is significantly involved in the band-impurity transition. Comparison of the theory 4.18 and the experimental measurements of Williams and Bebb [109] is shown in Figure 5.2. The results are in excellent agreement with experiment for the peak and higher energy portion of the spectral line for temperatures in the range 15-80K. At low temperatures other broadening mechanisms dominate.

Discrete-discrete transitions between donors and acceptors will be treated in-depth in Chapter 7. For now, it is clear from Figure 7.2 that the sharp form of the spectral shape 4.13 can be observed in practice.

This Figure has been removed for Copyright reasons.

Figure 5.2: Band-acceptor recombination: comparison of theory and experiment. (From [110].)

The agreement between theory and experiment for the actual energy of the luminescence transition has already been discussed (Chapter 2) for exciton states, substitutional impurities and deep levels.

## 5.2 Spectral Lines of GaAs

In this section I consider all of the photoluminescent transitions that may be present in the crystal. Of course, a single photoluminescent spectrum taken from a localized area of material will only show the lines characteristic of that particular locality in that particular crystal. However, many measurements over different crystal growth types and doping levels reveals the full structure of photoluminescent lines.

Comprehensive reviews of photoluminescent lines have been provided by Williams and Bebb [110] and in the EMIS Datareview series [47]. The precise

classification of lines in the spectrum can be difficult, especially when comparing spectra from crystals grown in different ways. Thewalt [94] has reviewed various techniques for characterising the photoluminescent lines.

Of the different crystal growth types, ~~SI~~ LEC GaAs is becoming the most technologically important. Its impurity concentration has already been described in Section 2.3 and, in Section 2.4, its semi-insulating property was described as arising from the deep levels.

There are other important growth methods of GaAs crystals:

- liquid phase epitaxy (LPE) layers of GaAs have been important for the identification of impurities and defect levels [35,92];
- vapour phase epitaxy (VPE), which may be sub-divided into hydride and chloride VPE depending on the starting materials (both methods involve the same reactants at the growth surface, though the hydride process offers more flexibility of the As/Ga ratio [47] [35];)
- metalorganic chemical vapour deposition (MOCVD) is a useful technique for producing thin layers and abrupt interfaces; [96,86]
- molecular beam epitaxy (MBE) is a technologically important growth technique, enabling thin films of very high quality to be grown [34].

This Figure has been removed for Copyright reasons.

Figure 5.3: Free exciton transitions for upper and lower polariton branches. (From [90].)

These are the lines that are identified in the photoluminescence spectrum of GaAs:

- **Free Exciton Lines.** Sell et. al. [90] detected the luminescence resulting from free excitons. These excitons interact with photons to form polaritons. Two lines are visible, corresponding to the upper and lower polariton branches. See Figure 5.3, [90].
- **Bound Exciton Lines.** Reasonable agreement is found with theory. Excitons bind to donors or acceptors, but the binding energy is too small to make a chemical identification of the impurity possible [94]. See Figure 5.4.
- **Two-Electron Transitions.** A partial Auger recombination leads to duplication of bound-exciton lines, separated by the electron energy. See Figure 5.5.

This Figure has been removed for Copyright reasons.

Figure 5.4: Exciton transitions. (From [92].)

This Figure has been removed for Copyright reasons.

Figure 5.5: Two-electron partial Auger recombinations. (From [84].)

This Figure has been removed for Copyright reasons.

Figure 5.6: KP lines. (From [80].)

- **KP Lines.** These were a source of controversy when first seen by Kunzel and Ploog [56]. Reynolds et. al. [80] thought that they were observing a discrete donor-acceptor pair structure. However, this interpretation has been discredited. Recent papers [2,23] indicate that they can be split into two groups. One peak is suggested to arise due to an exciton bound to a neutral acceptor complex defect. The set of lines at lower energies is due to exciton recombinations at axially orientated complex defects. Generally, KP lines are not visible in non-MBE samples, although lines in the same spectral region emitted by MOCVD layers may be related. See [11] for a recent study. See Figure 5.6.
- **Free-Bound Recombination.** The peak position of this line may vary by 0.5meV, dependent on the impurity concentration. Figure 5.7 shows typical band-acceptor transitions.

This Figure has been removed for Copyright reasons.

Figure 5.7: Band-acceptor transitions. (From [92].)

- **Donor-Acceptor Complexes.** The donor-acceptor recombination energy is given by 7.1. The peak position of the donor-acceptor pair spectra is given by the most probable pair separation, which is a function of impurity concentration. The recombination band is wide, its actual width also being related to concentration. Thus, the positions of the peaks are not exact and may vary by up to 1meV. Knowledge of the residual impurity concentration allows identification of the peaks.
- **Complex Centres.** The 1.49eV and 1.47eV bands seen in MBE samples were first measured by Briones and Collins [7]. They are attributed to complex centres involving carbon and a vacancy, of the type C-V(Ga) and C-Va(As).
- **Deep Centres.** The broad-band photoluminescence seen by Tajima is shown in Figure 5.8.

This Figure has been removed for Copyright reasons.

Figure 5.8: Deep levels. (Adapted from [97].)

- **Phonon Replicas.** These occur of lines for which it is probable that a phonon transition can take place [110]. The strength of the phonon coupling is greater for increased binding energy of hole or electron. Coupling is most probable with the LO phonon because of the polarization field. The LO phonon energy is 36.5meV and that of the TA phonon, the next likely to couple, is 10meV. In VPE samples replicas of the Mn and Cd deep impurities [110] are seen, see Figure 5.9.

Table 5.1 lists the energy positions of the photoluminescent lines [35,92,96,34,84].



This Figure has been removed for Copyright reasons.

Figure 5.9: Phonon replicas of luminescence lines. (From [110].)

TABLE OF ENERGIES

Energy	Identification	Material
1.5197	Not Observed (Band-Band recombination)	
1.5156	Free Exciton (X), upper polariton branch	MOCVD
1.5153	Free Exciton (X), upper polariton branch	LPE, VPE, MBE
1.5150	Free Exciton (X), lower polariton branch	LPE, VPE, MBE
1.5150   1.5146	Excited states of donor exciton (Do, X)*	LPE, VPE, MBE
1.5149   1.5145	Excited states of donor exciton (Do, X)*	MOCVD
1.5142	(Do, X)	MOCVD
1.5141	(Do, h) or (Do, X)	LPE
1.5141	(Do, X)	VPE, MBE
1.5136	(D+, X) or (Do, h)	MOCVD
1.5133	(D+, X)	LPE
1.5133	(D+, X) or (Do, h)	VPE, MBE
1.5128	(Ao, X) J=1/2	LPE, VPE, MBE
1.5126	(Ao, X)	MOCVD
1.5124	(Ao, X) J=3/2	LPE, VPE, MBE
1.5122	(Ao, X) J=5/2	LPE, VPE, MBE
1.5119	Defect-bound exciton	MOCVD
1.5112	Defect-bound exciton	MOCVD
1.5113   1.5056	Similar to KP lines	MOCVD
1.5110   1.5000	'KP' lines	MBE
1.5108	Two-electron transition (Do, X)	VPE
1.5101   1.5014	Two-electron transition (Do, X)*	VPE
1.5097	Two-electron transition (Do, X) donor n=2	VPE
1.5097	(Do, X) Donor left in n=2 excited state	LPE
1.5089	Two-electron transition (Do, C) donor n=3	VPE
1.4935	(C, e)	MOCVD
1.4932	(C, e)	VPE, VPE

1.4931	(C, e)		LPE
1.4930	(Dn=2, Ac)	ch ref	NOCVD ?
1.4915	(Be, e)		VPE
1.4914	(Hg, e)		LPE
1.4911	(Hg, e)		VPE, NOCVD
1.49	Broad Band		NBE
1.4895	DAP (Do-C, eh)		NOCVD
1.4894	(Zn, e)		VPE
1.4893	(Zn, e)		NOCVD
1.4892	DAP (Do-C, eh) ?notation		VPE, NBE
1.4891	DAP (Do-C, eh) ?notation		LPE
1.4875	DAP (Do-Hg, eh)		LPE
1.4870	DAP (Do-Hg, eh)		NOCVD
1.4854	DAP (Do-Zn)		VPE, NOCVD
1.4852	(Si, e)		NOCVD
1.4851	(Si, e)		LPE
1.4850	(Si, e)		VPE, NBE
1.4848	(Cd, e)		VPE
1.4820	DAP (Do-Si, eh)		NOCVD
1.4816	DAP (Do-Si, eh)		VPE
1.4814	DAP (Do-Si, eh)		LPE
1.4813	DAP (Do-Si, eh)		NBE
1.4785	(Ge, e)		NOCVD
1.4781	(Ge, e)		LPE, VPE(ch?)
1.4746	DAP (Do-Ge, eh)		LPE
1.4745	DAP (Do-Ge, eh)		NOCVD
1.47	Broad Band		NBE
1.4060	(Mn, e)		LPE, VPE
1.3556	(Cu, e)		VPE
1.3550	(Cu, e)		LPE
1.2200	Complex of donor and Ga vacancy		VPE
1.20	Ga vacancy		VPE
0.80	EL2 defect ?		LEC
0.68			LEC
0.65			LEC

Table 5.1: Energies of photoluminescence transitions.

# CHAPTER SIX

## TIME-DECAY OF PHOTOLUMINESCENCE

### 6.1 Evidence for Non-Radiative Processes

Luminescence has been a powerful tool for the study of impurities in GaAs and GaP. Luminescent lifetime studies have shown definitively that non-radiative recombination occurs.

Nelson et. al. [68] studied excitons bound to donors in GaP and Si. They measured the lifetime of the so-called C line in the luminescent spectrum of GaP and found it to be  $21 \pm 4 ns$ . This was about 500 times shorter than the theoretically predicted value of  $11 \mu s$ . They concluded that the decay of the bound exciton had to proceed mainly by a non-radiative process—the Auger effect. From the similarity between the theories of non-radiative recombination and internal conversion in nuclei, they were able to determine a value of 1200 as being the ratio between non-radiative and radiative processes. This figure is in good agreement with the absorption-emission discrepancy of the lifetimes.

### 6.2 Non-Exponential Behaviour

In Chapter 3 we saw that the processes of energy transfer in the crystal can lead to non-exponential decays. This was apparent from the continuity equation—the diffusion and surface recombination terms cause departure from exponential behaviour. In the simple excitation transfer model of Chimzak, the decay did certainly not follow a regular exponential—this was because of the transfer term that actually

caused the luminescence to increase for a short time after excitation had ceased. In the more complicated transfer theories, the presence of a discrete crystal lattice and a distance-dependent transfer interaction term also lead to non-exponential decays.

In Chapter 4 we saw that radiative decay itself does not always give exponential behaviour. It is clear that many different processes can lead to deviations from an ideal exponential decay and thus it is not possible solely on the basis of observation of non-exponential decay to determine which process or processes affected the decay.

Jonscher and de Polignac [49] point out that it has become accepted that the prevailing form of time dependence on response to excitation of duration short in comparison with the time of measurement is a power law of the form

$$L \propto t^{-s} \quad (6.1)$$

with the exponent  $s$  in the range 0.5 to 2. They showed evidence that a wide variety of materials exhibit power-law relaxation of their luminescence, often re-analyzing original data to show a better fit with power-law type behaviour.

Jonscher and de Polignac believed that the predominance of power-law decays amongst many different materials is a result of common general principles and suggested that many-body interactions may provide such principles. For the time-decay that is limited by de-trapping the de-trapping rate depends on the charge state of the trap and, following the release of a carrier, many charges re-distribute. The de-trapping rate is a complicated function resulting from many-body interactions. Jonscher and de Polignac argued that the long-term behaviour is proportional to  $t^{-k-1}$  where  $k$  depends critically on the degree of correlation between centres—strongly correlated centres have  $k \rightarrow 1$ , weakly correlated ones  $k \rightarrow 0$ . It was concluded that for experimentally observed cases of a single power law valid over time

that this corresponds with a single set of traps, while for cases in which two or more power law regions are observed in time, then there are multiple sets of traps.

Sakai et. al. [87] were able to break-up their non-exponential fluorescence decays into a sum of exponential terms. They found that a rising exponent was needed to explain the total decay. This term was found to be due to re-absorption of emitted light.

#### *a) Decay in GaAs*

Dingle [19] was one of the first to measure radiative lifetimes in GaAs and observe the time-resolved spectra. He noticed that the decay of the  $\sim 1.49$  eV band was considerably slower than other emission lines. For lightly doped samples it was slowest while for heavily doped samples it was much faster. Dingle was able to compare experimental results with the predictions of a theory by Thomas, Hopfield, and Augustyniak [100]. The decay at heavy doping seemed more likely due to a sort of free to bound recombination (this is the result of the heavy doping— an acceptor impurity band forms rather than localized impurity levels) while lower doped samples show behaviour that is consistent with discrete donor-acceptor pair recombination. At long times the decay behaves as  $t^{-1.3}$  in the light doped sample and  $t^{-1.8}$  in the heavy doped sample. This compares with the results from theory:  $t^{-1}$  for lightly doped samples and  $t^{-2}$  for heavily doped compensated crystals. The  $t^{-2}$  behaviour is appropriate as it represents the limit where the decay rate is dominated by the rate of hopping rather than by the optical decay rate.

Charbonneau, Thewalt and Steiner [11] used time-resolved photoluminescence measurements as a means of characterizing the discrete line structure that is seen in MBE samples, the so-called KP lines. Their measurements of lifetime allow

certain of the discrete lines to be distinctly grouped or characterized. A set of lines has lifetimes extending to around 100ns and is associated with excitons bound to acceptor pairs of varying separation.

Recent experimentors have been able to refine the techniques of time-resolved spectroscopy. Block, Shah and Gossard [4] (see Figure 6.1) have been able to obtain femtosecond time resolution on their measurements. With such resolution they are able to study the initial relaxation, or thermalization, of carriers in bands. This provides insight into carrier-carrier interactions. The data seen is consistent with a model of rapid thermalization of the electron-hole plasma by carrier-carrier scattering and subsequent cooling of the thermalized distribution of electrons and holes by phonon emission. Such a model would predict an increasing rise time with decreasing photon energy and decay times which can be substantially longer than rise times due to the radiative recombination process being much slower than the thermalization.

Teh's experimental work [98] showed luminescent decays decaying as power laws in time. The exponent of the power law,  $s$ , was found to obey a relationship,

$$s = -1 + \beta T \quad (6.2)$$

where  $\beta$  depends on the concentration of carbon impurities (acceptors substituting at the As lattice site). This power law behaviour was seen at long times, while initially a double exponential decay was observed. The two components of exponential decay are attributed to band-acceptor and donor-acceptor recombinations.

This Figure has been removed for Copyright reasons.

Figure 6.1: Immediate time-decay of luminescence from bands. (From [4].)



# CHAPTER SEVEN

## DONOR-ACCEPTOR PAIR PHOTOLUMINESCENCE

### 7.1 Recombination Spectra

The recombination of an electron trapped on a donor with a hole trapped on an acceptor constitutes an important mechanism of radiative recombination. The resulting recombination energy spectrum consists of a series of sharp lines, each corresponding to a particular electron-hole pair separation, and a broad band at low energies, where individual lines can no longer be resolved. The band cuts off at the energy of a non-interacting donor-acceptor pair.

The first treatments of donor-acceptor pair interaction [76,38] were concerned with associated pairs, that is, pairs occupying nearest neighbour sites. Prener and Williams [76] estimated the energy level structure by considering the electron and hole individually bound in a dipole field created by the other particle. Subsequently, Williams [111] refined the model to account for the overlap of electron and hole wavefunctions. It is found that up to a modest degree of overlap the interaction can be represented by an isotropic van der Waals' polarization interaction term, which arises from the secondary dipole-dipole interaction between the donor-acceptor pair fields.

The principal energy level structure for donor-acceptor pair recombination is then given by,

$$E(h\nu) = E_G - (E_A + E_D) + \frac{e^2}{\epsilon r} - \frac{e^2}{\epsilon r} \left( \frac{b}{r} \right)^5 \quad (7.1)$$

$E_G$  is the energy gap of the crystal,  $E_A$  and  $E_D$  are the acceptor and donor binding energies respectively, and the remaining two terms are the Coulomb and van der

Waals' interaction.  $r$  is the separation between the donor and acceptor.

For some materials, however, further fine structure is visible. For example, in III - V compounds there is a strong accumulation of electrons on the tetrahedral bonds [105]. This leads to a directional dependence in the interaction energy terms and so pairs of identical separation but in different directions recombine at slightly differing energies.

Further effects on the donor-acceptor interaction energy have recently been calculated—Breitenstein [6] calculated the broadening of donor-acceptor pair lines due to the Coulomb potentials of ionized impurities and Inglis and Williams [45] have included the effect of lattice polarization into a calculation of pair energies.

The spatial distribution of donor-acceptor pairs is something that is determined during crystal growth. At the high temperatures of growth, the impurities are ionized. If the donors and acceptors are allowed to migrate together under the influence of Coulomb attraction then associated near-neighbour pairs are formed. Usually, however, the crystal is rapidly cooled from high temperature and the impurities are not significantly influenced by the Coulomb interaction. The spatial distribution of donors and acceptors is then random.

In order to make a calculation of the intensity profile expected for radiative recombination of donor-acceptor pairs, we need to know the statistical distribution of pairs of different radii. Lannoo and Bourgoin [59] show that for associated pairs the distribution of pairs at distance  $r$  is  $e^{e^2/erkT}$ . Dunstan [20] has considered the distributions when the impurities are randomly spread. For a continuous space of donors and acceptors, the probability of forming a donor-acceptor pair of separation  $r$  is proportional to the probability of a donor existing in a volume element at a distance  $r$  from an acceptor multiplied by the probability that no other donor exists

nearer to the acceptor than distance  $r$ ,

$$P(r) = 4\pi r^2 \rho \, dR \int_r^\infty P(u) du \quad (7.2)$$

which is easily solved to give,

$$P_{NN}(r) = 4\pi r^2 \rho e^{-\frac{4\pi}{3}r^3 \rho} \quad (7.3)$$

This is the distribution of nearest neighbour pairs, it is a type of Poisson distribution. This distribution cannot be used to characterize donor-acceptor pairs, however, since it is a distribution of nearest-neighbours and not nearest-available-neighbours. The distinction is important since in a random population exactly one half of the carriers are not the nearest-neighbour of their own nearest-neighbour [20]. Also, there is a certain probability that another acceptor may exist nearer to the acceptor than the donor does. Taking account of these considerations, Dunstan [21] derives

$$P_{NAN}(r) = \frac{4\pi r^2 \rho}{(1 + \frac{4}{3}\pi r^3 \rho)^2} \quad (7.4)$$

as the distribution of “nearest available neighbours” in exactly compensated samples.

In order to translate this continuous distribution into the discrete distribution that is expected to arise in the solid, we need to consider some details of the crystal lattice. Prener [77] wrote down the equation for associated ion pairs distributed on a lattice as

$$\alpha_i = A z_i \exp\left(\frac{e^2}{D r_i k T}\right) \left[1 - \sum_{j=1}^{i-1} \alpha_j \frac{\exp(-e^2 / \rho r_j k T) N}{n \sum_j z_j}\right] \quad (7.5)$$

where  $\alpha_i$  is the fraction of ion pairs with separation  $r_i$  and  $z_i$  is the number of equivalent sites available to a positively charged impurity at a distance  $r_i$  from a

negative impurity. Equation 7.5 was written in direct analogy to the Reiss' distribution function for ion pairs under Coulomb interaction [79],

$$G(r) = A4\pi r^2 \exp\left(\frac{e^2}{DrkT}\right) \left[1 - \int^r G(x) \exp\left(\frac{-e^2}{DxkT}\right) \frac{dx}{A}\right] \frac{N}{V} \quad (7.6)$$

Onton and Lorenz [71] expressed the result 7.5 in the form

$$G(r_i) = Az_i C \exp\left(\frac{e^2}{\epsilon r_i kT}\right) \sum_{j=1}^i i - 1(1 - z_j c) \quad (7.7)$$

where  $z_i$  is the number of equivalent sites available to an impurity at a distance  $r_i$  from its pair partner. To perform any calculations with 7.5 or 7.7 it is necessary to calculate the  $z_i$ 's associated with the  $r_i$ 's. The pair separation distance is a property of the crystal. For a simple cubic lattice the separation can be expressed as

$$r_m = \sqrt{m}a_0 \quad (7.8)$$

where  $m$  is an integer, the shell index number, and  $a_0$  is the lattice constant. The degeneracy of each shell may easily be calculated.

For the common Zincblende crystal structure, two types of donor-acceptor pair spectra can be distinguished—Type I and Type II—depending on whether the donors and acceptors occupy the same or opposite face-centered-cubic sublattices respectively. Each pair spectrum can be identified from equation 7.7 once the number of available sites at a particular separation,  $z_i$ , is known. Dean [17] has tabulated the radii and occupation numbers for Type I and Type II donor-acceptor pair spectra on the zincblende lattice. A complete account for other crystal types has been given by Wiley and Siman [108].

The intensity of the pair lines of particular separation is proportional to the fraction that are ionized. Additional considerations than the calculated distributions, however, need to be taken because under experimental conditions not all

close pairs capture electrons and holes. It is often only the distant pairs that become completely ionized due to their longer recombination times. Capture cross-section variations with pair separation, therefore, also play a role in determining the final intensity profile.

## 7.2 Decay Characteristics

Thomas, Hopfield and Augustyniak [100] formulated a theory for the decay kinetics of donor-acceptor pair recombination. Assuming that the decay proceeds as isolated pairs recombine, they determined the decay rate as a function of pair separation. To do this they first derived a matrix element for the optical transition between the state of the crystal with the electron and hole present and the state with them absent.

In GaAs the binding energy of acceptors is about  $30\text{meV}$  while that of donors is about  $6\text{meV}$ . Because of this tight binding of the acceptor, the acceptor wavefunction is rigid and the hole sees no perturbation due to the neutral donor except in a small volume of space relative to the extent of the hole wavefunction. A product wavefunction can then be used and the matrix element is,

$$M(r) = \int \Psi_h^*(r_h)[P(\Psi_e(r_e))]\delta(r_e - r_u) d^3r_e \quad (7.9)$$

$\Psi_h$  is the hole wavefunction and  $\Psi_e$  is the electron wavefunction.  $P$  represents the interaction term. Under a further approximation that the hole wavefunction in the absence of the donor does not vary appreciably over the region of the donor and that the central bracket is only large in the small volume occupied by the donor wavefunction we write,

$$M(r) = \text{const.} \times \Psi_h^*(r) \quad (7.10)$$

For large  $r$  the hole wavefunction is expressible as a hydrogenic acceptor wavefunction,

$$\Psi_h(r) \propto e^{-(r/a)} \quad (7.11)$$

where  $a$  is the Bohr radius of the acceptor. Then the transition rate

$$W_{ij}(r) \propto |M(r)|^2 \quad (7.12)$$

becomes

$$W(r) = W_{max} e^{-(r/2a)} \quad (7.13)$$

Thus the transition rate is an intimate function of separation. This is why a crystal which contains a distribution of pairs is not characterized by a single decay time. The long and variable lifetimes of the distant pairs account for the long and non-exponential decay curves of the photoluminescence after excitation.

Having derived a transition rate, Thomas et. al. [100] attempted to calculate the decay of excitation between donors and acceptors when the donor and acceptor concentrations are equal (the case for a compensated crystal).

The equations they derived could only be solved numerically under a so-called Hartree approximation which neglects correlations in the occupations of lattice sites. Their solution predicts a  $t^{-2}$  time dependence for heavily doped, compensated samples at long times and a  $t^{-1}$  dependence for lightly doped samples. However, the nature of the approximation makes the long time and low concentration predictions particularly dubious.

Compensation introduces the possibility of a new physical effect— the hopping of electrons and/or holes from one impurity to another when the sample has partially decayed. Provided that sites are within  $kT$  of energy of each other then for long times, Thomas et. al. [100] claim that when hopping is rapid in comparison to optical processes, the consequent averaging out of the electron concentration in

the crystal ensures the correctness of the  $t^{-2}$  approximate solution. This decay is characteristic of bimolecular recombination and is a high temperature limit due to the energy requirement.

Dunstan [20,21] took a different approach to the recombination decay of donor-acceptor pairs. He showed that to a very good approximation the recombination may be treated analytically as the decay of independent centres. These independent centres are the donor-acceptor pairs and the distribution 7.4 for  $P_{NAN}$  is used to describe the decay.

The total ensemble decays as

$$n = \int_{r=0}^{\infty} P_{NAN}(r) e^{-t/\tau(r)} dr \quad (7.14)$$

where the recombination time is obtained from 7.13,

$$\tau = \tau_0 e^{r/2a} \quad (7.15)$$

and the possibility that recombination may occur with other than mutually nearest neighbours has been neglected. The resultant luminescent intensity is then

$$I(t) = \int_{r=0}^{\infty} P_{NAN}(r) r^{-1} e^{-t/\tau(r)} dr \quad (7.16)$$

Eggert [24,25] has performed Monte Carlo calculations of the donor-acceptor distributions and recombination kinetics. His work improved upon the pair distribution used by Dunstan but at the expense of a computationally intensive technique. At low excitation densities, the photoluminescent decay curves of Dunstan and Eggert are practically identical [22] (see Figure 7.1) while at higher carrier densities the theoretical predictions differ only at very long times [26].

This Figure has been removed for Copyright reasons.

Figure 7.1: Dispersion of the Dunstan and Eggert solutions; a) Dunstan b) Eggert and c) the decay of a near-neighbour distribution ( $P_{NN}$ ). (From [22].)



Paasch [73] used a distribution of pairs on discrete sites in his calculation of time decay. This lead to the effect of suppressing high powers of time in comparison with the continuous distribution.

When the donor and acceptor populations are unequal the luminescent time decay is much easier to determine than in the compensated case. The exact solution is more given by [100]

$$I(t) = 4\pi\rho \int_{r=0}^{\infty} r^2 \tau^{-1}(r) e^{-t/\tau(r)} dr \times \exp[4\pi\rho \int_{r=0}^{\infty} (e^{-t/\tau(r)} - 1) r^2 dr] \quad (7.17)$$

Onsager and Stewart [70] have shown that this expression reduces, at long times, to

$$I(t) \propto \frac{\log_e t}{t} e^{-(\log_e t)^3} \quad (7.18)$$

This expression becomes accurate as soon as the closest pairs have decayed completely. For shorter times a power series may be used to calculate the initial decay, but Onsager and Stewart point out that preferential pairing effects need to be considered and thus theories for capture cross-section as well as tunnelling and emission probabilities are needed.

Capture cross-section effects do play an important role in the excitation and recombination processes. When a pair decays, the donor and acceptor are left ionized. The capture cross-section for this ionized donor-acceptor pair is a strong function of separation. For large separations the capture cross-section is that of an isolated ionized acceptor (or donor) and is very large. For small separations the pair appears neutral and has a much smaller cross-section. Therefore, the donor-acceptor emission is more efficient at low excitations, when a large proportion of incident energy can be absorbed.

Golka [27,28] considered the effects on the recombination rate if it is no longer assumed that donor-acceptor pairs are isolated. He considered the interaction of

pairs with additional donor ions. In a material such as n-type GaAs where the wavefunction of shallow hydrogenic donors has an extremely large spatial extent, he found that the recombination time depends very sensitively on the presence of an additional donor ion. Even if an additional donor ion is separated by as much as  $10a_d$  from the donor of a donor-acceptor pair, its presence can increase the transition rate by one or two orders of magnitude.

A specific theory of the hopping effect of electrons and holes was formulated by Kostadinov [51]. He considered that diffusion is the slowest process in the distant electron-hole pair recombination and thus it determines the tail of the luminescence decay. He used a hopping transport theory which was based on "percolation" methods of statistical mechanics. His considerations of pair recombination predicted a power law decay of the luminescence with the exponent of the power showing a weak temperature dependence.

$$\alpha = 1 + \left(\frac{3}{4}\right)^{\frac{4}{3}} \left[1 - \frac{3T^{3/2}}{2}\right] \quad (7.19)$$

$$\alpha(0) = 1.316$$

Comparison of this result with that of published work by Dean [18] lead Kostadinov to conclude that a variable activation energy is present in the hopping process.

### 7.3 Observations

Agreement between the theoretical predictions of equation 7.1 and experimental findings was striking. Observations were made [29,103] of amazingly complicated spectra with at least 100 sharp lines near the band gap energy in the fluorescence spectra of GaP. Hopfield, Thomas and Gershenson [39,99] published papers reporting the comparison of their experimental luminescent lines with the simple theory.

This Figure has been removed for Copyright reasons.

Figure 7.2: Photoluminescence spectrum of GaP. (From [17].)

They distinguished Type I and Type II spectra and noticed a splitting of many experimental lines. They proved the existence of the donor-acceptor pair recombination mechanism beyond doubt. Figure 7.2 shows the spectrum of Dean et. al. [17] on GaP lightly doped with P-site donor S and Ga-site acceptor Mg. Figure 7.3 shows the fit of the observed energy to that predicted from theory. Chemical identification of impurities is possible with a knowledge of the activation energies of donors and acceptors.

The decay kinetics of green pair luminescence in GaP were studied by Thomas et. al. [99]. They discovered a non-exponential power law form of the decay.

Certainly, the early energy expended into the analysis of pair spectra in GaP proved to be worthwhile with the subsequent recognition of properties characteristic of pair recombination in other crystals. It is now clear that donor-acceptor pair recombination is a prominent general feature of the low temperature luminescence

This Figure has been removed for Copyright reasons.

Figure 7.3: Energy vs. separation relationship for donor-acceptor pair recombination. (From [17].)

of dilutely doped, compensated semiconductors [17].

GaAs is a direct gap semiconductor. For hydrogenic donors and acceptors, we find that  $E(r \rightarrow \infty)$  of equation 7.1 is  $39\text{meV}$ . Using,

$$E(h\nu) = E_G - (E_A + E_D) + \frac{e^2}{\epsilon r}$$

it is clear that the energy transitions for  $r < 350\text{\AA}$  will not be visible because the transition energy is greater than the band gap energy. Those lines that are visible merge into a continuum due to the finite width of each line and the close energy spacing at further separations.

In photoluminescence studies of GaAs, the broad band at  $\sim 1.49\text{ eV}$  was first suggested to be associated with donor-acceptor pair recombination by Lucovsky et. al. [62] and thorough subsequent investigation by Leite and DiGiovanni confirmed this [61]. They observed characteristics of the  $\sim 1.49\text{ eV}$  line which they considered to be evidence for donor-acceptor emission: a shift of line to higher energies as excitation intensity increases; a narrowing of the band as intensity increases; a shift of the band towards higher energies as doping increases; and a dramatic decrease in intensity of luminescence as the temperature is increased from  $25\text{K}$  to  $35\text{K}$ . The first two observations arise from the effect of saturation of distant pairs; the shift with increasing doping is due to a reduced average donor-acceptor separation; the intensity drops off with temperature because of competitive non-radiative processes but the temperature dependence indicates other mechanisms influencing the spectrum—exciton recombinations, band-acceptor transitions, transitions involving excited states of impurities and phonon replica transitions.

Compelling evidence for donor-acceptor pair bands in GaAs came from measurements of the radiative lifetime by Dingle [19]. He was able to measure power law time decays for differently doped crystals. His research indicated a decay  $t^{-2}$

for heavily doped crystals and  $t^{-1}$  for lightly doped ones. The  $t^{-2}$  behaviour seems to agree with the limit of the Hartree approximation of theory [100].

The band at  $\sim 1.49$  eV, as well as shifting its peak with temperature, also shows the emergence of a second band. Shah et. al. [91] thought that this was an effect of donor-acceptor recombination but involving the excited state of the donor. Subsequent evidence proved this hypothesis to be false— the high energy band exhibited a large linear magnetic shift rate which is indicative of a free to bound transition [85].

More recently, however, Skromme and Stillman [93] identified a small third peak between the donor-acceptor and band-acceptor transitions. They considered this as an excited state donor-acceptor transition. They found excellent agreement with theory for its lineshape.

Paget [72] has recently shown evidence of donor-acceptor pair bands overlapping one another. He argues that this arises from a continuous distribution of traps.

## **Part II**

### **De-Trapping Model of Luminescence Decay**

# CHAPTER EIGHT

## ENERGY DE-TRAPPING

### 8.1 Semiconductor Thermodynamics

This is a study of one physical process in the semiconductor. The process, energy de-trapping, is important in determining the long-time behaviour of luminescence. De-trapping occurs on a relatively long timescale, much longer than for the physical processes of thermalization or radiative recombination. Usually, on a timescale long enough that the rest of the crystal can be considered to have reached thermal equilibrium following the initial photo-excitation.

The study of thermodynamics involves the study of heat energy. Thermodynamics provides remarkable insight into the properties of the thermal equilibrium state of a system once something is known about the constraints on the system. Using mathematical relations derived from thermodynamics it is possible to describe the equilibrium distribution of energy-carrying particles among the energy states of a system and to determine the equilibrium, “detailed balance”, rate of a reaction.

In order to study the de-trapping of energy in the semiconductor crystal we need to understand several things:

- a) the various particle reactions that take the system to thermal equilibrium
- b) the equilibrium distribution of energy-carrying particles among the energy states of the system after thermalization and radiative recombination.
- c) the rate of thermal de-trapping of energy from the traps.

Thermodynamics can help us with these problems. We consider the semiconductor as an isolated system made up of four subsystems. These four subsystems represent



the four independent types of particle— electrons, holes, phonons and photons. They are enclosed in a cavity with perfectly reflecting walls.

*a) Particle Reactions and Equilibrium Conditions*

Among the four independent types of particle, four reactions occur to bring the semiconductor system to thermal equilibrium [121]. They are:

$$e + h \rightleftharpoons \gamma \quad (8.1)$$

$$e + h \rightleftharpoons \nu \Gamma \quad (8.2)$$

$$e + \nu \Gamma \rightleftharpoons e \quad (8.3)$$

$$h + \nu \Gamma \rightleftharpoons h \quad (8.4)$$

$e$  is an electron,  $h$  a hole,  $\gamma$  a photon and  $\Gamma$  a phonon.  $\nu$  is the number of phonons created.

8.1 represents radiative recombination of an  $e - h$  pair

8.2 represents non-radiative recombination of an  $e - h$  pair, either Auger or phonon-cascade process

8.3 represents energy exchange between an electron and  $\nu$  phonons

8.4 represents energy exchange between a hole and  $\nu$  phonons

The reactions are illustrated in Figure 8.1 for a simple two-band model system. Several other reactions have been ignored. Firstly, phonon-photon interaction is neglected because of their unequal momenta. Secondly, there is no process which transforms an electron into a hole. The numbers of electrons and holes is determined by the position of the Fermi level in equilibrium. Off-equilibrium, these number are supplemented equally by electrons or holes according to the number of photons absorbed. Thirdly, electron-photon and hole-photon reactions are ignored— photons

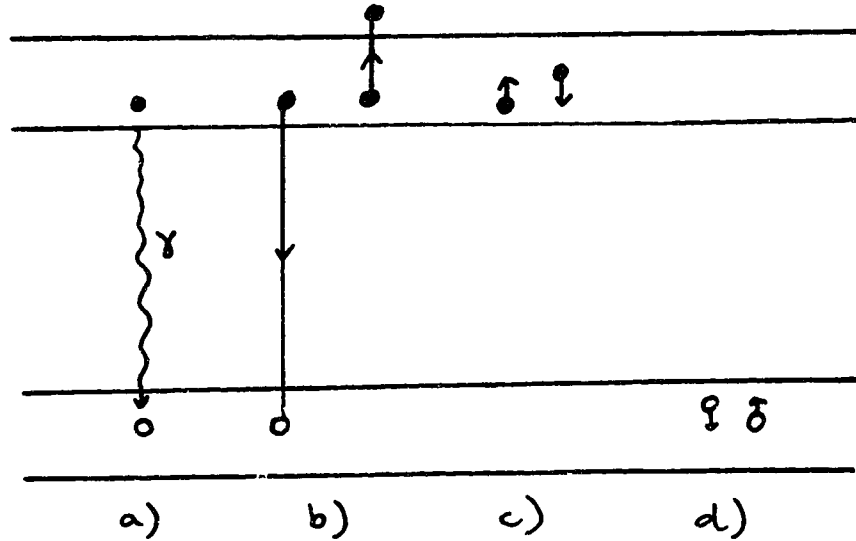


Figure 8.1: The particle reactions in a semiconductor; a) radiative recombination of an electron-hole pair b) non-radiative recombination of an electron-hole pair c) energy exchange between an electron and  $\nu$  phonons d) energy exchange between a hole and  $\nu$  phonons.

are most likely to create  $e-h$  pairs with radiation of energy greater than the band gap.

We assume that the phonon system acts as a heat bath to the electrons and holes: phonons may be freely given to or taken from the heat bath without affecting its temperature.

According to thermodynamics, a change of the energy  $E$  of a system is related to a change of its extensive variables by

$$dE = TdS - pdV + \sum_i \mu_i dN_i \quad (8.5)$$

The extensive variables are the entropy  $S$ , the volume  $V$  and the number of particles

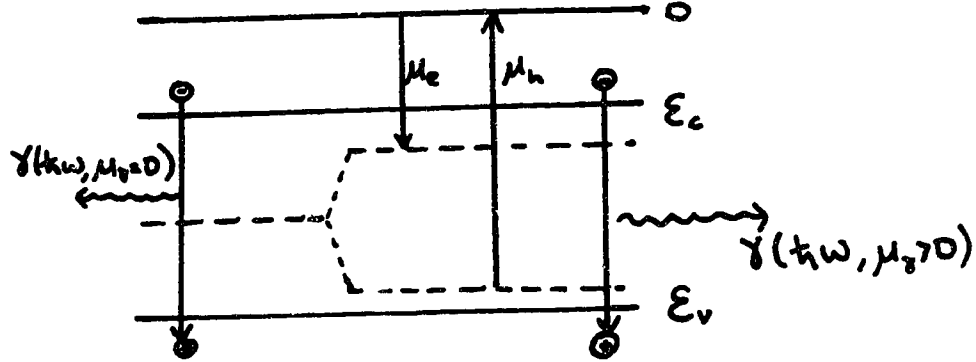


Figure 8.2: Energy diagram of electron-hole system: right-side shows the off-equilibrium state—electrons and holes are associated with separate quasi-Fermi levels and the left-side is at equilibrium—there is a common Fermi level.

$N_i$  of kind  $i$ . The intensive variables are the temperature  $T$ , the pressure  $P$ , and the chemical potentials  $\mu_i$ , see Figure 8.2.

For the particle reactions the extensive variables  $S$  and  $V$  are held constant. In equilibrium energy is a minimum. Therefore,

$$dE = \sum_i \mu_i dN_i = 0 \quad (8.6)$$

where the sum over  $i$  is a sum over the electrons, holes, phonons and photons.

Now consider the conditions imposed by equilibrium for the different reactions. For 8.1

$$dN_e = dN_h = -dN_\gamma \quad (8.7)$$

and thus from 8.6 equilibrium is achieved when

$$\mu_e + \mu_h = \mu_\gamma \quad (8.8)$$

For 8.2

$$dN_e = dN_h = -\nu.dN_\Gamma \quad (8.9)$$

and thus from 8.6 equilibrium is achieved when

$$\mu_e + \mu_h = \nu.\mu_\Gamma \quad (8.10)$$

For 8.3

$$dN_e = 0, dN_\Gamma = \pm 1 \quad (8.11)$$

and from 8.6, equilibrium is achieved when

$$\mu_\Gamma = 0 \quad (8.12)$$

Reaction 8.4 gives the same condition as 8.12.

In full thermal equilibrium, of course, all three conditions must be satisfied.

Therefore,

$$\mu_\Gamma = 0 \quad (8.13)$$

$$\mu_e = -\mu_h \quad (8.14)$$

$$\mu_\gamma = 0 \quad (8.15)$$

the chemical potentials coincide (see Figure 8.2) and the chemical potential of the photons is zero.

Full thermal equilibrium is not the only equilibrium between the particles in the semiconductor. Each of the reactions 8.1-8.4 can reach equilibrium without a full thermal equilibrium of the system. This has important consequences for the semi-conductor.

- Reactions 8.3 and 8.4 represent the interaction of the electronic particles with the heat bath of phonons; the reactions act to bring the electrons and holes

into equilibrium with it. This equilibrium is established very quickly. Suppose that a characteristic time  $\tau_{th}$  can be used to describe the process. Then the temperature of electrons and holes is the same as the phonon temperature,  $T$ , and we may use the Fermi-Dirac distribution of fermions to describe the electrons and holes [113]. This equilibrium-creating reaction between electrons or holes and phonons is known as “thermalization”.

The thermalization process, however, applies to the equilibrium of 8.1 only as far as  $\nu = 1$ , that is, it occurs through the exchange of single phonons. It must therefore be separated from the more general reaction for  $\nu \neq 1$ . The latter process is the important one for de-trapping electrons or holes. Use a characteristic time  $\tau_{tr}$  to describe the de-trapping rate.

- Equilibrium between photons and electron-hole pairs (reaction 8.1) is established on a timescale much longer than that for thermalization. Use a characteristic time  $\tau_\gamma$ .
- Equilibrium between phonons and electron-hole pairs (reaction 8.2) is of little importance to the semiconductor equilibrium. The condition  $\mu_e = -\mu_h$ , from 8.2, is usually quickly reached anyway as the electron-hole pairs recombine after photo-excitation and the photon density returns to its black body spectrum ( $\mu_\gamma = 0$ ). During the time when this equilibrium does not exist the luminescence spectrum is associated with a boson distribution for  $\mu_\gamma \neq 0$ .

We can use the individual reaction times  $\tau_{th}$ ,  $\tau_{tr}$  and  $\tau_\gamma$  to describe the return of the whole system to thermal equilibrium. This will be done in the next section and used to set up dynamical equations for the semiconductor.

*b) Fermi-Dirac Distribution*

Electrons, and their counterpart holes, are fermions. According to quantum statistics, no two fermions may exist with the same quantum numbers. This means that a fermion state has occupation either 0 or 1 and energy either 0 or  $\epsilon$ .

The equilibrium energy distribution of a system of weakly interacting fermions in equilibrium with a reservoir can be derived from the Gibbs distribution [119], it is

$$f_j = \frac{1}{e^{-(\epsilon_j - \mu)/kT} + 1} \quad (8.16)$$

This is the Fermi-Dirac distribution. It describes the occupation probability of any electron state in equilibrium.

*c) Arrhenius Relation*

The Arrhenius relation is the basic relation that we use to describe the rate of thermal de-trapping. Thermal de-trapping constitutes a non-radiative transition process which acts to restore a non-equilibrium population of carriers from the traps. The rate cannot be derived from thermodynamics but it can be given considerable justification.

The problem of determining the rate of thermal de-trapping is analogous to the problem in physical chemistry of determining a general theory of reaction rates. Thermodynamics and statistical mechanics alone cannot provide a solution, and so additional assumptions need to be introduced.

Eyring's theory of absolute reaction rates [115] took an approach based on the law of mass action. This law is very simply derived from thermodynamics, from

the equilibrium condition for a system of uncondensed particles. It states,

$$\frac{\prod N_r^{R_r}}{\prod N_p^{P_p}} = K(T, V) \quad (8.17)$$

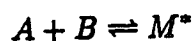
where  $N_r$  and  $N_p$  are the equilibrium populations of reactants and products respectively.  $R_r$  is the reagent number and is the number of molecules of the  $r$ 'th species disappearing; similarly,  $P_p$  is the product number. The products are taken over the different reagent and product species.

$K$  is the equilibrium constant and is defined in terms of the molecular partition functions,  $f$ , derived from the Gibbs distribution.

$$K = \frac{\prod f_r}{\prod f_p} \quad (8.18)$$

The additional assumption introduced by Eyring is that the reactants are always in equilibrium with activated complexes, see Figure 8.3.

For a simple reaction the equilibrium is written



and the equilibrium constant from the law of mass action is

$$K = \frac{N_A N_B}{N_{M^*}} \quad (8.19)$$

Therefore the number of activated complexes is

$$N_{M^*} = \frac{N_A N_B}{K} \quad (8.20)$$

Now we need to find the rate of the reaction



For the thermal activation that we are considering, the activated complex may be thought of as having one special vibration with respect to which it is unstable. This

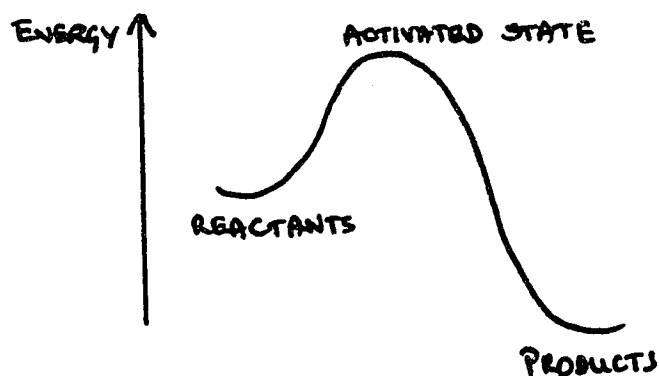


Figure 8.3: Energy diagram for reaction.

vibration leads to disassociation of the complex into products. If the frequency of this vibration is  $\nu$ , then the rate at which products are formed is

$$\text{rate} = \nu N_M.$$

then using 8.19 this becomes

$$\text{rate} = \frac{\nu N_A N_B}{K} \quad (8.21)$$

However, the elementary reaction,  $A + B \rightarrow \text{Products}$  has the rate,

$$\text{rate} = k N_A N_B \quad (8.22)$$

Thus, comparing 8.21 and 8.22 we find the rate constant  $k$  to be

$$k = \frac{\nu}{K} \quad (8.23)$$

This is correct for any elementary reaction.

The values of  $\nu$  and  $K$  can be calculated from writing the equilibrium constant in terms of the partition functions 8.18,

$$K = \left( \frac{f_A' f_B'}{f_{M^*}'} \right) \quad (8.24)$$



Castellin [115] derives

$$\frac{1}{K} = \frac{kT}{h\nu} \left( \frac{f_{M^*}}{f_A f_B} \right) e^{-(\Delta E/kT)} \quad (8.25)$$

by factoring out of  $f_{M^*}$  the vibrational partition function.  $\Delta E$  is the difference in zero point energies between the activated complex and the reactants. Hence,

$$k = \frac{kT}{h\nu} \left( \frac{f_{M^*}}{f_A f_B} \right) e^{-(\Delta E/kT)} \quad (8.26)$$

This is the Eyring equation for the rate constant of a reaction.

This derivation of the reaction rate, based as it is on the assumptions and conditions of the theory of absolute reaction rates provides justification for the form of the Arrhenius relation commonly observed experimentally for chemical reactions,

$$k = A e^{-(\Delta E/kT)} \quad (8.27)$$

or for the lifetime,

$$\tau = \tau_0 e^{(\Delta E/kT)} \quad (8.28)$$

## 8.2 Dynamical Equations

Immediately following photo-excitation a non-equilibrium distribution of electrons and holes is set up in the bands. Subsequently, the carriers thermalize in their respective bands and radiatively recombine. Some carriers jump to impurity levels, trapping levels or deep levels but the majority recombine radiatively.

In the previous section we identified three characteristic recombination times:  $\tau_r$  the radiative recombination time,  $\tau_{th}$  the thermalization time, and  $\tau_{tr}$  the de-

trapping time.  $\tau_{tr}$  is only relevant to certain trap energy levels. The three characteristic times are very different from one another—thermalization is a very fast process while de-trapping is a very slow process. Therefore, consider the dynamics of the three processes separately.

*a) Thermalization*

Consider the effect of the  $\tau_{th}$  process on the electron and hole populations of each energy level. Assume that  $\tau_{th}$  is independent of phonon or photon energies.

Thermalization occurs so as to establish equilibrium between the carriers and phonons. The rate of change of an electron level due to a non-equilibrium distribution of carriers is

$$\left[ \frac{dn_c}{dt} \right]_{th} = -\frac{(n_c - n_{cth})}{\tau_{th}} \quad (8.29)$$

$n_{cth}$  is the thermalized distribution and is given by  $n_{cth} = g_c f_c$  where  $g_c$  is the density of states and  $f_c$  is the occupancy, the Fermi-Dirac function, determined by  $\mu$ , the “quasi-Fermi” level for the number of electrons present.

The solution of this equation is

$$n_c = n_{cs} e^{-t/\tau_{th}} + n_{cth} (1 - e^{-t/\tau_{th}}) \quad (8.30)$$

where  $n_{cs}$  is the electron population immediately after excitation.

Holes also thermalize in the valence band. The hole population of a valence level  $p_v$  will obey

$$p_v = p_{vs} e^{-t/\tau_{th}} + p_{vth} (1 - e^{-t/\tau_{th}}) \quad (8.31)$$

For a whole band consider the total population

$$N_c = \sum_c n_c \quad (8.32)$$

and

$$P_v = \sum_v p_v \quad (8.33)$$

### b) Radiative Recombination

Radiative recombination requires the presence of an electron and a hole. Assume that  $\tau_\gamma$  is independent of energy. The recombination rate is given by

$$\left[ \frac{dn_c}{dt} \right]_\gamma = - \frac{(n_c p - n_{c0} p_0)}{\tau_\gamma} \quad (8.34)$$

$p$  is the total number of holes,  $n_{c0}$  and  $p_0$  are the thermal equilibrium populations.

In the case that  $p \sim p_0$ , then this may be solved.

$$n_c = n_{c0} e^{-t/\tau_\gamma} + n_{c0} (1 - e^{-t/\tau_\gamma}) \quad (8.35)$$

This case applies only when photo-excitation creates relatively few carriers compared to the thermal equilibrium population of holes.

Again, for the whole band consider

$$N_c = \sum_c n_c \quad (8.36)$$

### c) De-Trapping

Energy becomes trapped in certain levels following photo-excitation of carriers into the bands and the subsequent decay from the bands. Trapped energy constitutes a departure from thermal equilibrium. The rate of decay of an electron trap level is equal to the recombination rate  $\frac{1}{\tau_{tr}}$  multiplied by the above equilibrium population of electrons in the trap and the equilibrium number of available states of the upper

level,  $(N'_c - n_{c0})$ .

$$\frac{dn_t}{dt} = -(N'_c - n_{c0}) \frac{(n_t - n_{t0})}{\tau_{tr}} \quad (8.37)$$

where  $\tau_{tr} = \tau_0 e^{\frac{\Delta E}{kT}}$  and  $N'_c$  is the total number of states in the conduction energy band. The solution is

$$n_t = n_{t,s} e^{-t(N'_c - n_{c0})/\tau_{tr}} + n_{t,e} (1 - e^{-t(N'_c - n_{c0})/\tau_{tr}}) \quad (8.38)$$

Similarly for a hole trap,

$$p_t = p_{t,s} e^{-t(P'_v - p_{v0})/\tau_{tr}} + p_{t,e} (1 - e^{-t(P'_v - p_{v0})/\tau_{tr}}) \quad (8.39)$$

Assume that  $n_{t,e} \ll n_{t,s}$  and  $p_{t,e} \ll p_{t,s}$ , that is that the equilibrium occupation of the trap is very small compared to the initial excitation. This is reasonable since the traps are localized energy levels of the crystal and near the surface, where absorption takes place, almost all of the traps will become occupied. We therefore neglect the second term of 8.38 and 8.39.

For a distribution of trap levels de-trapping into a single level, we take a sum over states

$$N_t = \sum_i n_{t,s} e^{-t/\tau_{tr}} \quad (8.40)$$

and

$$P_t = \sum_i p_{t,s} e^{-t/\tau_{tr}} \quad (8.41)$$

The equilibrium occupation of the upper level  $(N'_c - n_{c0})$  or  $(P'_v - p_{v0})$  has been incorporated into the constant of  $\tau_{tr}$ .

The total above-equilibrium electron population in conduction band and traps is given by

$$N = N_c + N_t \quad (8.42)$$

Now,  $\tau_{tr} \gg \tau_r \gg \tau_{th}$  the decay of the traps dominates the long time behaviour of the crystal.

$$\begin{aligned} N &= N_c + N_t \\ &= N_t \text{ as } t \rightarrow \infty \end{aligned} \quad (8.43)$$

After de-trapping of excitation, radiative recombination is most likely to occur. Thus the luminescence is limited by the de-trapping process

$$L(t) = -\frac{dN_t}{dt} \quad (8.44)$$

$$= -\frac{d}{dt} \left( \sum_i n_{ts} e^{-t/\tau_{tr}} \right) \quad (8.45)$$

$$= \sum_i \frac{n_{ts}}{\tau_{tr}} e^{-t/\tau_{tr}} \quad (8.46)$$

In deriving 8.46 the assumption of first order kinetic processes allowed a sum of exponential functions to be used to represent the decay between energy levels. The assumption is valid on the grounds that the occupation of the upper level is sufficiently close to equilibrium that it does not affect the kinetics. De-trapping occurs on a timescale much longer than radiative recombination which brings the system to equilibrium. Further, once a carrier is released from a trap it recombines very quickly to give luminescence. Thus the occupation of the upper level or levels is fairly constant following the fast initial processes.

# CHAPTER NINE

## COMPUTER SIMULATION AND RESULTS

### 9.1 Background

The form of the luminescence decay 8.46

$$L(t) = \sum_E \frac{n_s(E)}{\tau(E)} e^{-t/\tau(E)}$$

is exactly the same as was considered for the decay of phosphorescence in crystals [78,118,116,13].

Randall and Wilkins [78] were the first to give a theoretical account of the phenomena of phosphorescence. They studied isothermal decay behaviour assuming continuous trap distributions. They used uniform and exponential distributions of trap density and assumed the simple form for the activation kinetics which leads to exponential decays. For a uniform distribution of traps extending from 0 to  $\infty$  they showed that the time dependence of phosphorescence behaved as

$$L(t) \propto t^{-1} \quad (9.1)$$

When the trap distribution was exponential,

$$n_s(E_T) = A e^{-\alpha E_T} \quad (9.2)$$

they showed that a time decay

$$L(t) \propto t^{-(\alpha kT+1)} \quad (9.3)$$

was obeyed.

Medlin [118] investigated the phosphorescence behaviour associated with trap dis-

tributions obeying a Gaussian form,

$$n_s(E_T) = Ae^{-\alpha(E_T-E_0)^2} \quad (9.4)$$

He showed that the decay behaved as

$$L(t) = (1 + bt)^{-m} \quad (9.5)$$

where  $b$  and  $m$  are constants. Medlin was not able to furnish a relation between the exponent  $m$  and the parameters in 9.4.

Hornyak and Chen [116] investigated numerically the phosphorescence from continuous distributions of traps with uniform and Gaussian distributions. They showed that broad distributions quite generally result in  $t^{-1}$  phosphorescence behaviour, while narrow distributions result in exponential decay. They found that for both Gaussian and truncated uniform distribution of trap energies the critical parameter controlling the change from exponential to inverse time dependence is the quantity  $y = kT\sqrt{\alpha}$  for the Gaussian case and  $y = kT/\Delta E$  for the truncated uniform case, where  $\Delta E$  is the width of the distribution. The power law  $t^{-1}$  behaviour was seen for values of the parameter satisfying  $y \leq \sim 0.15$

## 9.2 Simulation

I investigated the luminescence decay form 8.46 with various discrete trap distributions. I considered the dependence of the final decay forms on the parameters of  $n_s(E)$  such as the width of the distribution and the number of trapping states.

I made computations on an IBM-PC compatible machine having written the routines in BASIC using double precision numbers (15 decimal places). Appendix B

lists the computer program I wrote to generate the luminescence data from Equation 8.46. A file needs to be specified for  $n_s(E)$ . Data for luminescence response was obtained by summing individual exponential decays over the distribution specified by  $n_s(E)$ . The luminescence response,  $L(t)$ , could then be analyzed by re-plotting the data in any of the following forms,

$$\begin{aligned}
 &L(t) \text{ vs. } t \\
 &\ln L(t) \text{ vs. } t \\
 &\ln L(t) \text{ vs. } \ln t \\
 &L(t) \text{ vs. } \ln t
 \end{aligned}
 \tag{9.6}$$

If the decay follows a classical exponential decay, then a plot of  $\ln L(t)$  vs.  $t$  is linear whereas if it follows a power-law decay then  $\ln L(t)$  vs.  $\ln t$  is linear. A straight line fit could be determined for any portion of the decay and the closeness of fit could be determined by plotting the difference between the decay and the best fit line.

#### a) Parameters and Range

In modelling 8.46, I chose values of the parameters  $\tau_0$ ,  $\Delta E$  and  $T$  suitable to fit the luminescence decays observed in GaAs [98]. Observing the  $\sim 1.49\text{eV}$  line, Teh measured two exponential decays immediately after excitation. At 32K they corresponded to decay times of approximately 31ns and 115ns and activation energies 6meV and 15meV respectively. Using these values with the Arrhenius relation

$$\tau = \tau_0 e^{\Delta E/kT}$$



two values of  $\tau_0$  are obtained,  $\tau_0 = 3.5ns$  for the  $31ns$  and  $\tau_0 = 0.5ns$  for the  $115ns$  decay.

We are concerned about observing decay times over as many orders of magnitude of time as possible in order to accurately determine the shape of the decay. We are limited by the numerical ability of the computer. The magnitude of double precision numbers can extend from  $1 \times 10^{250}$  to  $1 \times 10^{-250}$ . This range of magnitudes can be used for the decaying luminescent intensity,  $L(t)$ . If the decay is non-exponential then this range of  $L(t)$  typically covers many tens of orders of magnitude of time. If, however, the decay is exponential, then the range of the time variable cannot be nearly as great. For a typical  $\tau$  of  $50-100ns$ , a change of 500 orders of magnitude for  $L(t)$  occurs over 4-5 orders of magnitude of time.

### 9.3 De-Trapping Scenarios

Once the carrier has been released from its trap it can recombine with another carrier and luminescence results. We consider two scenarios for the de-trapping of the carrier, see Figure 9.1:

- a) de-trapping from a group of traps to a single energy level
- b) de-trapping from a single trap to an energy band.

#### *a) De-trapping from a group of traps to a single energy level*

This is the primary scenario for the modelling of de-trapping. It shows decay behaviour which is in good agreement with that observed experimentally. We consider the time-decays from various trap distributions:

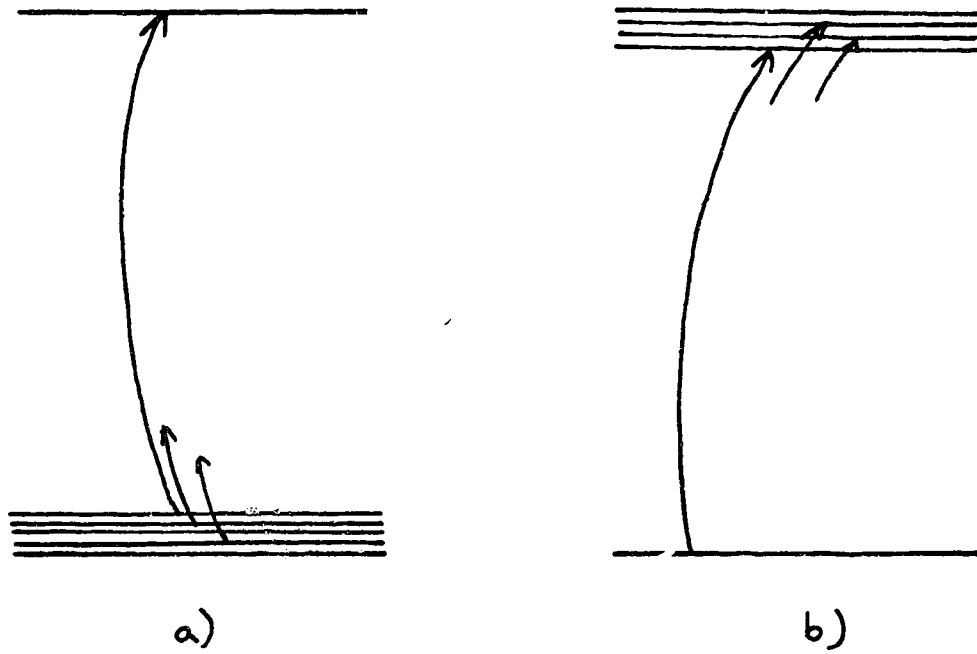


Figure 9.1: De-trapping scenarios: a) de-trapping from a group of traps to a single energy level b) de-trapping from a single trap to an energy band. The trap depth is very small ( $\sim 10 - 50 meV$ ) compared to the band-gap energy of the semiconductor ( $\sim 1.5 eV$ ).

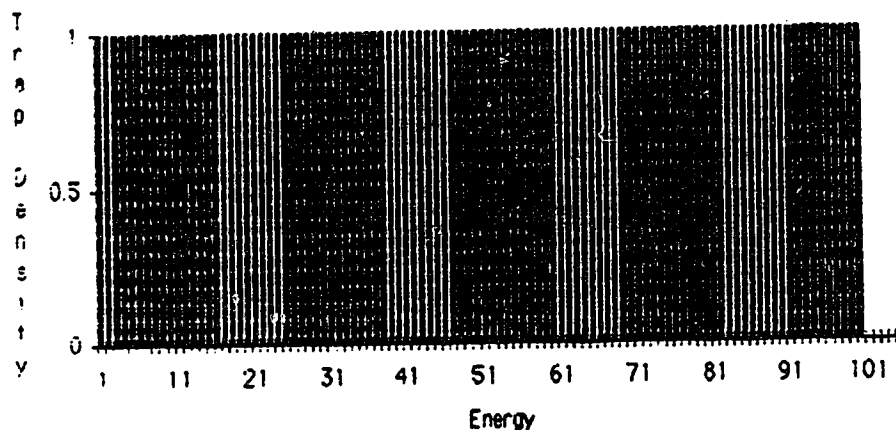


Figure 9.2: Trap Distribution

*Uniform trap distribution*

A power-law decay is typically observed from a uniform distribution of traps de-trapping into a single upper level. The exponent of the power law is 1. The power law can exist over many orders of magnitude of  $t$ , dependent on the width of the uniform distribution. Significantly, the power-law decay is preceded by an exponential decay whose time constant is in accord with the initial decay being dominated by activation from the shallowest traps. At very long times, the decay is again exponential. This is due to the fact that the distribution is finite in width—the decay becomes dominated by the deepest, slowly activated traps. Reducing the width of the distribution leads to the sooner onset of the final exponential decay.

I modelled the luminescence using  $\tau_0 = 0.5ns$ , appropriate to the  $115ns$  decay in GaAs. Figure 9.2 shows the uniform distribution of 100 traps, each separated by  $1meV$ . Their activation energies from 1 to  $100meV$  represent the situation of a set of traps (hole or electron) immediately jumping into the band. A power law decay is observed with the exponent  $p = 1$ , Figure 9.3. The power law behaviour extends over 15 orders of magnitude of time.

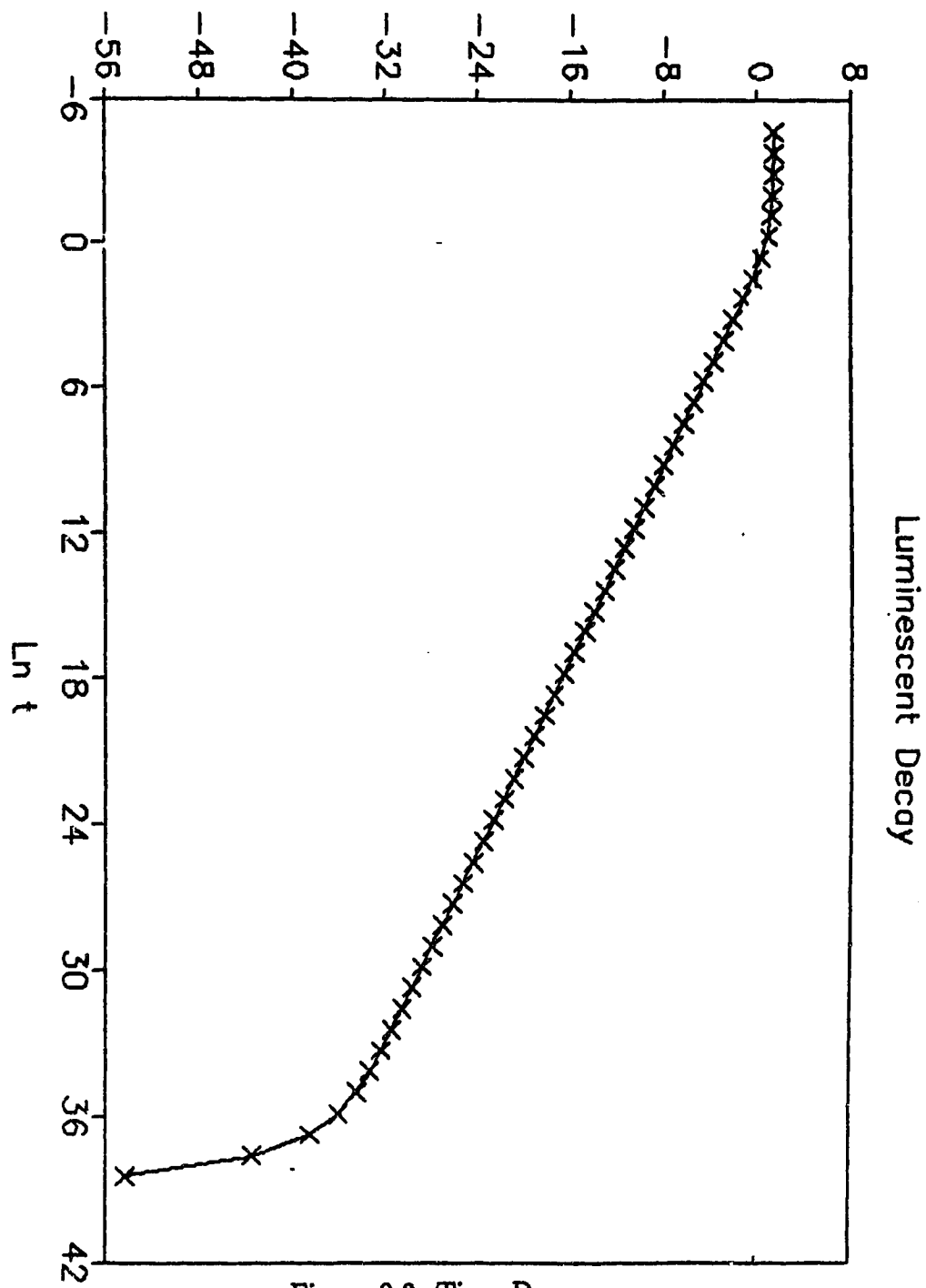


Figure 9.3: Time Decay

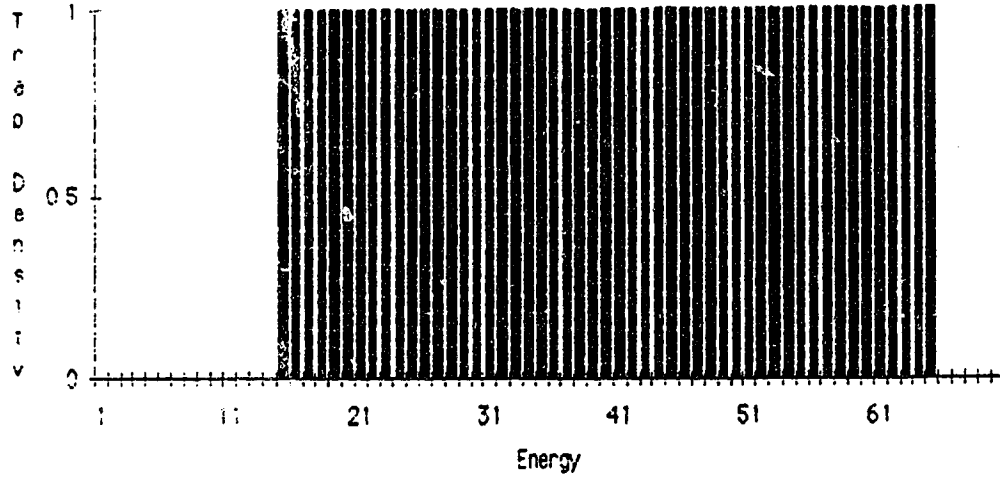


Figure 9.4: Trap Distribution

More interesting is Figure 9.5 which simulates the decay from a distribution of traps separated from the band by an energy gap of  $15\text{meV}$  (Figure 9.4). The trap distribution shown has half the width but the same energy spacing as the distribution of Figure 9.2. The power law now extends over only 7 orders of magnitude. The initial decay is exponential, see Figure 9.6. It has a decay time of  $\tau = 201\text{ns}$  even though the decay time of the first trap is only  $\tau = 115\text{ns}$ . The decay  $\tau = 201\text{ns}$  represents excitation from a trap of depth  $16.5\text{meV}$ , still very close to the band-gap energy.

#### *Exponential trap distribution*

The results of this type of distribution are qualitatively exactly the same as that of the uniform distribution. From equation 8.46, when a sum is made over a uniform distribution, the  $\tau$  in the denominator introduces an exponentially varying factor. This may be seen as follows: for a fully occupied initial distribution

$$N_S(E) = Ae^{-\alpha(E_T - E_0)} \quad (9.7)$$

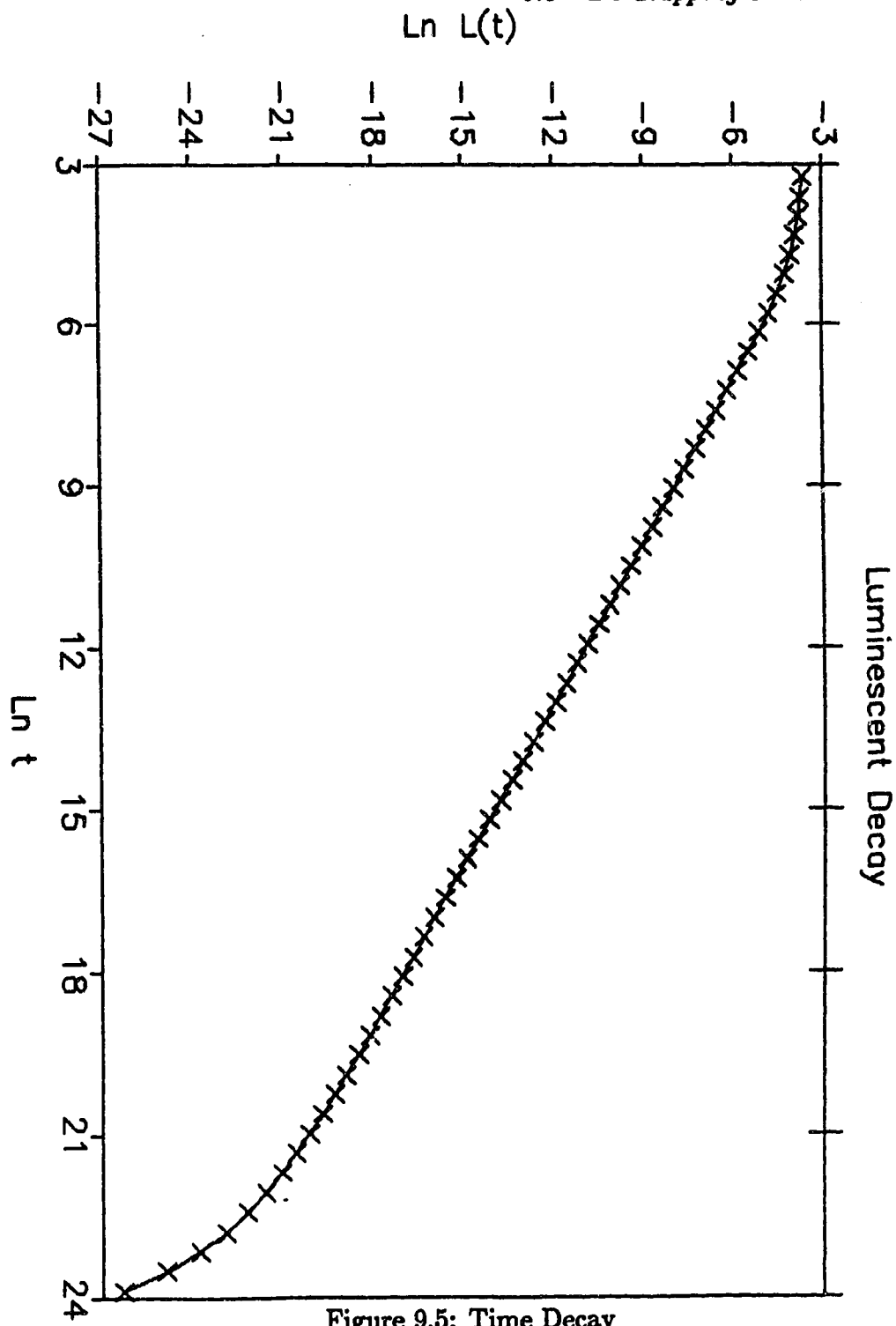


Figure 9.5: Time Decay

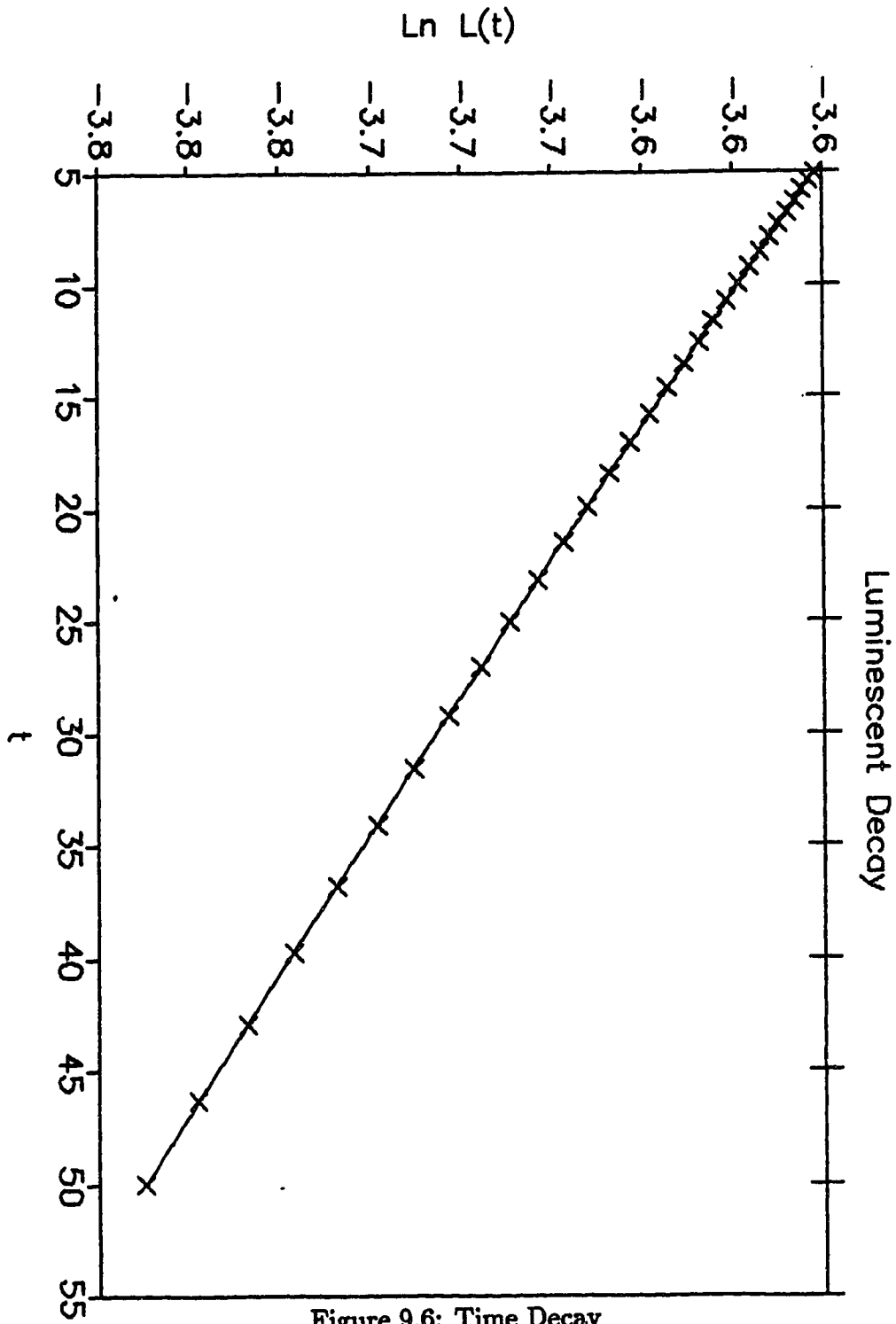


Figure 9.6: Time Decay

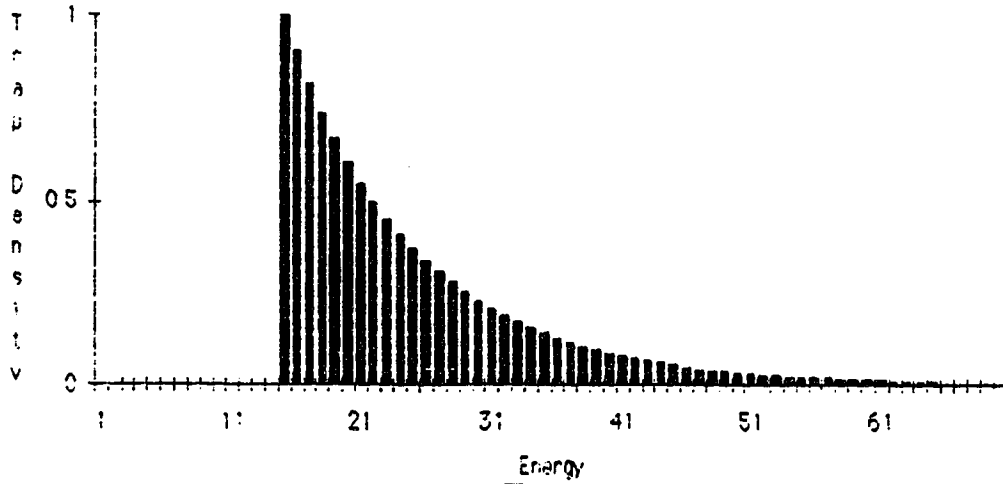


Figure 9.7: Trap Distribution

then

$$\frac{N_S(E)}{\tau} \propto A e^{-(\alpha+1/kT)E_T} \quad (9.8)$$

which compares to

$$\frac{N_S(E)}{\tau} \propto A e^{-(E_T/kT)} \quad (9.9)$$

for a uniform distribution.

The only change to the luminescence intensity 8.46

$$L(t) = \sum \frac{N_S(E)}{\tau} e^{-t/\tau}$$

results from the different exponential value of  $\frac{N_S(E)}{\tau}$ . We thus still expect to see power-law behaviour. We indeed find a time-decay  $t^{-p}$  where,

$$p = 1 + \alpha kT \quad (9.10)$$

This is shown in Figure 9.8 for the trap distribution of Figure 9.7. The slope of the line equals  $\alpha$ . The seemingly reduced 'width' of a distribution with large  $\alpha$  does not affect the condition on  $\gamma$ . The important width is actually the extent of the trap distribution.



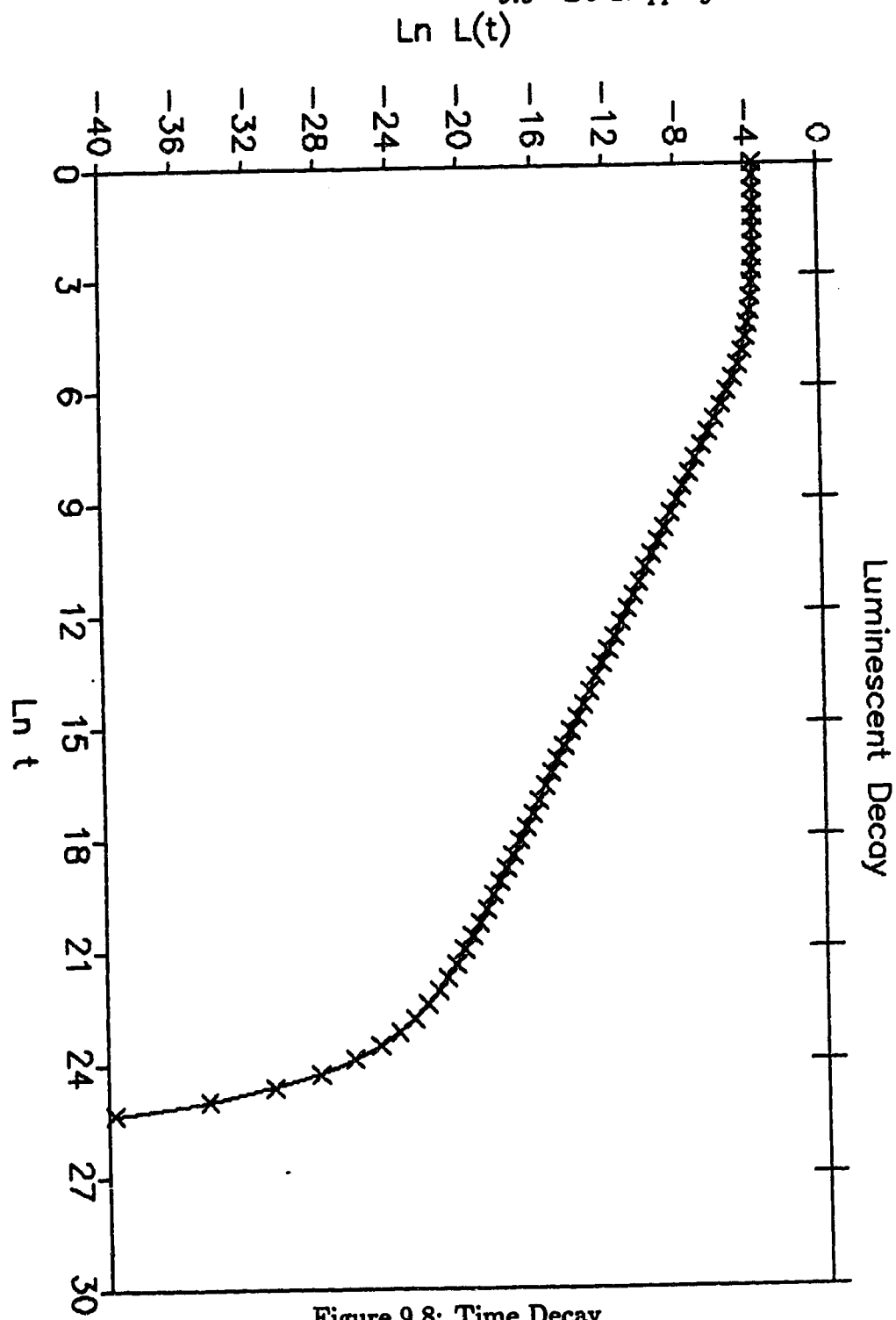


Figure 9.8: Time Decay

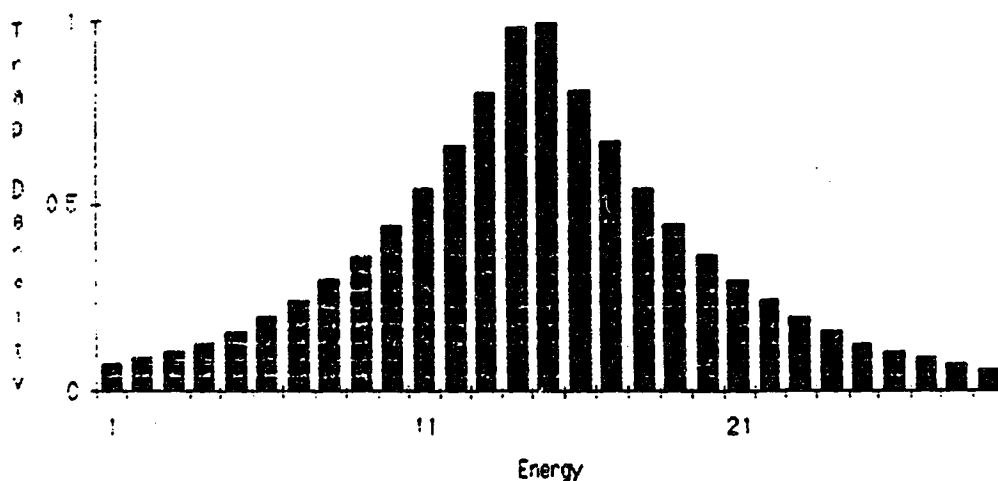


Figure 9.9: Trap Distribution

*Two-sided exponential trap distribution*

Consider a trap distribution as shown in Figure 9.9, characterized by

$$N_S(E) = Ae^{-\alpha|E-E_0|} \quad (9.11)$$

The behaviour of each side of the distribution of Figure 9.9 can be considered separately. The right-hand side has already been considered—it gives power-law decay. Considering separately the luminescence from the distribution of Figure 9.10 we see that the final luminescence does not decay—its amplitude is maintained over time. However, due to the finite width of the distribution, the constant luminescence persists only up to a certain point and then decays exponentially, see Figure 9.11.

*Gaussian trap distribution*

The decay from a Gaussian distribution is of considerable interest because if traps are randomly distributed around a mean energy then we would expect to observe a

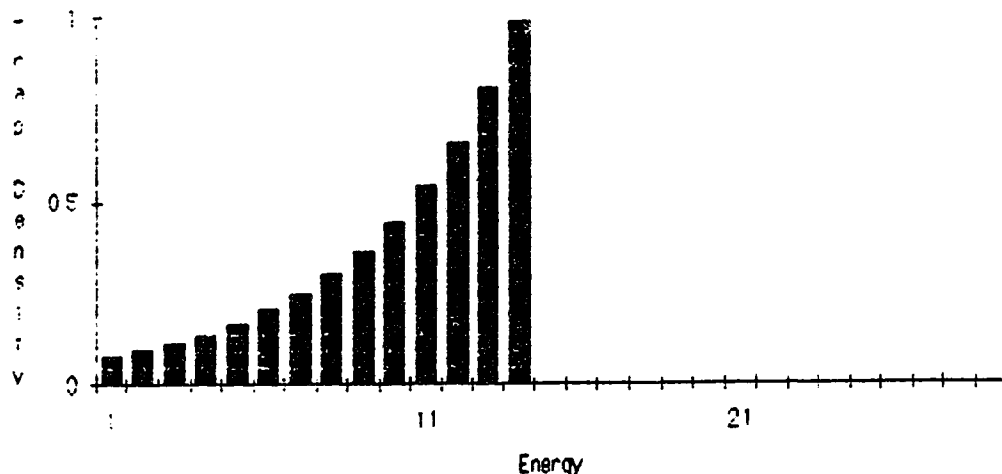


Figure 9.10: Trap Distribution

Gaussian density distribution. For the function,

$$N_S(E) = Ae^{-\alpha(E-E_0)^2} \quad (9.12)$$

the observed decay of 8.46 does not appear simple. As [116] showed, broad distributions lead to  $t^{-1}$  behaviour. For  $\alpha = 0.001$  see Figures 9.12 and 9.13.

*b) De-trapping from a single trap to an energy band*

Equation 8.46 applies equally well to describe the luminescence from a single trap level to a group of higher energy levels, a band. The decays of the previous section for various trap distributions will therefore be the same as these decays if an equivalence is made between the previous trap distributions and the energy band distributions. However, in modelling an energy band we need to consider distributions which are physically reasonable.

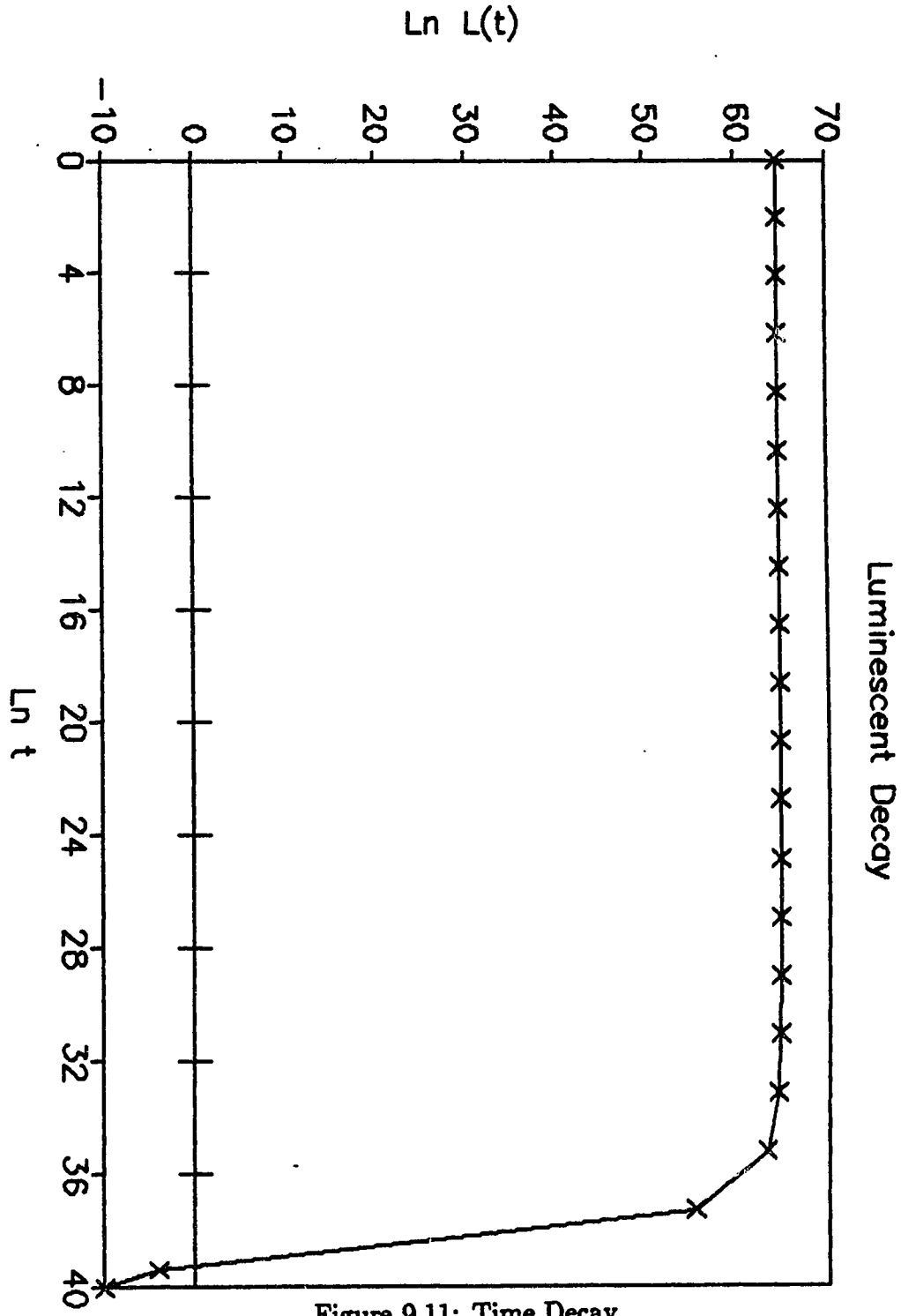


Figure 9.11: Time Decay

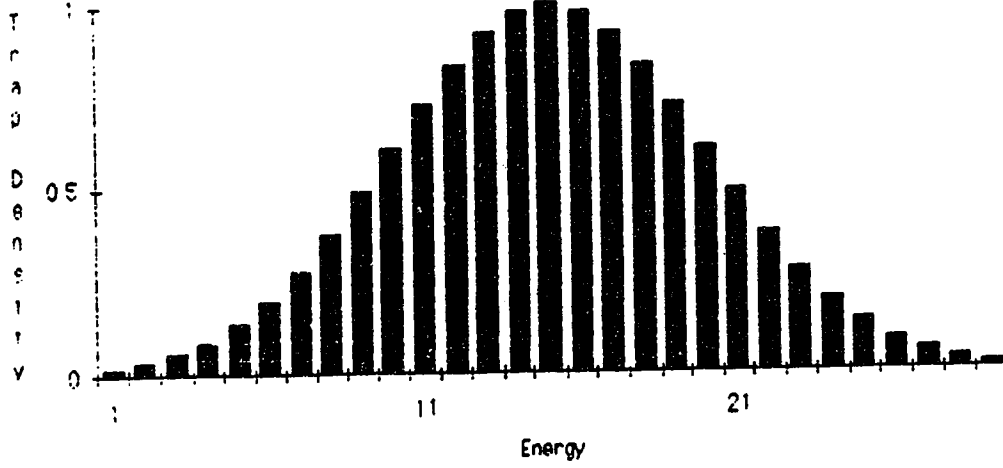


Figure 9.12: Trap Distribution

*Parabolic band*

For a simple band,

$$E = E_c + \frac{\hbar^2 k^2}{2m_c} \quad (9.13)$$

and the density of states is,

$$g(E) = 4\pi \left( \frac{2m_c}{\hbar^2} \right)^{3/2} (E - E_c)^{1/2} \quad (9.14)$$

This is a weakly increasing function of energy. It is therefore different from the previous trap distributions which were either uniform, decreasing exponentially with energy, or decreasing in a Gaussian manner.

The results of the decay from a single level (at  $E = 0$ ) to a parabolic band distribution (Figure 9.14) are shown in Figure 9.15. The decay follows a power-law with the exponent  $p = 1$ . This is not altogether surprising since the decay to a weakly increasing density of states is still dominated by the exponential denominator  $\tau$  of Equation 9.9 and thus leads to the  $t^{-1}$  form of decay.

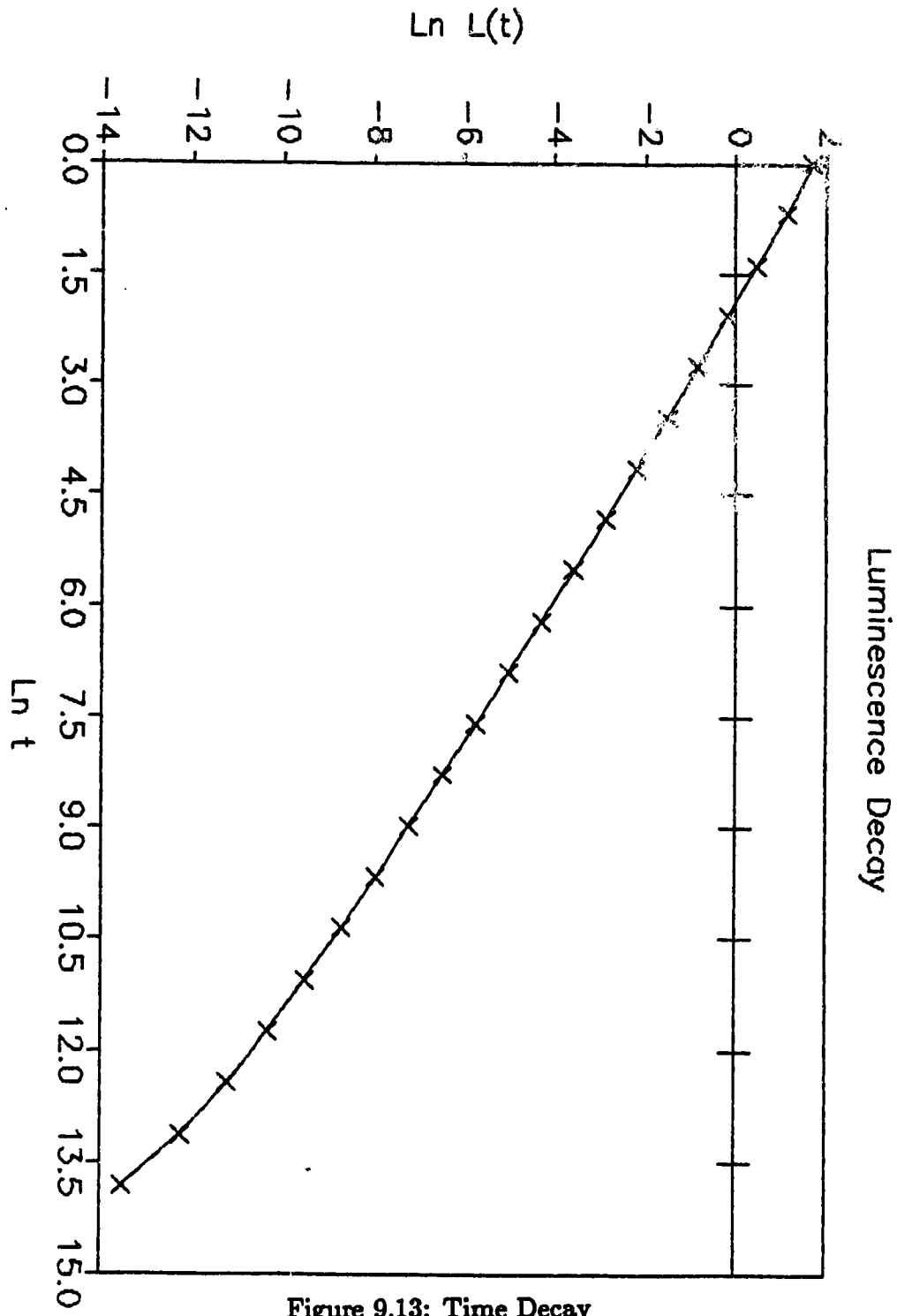


Figure 9.13: Time Decay

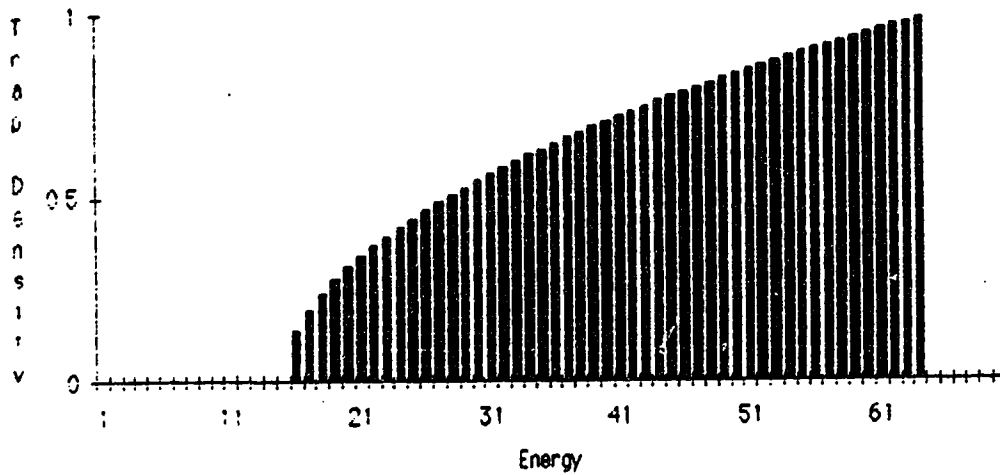


Figure 9.14: Trap Distribution

## 9.4 Critical Parameters

One general conclusion that can be drawn from the de-trapping scenarios is that power-law decays can result from many different trap and energy distributions—basically, whenever the form of the decay is dominated by the exponential dependence of  $\tau$  (see equation 9.9) or the distribution is exponentially varying.

My results from computer simulation are in substantial agreement with the previous investigations of phosphorescence. What is new about these investigations, however, is that discrete distributions of traps have been considered.

Power law behaviour results quite generally from summing a set of exponential functions when the close, quicker-decaying functions have a higher magnitude, so that the would-be exponential decay is slowed by the presence of very shallow exponentials and power-law decay results.

Hornyak and Chen defined critical parameters for the onset of power-law decay from a continuous distribution of traps. I have been able to confirm their values with the computer simulations I made. Additionally, I determined a new

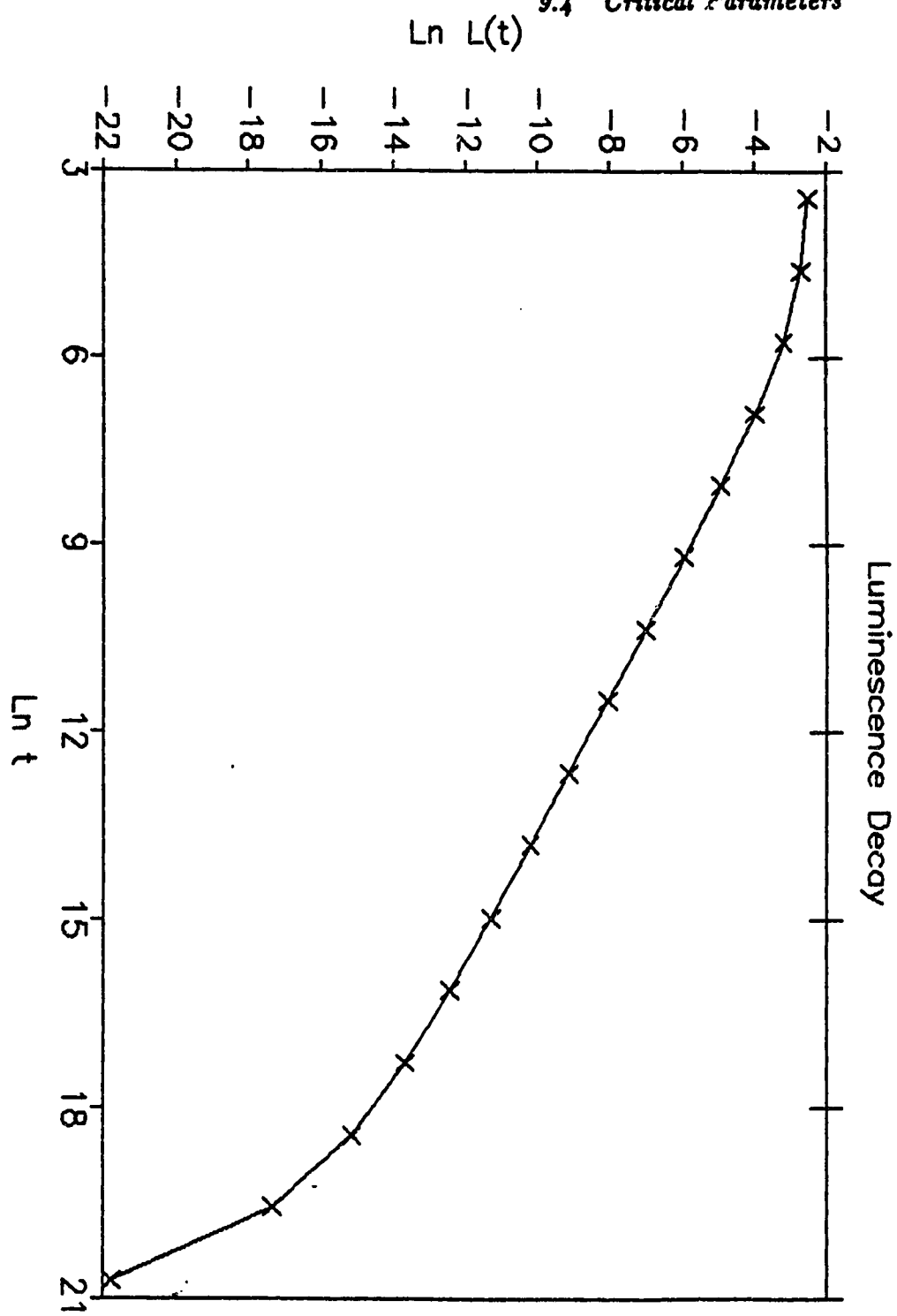


Figure 9.15: Time Decay



critical parameter that could be used to determine when the discrete distributions begin to behave like continuous distributions.

*a) The critical parameter for power-law decay*

It is relatively easy to verify the dependence of power-law behaviour on the parameter identified by Hornyak and Chen [116],  $y = kT/\Delta E$ .  $\Delta E$  is the width of the distribution. For Figure 9.4,  $\Delta E = 50\text{meV}$  and  $kT = 2.76\text{meV}$  therefore  $y = 0.0552$ , well below the critical value of 0.15. If the same distribution is used but the temperature changed, the final decay form changes with the value of  $y$ . Figure 9.16 shows that at  $100\text{K}$  ( $kT = 8.63\text{meV}$ ) the power-law behaviour has disappeared. The critical value of  $T$  is around  $60\text{K}$ , indicating a value of  $y$  of 0.104. Similarly, at  $32\text{K}$  the minimum energy width of the distribution that leads to power law behaviour is  $40\text{meV}$ , indicating  $y \leq \sim 0.07$ .

For the Gaussian distribution, the critical value of  $\alpha$  at  $32\text{K}$  was 0.002 giving  $y \leq \sim 0.12$ , in agreement with [116]. The more detailed decay form derived by Medlin (Equation 9.5) does not show simple power-law behaviour, except in the “wide-distribution” limit above.

*b) A critical parameter for discrete distributions*

A power-law decay can be obtained from making a sum of exponential functions. The fast-decaying exponentials must have high initial magnitude so that the fast decaying component is maintained together with a slowly-decaying component from slow exponentials of smaller magnitude.

I found from computer simulations that the individual levels could not be spaced

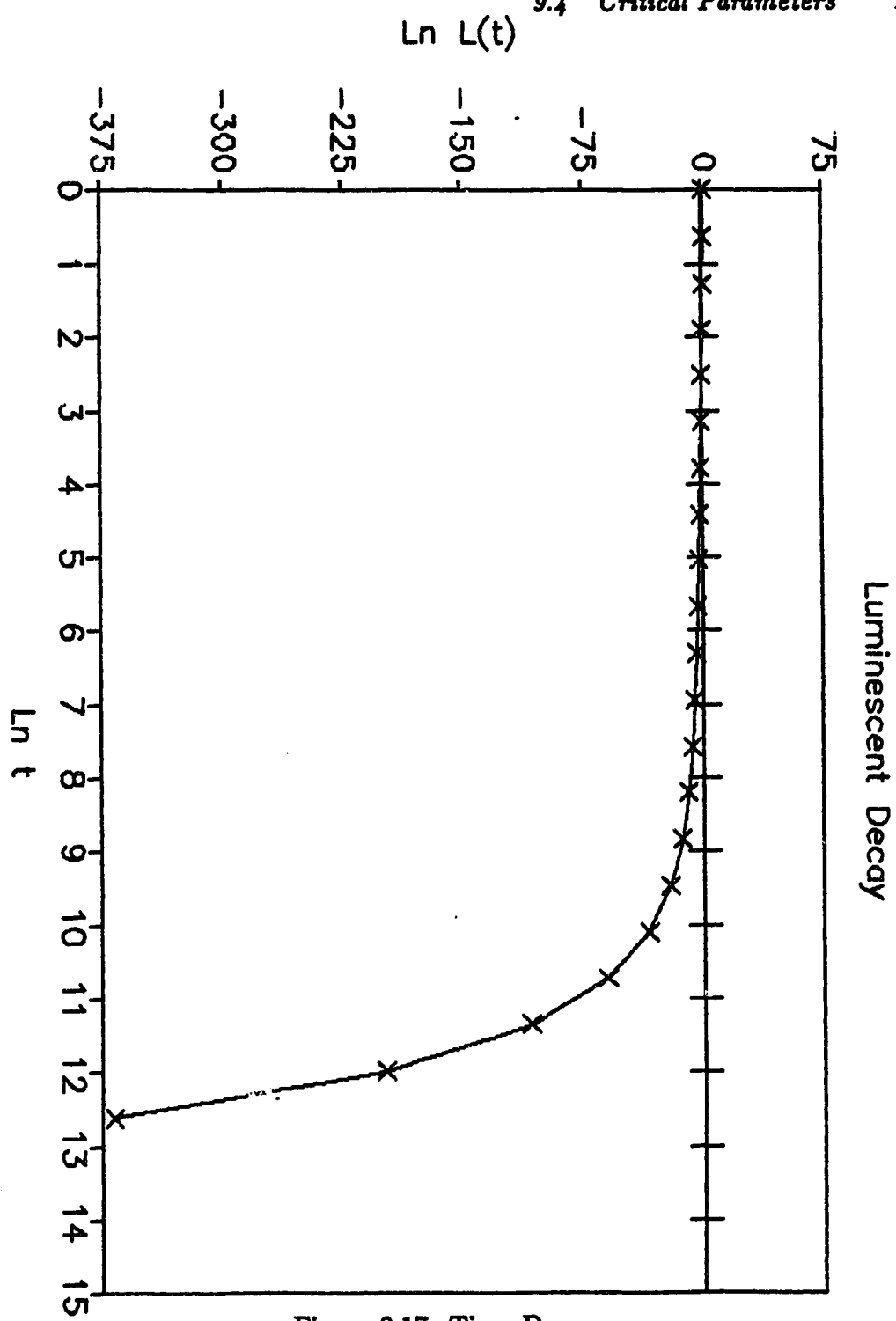


Figure 9.17: Time Decay

too far apart in energy because then the time constants of their decays would be very different and the overall decay would resemble an exponential rather than a power-law. For power law decay, the levels must be closely enough spaced so that successive exponentials can help to sustain the decay from the previous ones. I considered the difference in decay times  $\Delta\tau$  between traps. The critical parameter for seeing power law decay from a discrete distribution seems to be  $\Delta\tau/\tau$ . Call this parameter  $m$  and from 8.28 this is

$$m = \frac{\Delta\tau}{\tau} = \frac{\Delta E}{kT} \quad (9.15)$$

The distribution of Figure 9.4 has  $\Delta E = 1\text{meV}$ ,  $kT = 2.76\text{meV}$  and  $m = 0.36$ . We observe the power for  $\Delta E \sim 15\text{meV}$  and  $kT \sim 32\text{K}$  indicating that the critical value for  $m$  is  $m \leq \sim 5.5$ .

# CHAPTER TEN

## DE-TRAPPING IN GAAS

### 10.1 Trap Population in GaAs

Immediately after excitation, huge numbers of non-equilibrium carriers exist in the bands, spatially localized near to the excitation surface. An order of magnitude calculation can give an approximate rate of creation of carriers. Imagine an incident intensity of  $1.7\text{eV}$  and  $10\text{mW/cm}^{-2}$  focused to a  $2\text{mm}$  spot of light that excites photons across the band gap. Then

$$\begin{aligned}
 \text{Intensity} &= \text{Power/Area} \\
 &= \frac{\text{Energy of Photon} \times \text{No. of photons/sec}}{\text{Area}} \\
 10 \times 10^{-3} &= \frac{1.7 \times 1.6 \times 10^{-19} \times N}{\pi(0.2)^2} \\
 \Rightarrow N &= 4.6 \times 10^{15} \text{photons/sec}
 \end{aligned} \tag{10.1}$$

Weiner and Yu [107] have shown that the band-band energy decays in  $100\text{-}200\text{ps}$ . Nelson and Sobers [69] found radiative lifetime of near band-edge luminescence to be  $1\text{-}1000\text{ns}$ . From these figures we can estimate the number of above-equilibrium electrons or holes existing during the excitation period:

1. In the conduction band, spatially localized near the excitation surface

$$\begin{aligned}
 \text{No.} &= 4.6 \times 10^{15} \text{s}^{-1} \cdot 500\text{ps} \\
 &= 2.3 \times 10^6
 \end{aligned} \tag{10.2}$$

2. In the near band-edge region, spatially localized near the excitation surface

$$\text{No.} = 4.6 \times 10^{15} \text{s}^{-1} \cdot 500\text{ns}$$

$$= 2.3 \times 10^9 \quad (10.3)$$

Excitation from the laser is absorbed by the crystal near to the surface. The absorbed radiation creates a 'wave-packet' of excitons which subsequently diffuses through the crystal or dissolves through the process of recombination.

The estimate of the maximum number of above-equilibrium electrons and holes in the bands under conditions of continuous ( $> \sim 500ns$  duration) excitation assumes that all electrons created in the band decay into the near-band region (presumably through the thermalization process) and then decay radiatively. The first stage is probably correct because of the extreme difficulty of observing band-band recombination. However, not all carriers decay radiatively from the near-edge region. The rate of loss of near-band electrons attributed to non-radiative transitions can be estimated from the difference between the observed decay time and the theoretically expected radiative decay time.

We expect that the number of electrons recombining non-radiatively is relatively small. If the total recombination rate is greater than the radiative rate by 10% for example, then 10% of the carriers will dissipate through non-radiative processes. So, for the previous  $500ns$  pulse,  $2.3 \times 10^9$  is the stationary number in the near band-edge region under excitation. Then  $2.6 \times 10^8 s^{-1}$  are dissipated from the near band-edge region by non-radiative processes. We assume that this number become trapped just below the near band-edge region.

## 10.2 De-Trapping in GaAs

Teh [98] obtained experimental evidence of the time decays of LEC-grown SI GaAs in which carbon forms an acceptor level,  $C_{As}$ , which is responsible for the  $\sim 1.49eV$

donor-acceptor pair radiative recombination at low temperatures. She measured the decay and the line shape of the photoluminescence signals at and near the donor-acceptor emission peak for temperatures ranging from 4.1K to 34K for several samples of LEC SI GaAs with different carbon concentrations.

The photoluminescence decay was found to follow a double exponential law at the early stage of the decay but followed a power-law of the form  $L(t) \propto t^{-p}$  at a later stage. Analysis of the temperature dependence of the exponential components gave two activation energies of  $\sim 5.7\text{meV}$  and  $\sim 15\text{meV}$ . The exponent,  $p$ , of the power law decay was found to be both temperature and concentration dependent. For the undoped sample, Teh found the decay to be of the form

$$p = -1.2 \pm 0.2 + \beta T \quad (10.4)$$

where  $\beta$  is proportional to the concentration of the acceptors,  $C_A$ , in the temperature range  $18 < T < 30\text{K}$ . The value of  $p = 1.4$  at 4.1K agreed with Dingle's result [19].

Figure 10.1 shows the lineshape of the  $\sim 1.49\text{eV}$  luminescence observed by Teh. It clearly shows the luminescence to be made up of two components— identified as a donor-acceptor component on the low energy side and a band-acceptor component on the high energy side. Figure 10.2 shows the observed dependence of the exponent of the power-law,  $p$ , on temperature for samples of different carbon concentration.

Is the observed time decay consistent with a model of de-trapping from a discrete set of energy levels?

One immediate problem is that experiment shows

$$p = -1 + \beta T \quad (10.5)$$

This Figure has been removed for Copyright reasons.

Figure 10.1: Luminescence spectrum of  $\sim 1.49\text{eV}$  region at different temperatures. The donor-acceptor and band-acceptor transitions are indicated. (From [98].)

This Figure has been removed for Copyright reasons.

Figure 10.2: Temperature dependence of the exponent,  $p$ , for different carbon concentrations  $N$ . (From [98].)



whereas theory of decay from an exponential trap distribution predicts

$$p = 1 + \alpha kT \quad (10.6)$$

and from the flat and Gaussian distributions,

$$p = 1 \quad (10.7)$$

Apart from this discrepancy, the model of de-trapping from a set of levels does predict an initial exponential decay followed by a power law whose exponent increases with temperature and  $\alpha$ , the steepness of the exponential trap distribution. A comparison between the theoretical prediction of 10.6 and the experimental data is shown in Figure 10.3 using  $\alpha = 1.29 \text{ meV}^{-1}$  to model the results from the samples with concentration  $N = 11.6 \times 10^{15} \text{ cm}^{-3}$ .

Experimentally we observe two decays in the  $\sim 1.49 \text{ eV}$  region—the band-acceptor and donor-acceptor contributions. We see two initial decays and one final power law decay. This is consistent with a model of de-trapping from two sets of traps. The trap distributions would have to be of the same form so that  $\alpha$  is the same for both and the final power law is identical.

Experimentally,  $p$  increases with  $\beta$  and  $T$ . If we equate  $\alpha$  with  $\beta$  then we are led to the conclusion that the steepness of the exponential distribution is proportional to the carbon concentration, that is, the distribution is more sharply peaked at higher  $\beta$ , see Figure 10.4.

The possibility of traps existing in material is something that is, by nature, difficult to verify. Martin, Mitonneau, and Mircea did classify trap states in GaAs from

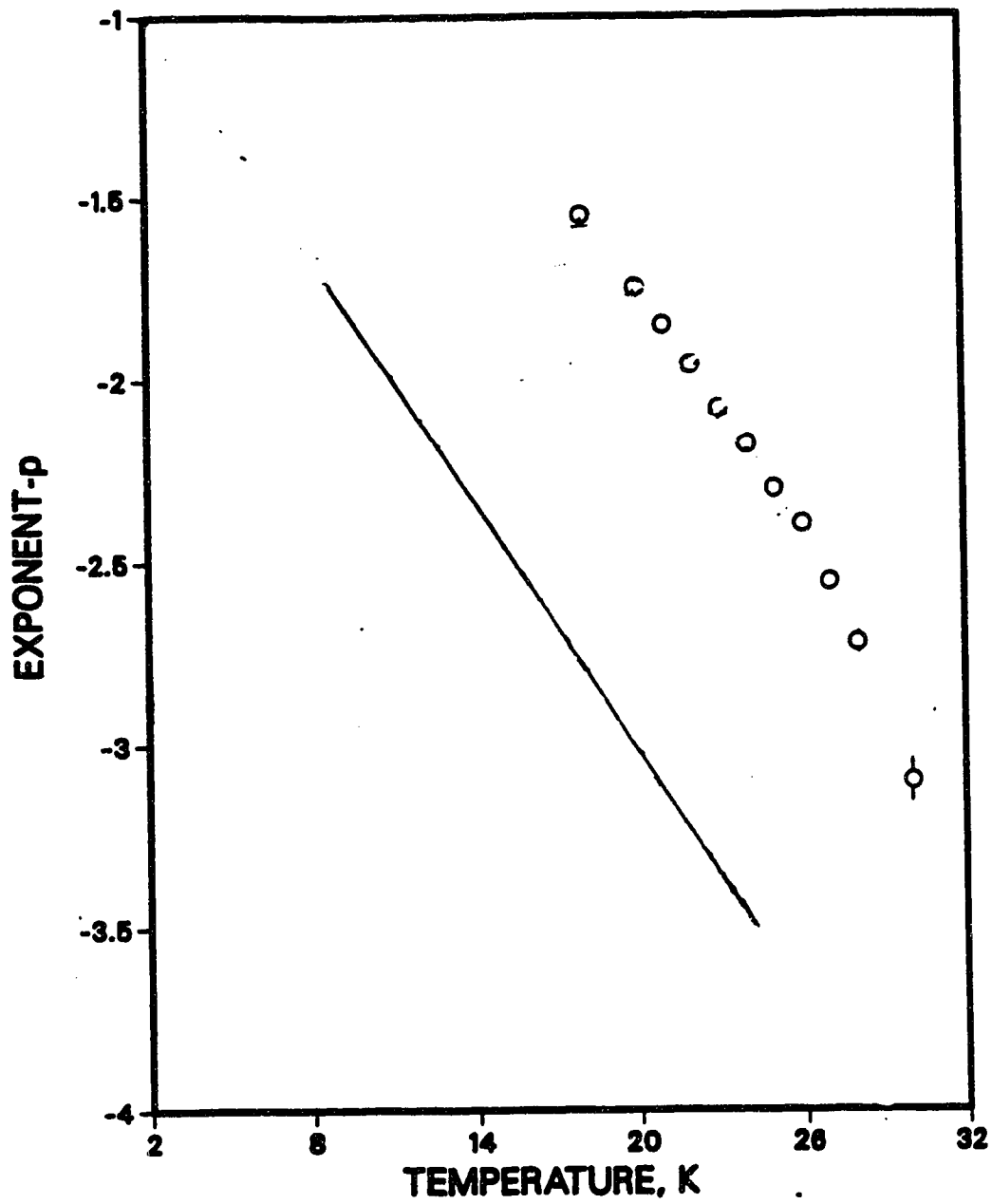
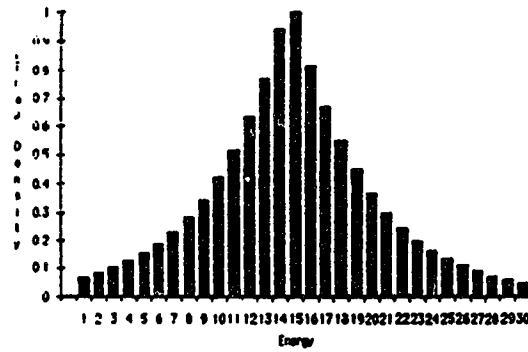


Figure 10.3: Comparison between theory and experiment for exponent of power-law decay



a)

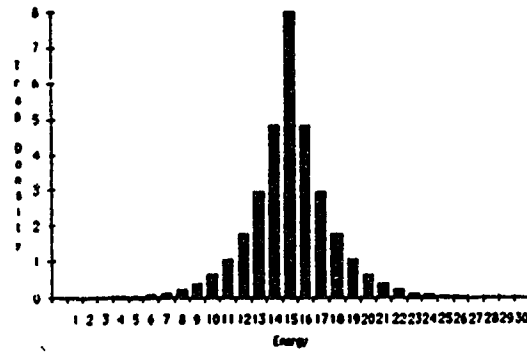


Figure 10.4: Trap Distributions a) low carbon concentration b) high carbon concentration.

DLTS experiments [64] but none of their observed activation energies are as small as the  $6\text{meV}$  or  $15\text{meV}$  seen by Teh.

Walukiewicz et. al. [120] have reported the presence of a new shallow donor level  $20\text{-}30\text{meV}$  below the conduction band with concentrations similar to those of the EL2 defect. The shallow donor could act as an electron trap from which electrons are excited into the conduction band or donor level.

Paget and Klein [72] have evidence from photoluminescence experiments for the presence of a continuous set of shallow donor levels. They say that the effect most probably results from the Coulomb interaction between the electron bound to the donor and charged impurities which arise as a result of the compensation process in SI GaAs.

Although no evidence so far points to the discrete distribution of traps that we have postulated, it may be hoped that more accurate experiments will be able to determine whether the possibility exists for two sets of trapping levels leading to donor-acceptor and band-acceptor luminescence in GaAs.

## BIBLIOGRAPHY

- [1] N. W. Ashcroft, N. D. Mermin, "Solid State Physics", Saunders College, Philadelphia, 1976
- [2] D. J. Ashen, P. J. Dean, and 4 others, J. Phys. Chem. Solids **36**, 1041, (1975)
- [3] H. B. Bebb, E. W. Williams, in "Semiconductors and Semimetals" (R. K. Willardson, A. C. Beer, Eds.), **8**, 181, (1972), Academic Press, New York
- [4] D. Block, J. Shah, A. C. Gossard, S. S. Commun. **59**, 527, (1986)
- [5] E. H. Bogardus, H. B. Bebb, Phys. Rev. **176**, 993, (1968)
- [6] O. Breitenstein, K. Unger, Phys. Stat. Sol. (b) **91**, 557, (1979)
- [7] F. Briones, D. M. Collins, J. Electron. Mater. (U.S.A.) **11**, 847, (1982)
- [8] M. R. Brozel, R. C. Newman, B. Özbay, J. Phys. C **12**, L785, (1979)
- [9] M. R. Burd, R. Braunstein, J. Phys. Chem. Solids **49**, 731, (1988)
- [10] J. Callaway, "Quantum Theory of the Solid State", Academic Press, New York, (1974)
- [11] S. Charbonneau, M. L. W. Thewalt, T. Steiner, Can. J. Phys. **65**, 838, (1987)
- [12] J. R. Chelikowsky, M. L. Cohen, Phys. Rev. B **14**, 556, (1976)
- [13] R. Chen, Y. Kirsh, "Analysis of Thermally Stimulated Processes", Pergamon Press, Oxford, (1981)
- [14] E. Chimzak, Z. Phys. B **72**, 211, (1988)

- [15] M. L. Cohen, J. R. Chelikowsky, "Electronic Structure and Optical Properties of Semiconductors", Springer-Verlag, Berlin, (1988)
- [16] P. J. Dean, C. J. Frosch, C. H. Henry, J. Appl. Phys. **39**, 5631, (1968)
- [17] P. J. Dean, "Inter-impurity Recombinations in Semiconductors", Prog. S. S. Chem, **8**, 1, (1974)
- [18] P. J. Dean, B. I. Fitzpatrick, R. N. Bhargava, Phys. Rev. B **26**, 2016, (1982)
- [19] R. Dingle, Phys. Rev. **184**, 788, (1969)
- [20] D. J. Dunstan, Phil. Mag. B **46**, 579, (1982)
- [21] D. J. Dunstan, Phil. Mag. B **49**, 191, (1984)
- [22] D. J. Dunstan, Phys. Rev. B **32**, 6910, (1985)
- [23] D. M. Eagles, J. Phys. Chem. Solids **30**, 2225, (1969)
- [24] J. R. Eggert, Phys. Rev. B **29**, 6664, (1984)
- [25] J. R. Eggert, Phys. Rev. B **29**, 6669, (1984)
- [26] J. R. Eggert, Phys. Rev. B **32**, 6913, (1985)
- [27] J. Golka, S. S. Comm. **28**, 401, (1978)
- [28] J. Golka, S. S. Comm. **32**, 479, (1979)
- [29] E. F. Gross, D. S. Nedzvetskii, Dohl. Akad. Nauk. S. S. S. R. **146**, 1047, (1962)
- [30] H. Gummel, M. Lax, Phys. Rev. **97**, 1469, (1955)
- [31] W. A. Harrison, "Electronic Structure and the Properties of Solids: The Physics of the Chemical Bond", Freeman, San Francisco, (1980)

- [32] A. Haug, "Theoretical Solid State Physics", Pergamon Press, Oxford, (1972)
- [33] J. R. Haynes, *Phys. Rev. Lett.* **4**, 361, (1960)
- [34] M. Heiblum, E. E. Mendez, L. Osterling, *J. Appl. Phys.* **54**, 6982, (1983)
- [35] U. Heim, P. Hiesinger, *Phys. Stat. Sol.* **66**, 461, (1974)
- [36] C. H. Henry, D. V. Lang, *Phys. Rev. B* **15**, 989, (1977)
- [37] C. Hoffman, H. J. Gerritsen, A. V. Nurmikko, *J. Appl. Phys.* **51**, 1603, (1980)
- [38] W. Hoogenstraaten, *Philips Res. Rep.* **13**, 682, (1958)
- [39] J. J. Hopfield, D. G. Thomas, M. Gershenson, *Phys. Rev. Letts.* **10**, 162, (1963)
- [40] J. J. Hopfield, *Proc. of the Intl. Conf. on Phys. of Semiconductors*, Dunod, Paris, (1964)
- [41] K. Huang, A. Rhys, *Proc. Roy. Soc. A* **204**, 406, (1950)
- [42] D. L. Huber, *Phys. Rev. B* **20**, 2307, (1979)
- [43] D. L. Huber, *Phys. Rev. B* **20**, 5333, (1979)
- [44] D. L. Huber, D. S. Hamilton, B. Barnett, *Phys. Rev. B* **16**, 4642, (1977)
- [45] G. B. Inglis, F. Williams, *J. Lumin.* **12/13**, 525, (1976)
- [46] M. Inokuti, F. Hirayama, *J. Chem. Phys.* **43**, 1978, (1965)
- [47] INSPEC, Institute of Electrical Engineers, "Properties of GaAs", London, (1986)
- [48] D. E. Ioannou, R. J. Gledhill, *J. Appl. Phys.* **56**, 1797, (1984)

- [49] A. K. Jonscher, A. de Polignac, *J. Phys. C.* **17**, 6493, (1984)
- [50] M. Kaminska, *Phys. Scr.* **T19**, 551, (1987)
- [51] I. Z. Kostadinov, *Phys. Rev. B* **35**, 7613, (1987)
- [52] R. S. Knox, "Theory of Excitons", *Solid State Physics Supplement 5*, Academic Press, (1963)
- [53] V. A. Kovarskii, *Sov. Phys.- Solid State* **4**, 1200, (1962)
- [54] V. A. Kovarskii, E. P. Sinyavskii, *Sov. Phys.- Solid State* **4**, 2345, (1963)
- [55] R. Kubo, I. Toyazawa, *Prog. Theor. Phys.* **13**, 160, (1955)
- [56] H. Kunzel, K. Ploog, "Gallium Arsenide and Related Compounds, 1980", *Inst. Phys. Conf. Ser. No. 56*, 519
- [57] P. T. Landsberg, *Phys. Stat. Sol.* **41**, 457, (1970)
- [58] D. V. Lang, C. H. Henry, *Phys. Rev. Letts* **35**, 1525, (1975)
- [59] M. Lannoo, J. Bourgoin, "Point Defects in Semiconductors", Springer-Verlag, Berlin, (1981)
- [60] M. Lax, *J. Phys. Chem. Solids* **8**, 66, (1959)
- [61] A. C. Leite, A. E. DiGiovanni, *Phys. Rev.* **153**, 841, (1967)
- [62] G. Lucovsky, A. J. Varga, R. F. Schwarz, *S. S. Comm.* **3**, 9, (1965)
- [63] A. Mandelis, *Phys. Stat. Sol. (b)* **122**, 687, (1984)
- [64] G. M. Martin, A. Mittoneau, A. Mircea, *Electronics Letters* **13**, 191, (1977)
- [65] G. M. Martin, A. Mittoneau, A. Mircea, *Electronics Letters* **13**, 666, (1977)



- [66] J. P. McKelvey, "Solid State and Semiconductor Physics", Harper & Row, New York, (1966)
- [67] K. Misiakos, F. A. Lindholm, A. Neugroschel, J. Appl. Phys. **58**, 1647, (1985)
- [68] D. F. Nelson, J. D. Cuthbert, P. J. Dean, D. G. Thomas, Phys. Rev. Letts. **17**, 1262, (1966)
- [69] R. J. Nelson, R. G. Sobers, Appl. Phys. **49**, 6103, (1978)
- [70] L. Onsager, A. M. Stewart, J. Phys. C. **7**, 645, (1974)
- [71] A. Onton, M. R. Lorenz, Appl. Phys. Letts. **12**, 115, (1968)
- [72] D. Paget, P. B. Klein, Phys. Rev. B **34**, 971, (1986)
- [73] G. Paasch, E. Christie, M. Kausch, Phys. Stat. Sol. (b) **97**, 105, (1980)
- [74] R. Pässler, Phys. Stat. Sol. (b) **85**, 203, (1978)
- [75] L. Patrick, P. J. Dean, Phys. Rev. **188**, 1254, (1969)
- [76] J. S. Prener, F. E. Williams, Phys. Rev. **101**, 1427, (1956)
- [77] J. S. Prener, J. Chem. Phys. **25**, 1294, (1956)
- [78] J. T. Randall, M. H. F. Wilkins, Proc. Roy. Soc. **A184**, 390, (1945)
- [79] H. Reiss, J. Chem. Phys. **25**, 400, (1956)
- [80] D. C. Reynolds and 7 others, S. S. Comm. **52**, 685, (1984)
- [81] G. Richayzen, Proc. Roy. Soc. **A241**, 480, (1957)
- [82] B. K. Ridley, J. Phys. C **11**, 2323, (1978)

- [83] W. van Roosbroeck, W. Shockley, *Phys. Rev.* **94**, 1558, (1954)
- [84] J. A. Rossi, C. M. Wolfe, G. E. Stillman, J. O. Dimmock, *S. S. Comm.* **8**, 2021, (1970)
- [85] J. A. Rossi, C. M. Wolfe, J. O. Dimmock, *Phys. Rev. Lett.* **25**, 164, (1970)
- [86] A. P. Roth, R. G. Goodchild, S. Charbonneau, P. F. Williams, *J. Appl. Phys.* **54**, 3427, (1983)
- [87] Y. Sakai, M. Kawahigashi, T. Minami, T. Inoue, *J. Lumin.* **42**, 317, (1989)
- [88] W. Shockley, W. T. Read, Jr. , *Phys. Rev.* **87**, 835, (1952)
- [89] W. Shockley, "Electrons and Holes in Semiconductors", R. E. Krieger, New York, (1976)
- [90] D. D. Sell, R. Dingle, S. E. Stokowski, J. V. Di Lorenzo, *Phys. Rev. Letts.* **27**, 1644, (1971)
- [91] J. Shah, R. C. C. Leitte, J. P. Gordon, *Phys. Rev.* **176**, 932, (1968)
- [92] B. J. Skromme, T. S. Low, G. E. Stillman, *Inst. Phys. Conf. Ser. No.* **65**, 485, (1982)
- [93] B. J. Skromme, G. E. Stillman, *Phys. Rev. B* **29**, 1982, (1984)
- [94] T. Steiner, Y. Zhang, S. Charbonneau, A. Villemaire, M. L. W. Thewalt, *Can. J. Phys.* **67**, 242, (1989)
- [95] M. D. Sturge, *Phys. Rev.* **127**, 768, (1962)
- [96] V. Swaminatha, D. L. van Haren, J. L. Zilko, P. Y. Lu, N. E. Schumaker, *J. Appl. Phys.* **57**, 5349, (1985)

- [97] M. Tajima, in "Defects and Properties of Semiconductors: Defect Engineering" (J. Chikawa, K. Sumino, K. Wada, eds.), KTK, Tokyo, (1987)
- [98] C. K. Teh, Ph.D. thesis, University of Alberta, (1987)
- [99] D. G. Thomas, M. Gershenzon, F. A. Trumbore, Phys. Rev. **133**, A269, (1964)
- [100] D. G. Thomas, J. J. Hopfield, W. M. Augustyniak, Phys. Rev. **140**, A202, (1965)
- [101] M. S. Tyagi, J. F. Nijs, R. J. Van Overstaeten, S. S. Electron **25**, 411, (1982)
- [102] J. Vaitkus, Phys. Stat. Solidi **34**, 769, (1976)
- [103] A. T. Vink, C. Z. van Doorn, Phys. Letts. **1**, 332, (1962)
- [104] J. F. Wager, J. A. Van Vechten, Phys. Rev. B **35**, 2330, (1987)
- [105] J. P. Walter, M. L. Cohen, Phys. Rev. B **4**, 1877, (1971)
- [106] J. L. T. Waugh, G. Dolling, Phys. Rev. B **2**, 2410, (1963)
- [107] J. S. Weiner, P. Y. Yu, J. Appl. Phys. **55**, 3889, (1984)
- [108] J. D. Wiley, J. A. Seman, Bell. Syst. Tech. J. **50**, 355, (1970)
- [109] E. W. Williams, H. B. Bebb, J. Phys. Chem. Solids **30**, 1289, (1969)
- [110] E. W. Williams, H. B. Bebb, in "Semiconductors and Semimetals" (R. K. Willardson, A. C. Beer, Eds.), **8**, 321, (1972), Academic Press, New York
- [111] F. E. Williams, J. Phys. Chem. Solids **12**, 265, (1960)
- [112] D. E. Aspnes, Phys. Rev. B **14**, 5331, (1976)
- [113] J. S. Blakemore, "Semiconductor Statistics", Pergamon Press, Oxford, (1962)

- [114] J. S. Blakemore, J. Appl. Phys. **53**, R123, (1982)
- [115] G. W. Castellan, "Physical Chemistry", Addison-Wesley, (1977)
- [116] W. F. Hornyak, R. Chen, J. Lumin. **44**, 73, (1989)
- [117] E. O. Kane, J. Phys. Chem. Solids **1**, 249, (1957)
- [118] W. L. Medlin, Phys. Rev. **123**, 502, (1961)
- [119] J. R. Waldram, "The Theory of Thermodynamics", C.U.P., (1985)
- [120] W. Walukiewicz, J. Lagowski, H. C. Gatos, Appl. Phys. Lett. **43**, 112, (1983)
- [121] P. Würfel, W. Ruppel, J. Lumin. **24/25**, 925, (1981)

# APPENDIX A

## SIMPLE ENERGY TRANSFER MODEL

Chinnazak [14] derived the equations

$$\frac{dN_1}{dt} = -\alpha_1 N_1 \quad (\text{A.1})$$

$$\frac{dN_2}{dt} = -\frac{dN_1}{dt} - \alpha_2 N_2 \quad (\text{A.2})$$

Taking the Laplace transform of each

$$pL_1 - N_1(0) = -\alpha_1 L_1 \quad (\text{A.3})$$

$$pL_2 - N_2(0) = -\alpha_2 L_2 + \alpha_1 L_1 \quad (\text{A.4})$$

where  $L_1$  and  $L_2$  are the Laplace transforms of  $N_1$  and  $N_2$ , respectively.  $N_2(0) = 0$  since this centre is not initially excited.

Solving the above equations,

$$L_1 = \frac{N_1(0)}{p + \alpha_1} \quad (\text{A.5})$$

$$L_2 = \frac{N_1(0)\alpha_1}{(p + \alpha_1)(p + \alpha_2)} \quad (\text{A.6})$$

Taking the inverse Laplace transforms,

$$N_1 = N_1(0)e^{-\alpha_1 t} \quad (\text{A.7})$$

$$N_2 = N_1(0)\alpha_1 \left[ \frac{e^{-\alpha_1 t} - e^{-\alpha_2 t}}{\alpha_2 - \alpha_1} \right] \quad (\text{A.8})$$

The second centre is the emitting centre, so the luminescence is

$$I = -\frac{dN_2}{dt} \quad (\text{A.9})$$

$$= -\frac{N_1(0)\alpha_1}{\alpha_2 - \alpha_1} \left[ -\alpha_1 e^{-\alpha_1 t} + \alpha_2 e^{-\alpha_2 t} \right] \quad (\text{A.10})$$

using  $1/\tau_1 = \alpha_1$ ,  $1/\tau_2 = \alpha_2$

$$I = \frac{N_1(0)}{\tau_2 - \tau_1} \left[ e^{-t/\tau_2} - \frac{\tau_2}{\tau_1} e^{-t/\tau_1} \right] \quad (\text{A.11})$$

This luminescence peaks when

$$\frac{dI}{dt} = 0 \quad (\text{A.12})$$

Therefore,

$$\frac{N_1(0)}{\tau_2 - \tau_1} \left[ \frac{-1}{\tau_2} e^{-t/\tau_2} + \frac{\tau_2}{\tau_1^2} e^{-t/\tau_1} \right] = 0 \quad (\text{A.13})$$

$$t_{\max} = \frac{\tau_1 \tau_2}{\tau_2 - \tau_1} 2 \ln \frac{\tau_2}{\tau_1} \quad (\text{A.14})$$

# APPENDIX B

## COMPUTER PROGRAM

```

-----
----- COMBOPH 3/6/90 -----
-----
----- TRAPSLN -----
start:

SCREEN 3
VIEW PRINT
CLS
PRINT "Trap Decay"
PRINT
d$ = "\mark\bss\data2\

PRINT " 1) Generate Trap Data          2) Observe Time Data"
PRINT
b = VAL(INPUT$(1))
IF b <> 2 THEN GOTO tr
INPUT "Enter 'TIME' file name"; r$
MID$(d$, 17) = r$
GOTO 1:

tr:
INPUT "Enter Trap Distribution File"; r1$
r2$ = d$: MID$(r2$, 17) = r1$
OPEN r2$ FOR INPUT AS #2
INPUT #2, nt%

stime:
PRINT
d$ = "\mark\bss\data2\
INPUT "Enter 'TIME' file name"; r$
MID$(d$, 17) = r$

INPUT "Starting Time"; ti$
INPUT "Finishing Time"; tf$
INPUT "Number of Points"; n%
'ti$ = 1: tf$ = 1d9: n% = 11
PRINT
PRINT USING "Calculation Time  #.## mins."; nt% * n% * (.0010833333#)

```

```

'.....
'..... Set Parameters .....
'.....

sc# = 0#: kT# = (32# + .0863#): tau# = .5#: Ec# = 0#
ti# = LOG(ti#): tf# = LOG(tf#)
s# = (tf# - ti#) / (n# - 1)
DIM b#(n# - 1)

DEF iny# (t#, sc#, Eo#, Ec#, tau#, kT#) = EXP(sc# - (t# / (tau# * EXP((Ec# - Eo#) / kT#)))) * EXP(-(Ec# - Eo#) / kT#) / tau#

'Generate Data

FOR PX = 1 TO nt#
    INPUT #2, Eo#, W#
    FOR m# = 0 TO n# - 1
        t# = EXP((m# * s#) + ti#)
        b#(m#) = b#(m#) + W# * iny#(t#, sc#, Eo#, Ec#, tau#, kT#)
    NEXT m#
NEXT PX

'write to file

OPEN #1 FOR OUTPUT AS #1
WRITE #1, n#
FOR m# = 0 TO n# - 1
    t# = EXP((m# * s#) + ti#)
    WRITE #1, t#, b#(m#)
NEXT m#

CLOSE

SOUND 1000, 10

'-----
'----- DRAW -----

1 :
CLS
VIEW PRINT 24 TO 25
rn# = 1

2 :
'load data into array
GOSUB load

3 :
'Plot s#(n) for ns,np#
CLS 1
GOSUB findrange
GOSUB defwindow
GOSUB plot

```



GOTO menu

load:

```

dp% = 0: ex = 0
OPEN de FOR INPUT AS #1
INPUT #1, n%
nx = 1: np% = n%: nf% = 2 * n% - 1
IF rn% = 1 THEN DIM a%(nf% + 1): rn% = 0
FOR PX = 1 TO nx
    INPUT #1, x#: INPUT #1, y#
    a%(2 * PX - 1) = x#: a%(2 * PX) = y#
NEXT
CLOSE

```

RETURN

findrange:

```

dx% = 2 * nx - 1: df% = 2 * (nx + np% - 1) - 1
xmi% = a%(dx%): xma% = a%(df%): ymi% = a%(dx% + 1): yma% = a%(df% + 1)
FOR PX = dx% TO df% STEP 2
    x# = a%(PX): y# = a%(PX + 1)
    IF x# > xma% THEN xma% = x#
    IF x# < xmi% THEN xmi% = x#
    IF y# > yma% THEN yma% = y#
    IF y# < ymi% THEN ymi% = y#
NEXT
VIEW PRINT
LOCATE 1, 1
PRINT r#
PRINT
SELECT CASE ex
    CASE 0
        PRINT "Y - X"
    CASE 1
        PRINT "Y - ln X"
    CASE 2
        PRINT "ln Y - X"
    CASE 3
        PRINT "ln Y - ln X"
END SELECT
PRINT
PRINT USING "xmi= ###.####"; xmi%
PRINT USING "xma= ###.####"; xma%
PRINT USING "ymi= ###.####"; ymi%
PRINT USING "yma= ###.####"; yma%
PRINT
PRINT "Data Points"
PRINT nx; "to "; nx + np% - 1; "
PRINT " of "; n%
PRINT
PRINT "Dp "; dp%
LOCATE 16, 1: PRINT : PRINT
LOCATE 16, 1

```

```

PRINT USING "m= #.###^"; m#
PRINT USING "i= #.###^"; i#
VIEW PRINT 23 TO 24

```

```

RETURN

```

```

defvindow:

```

```

WINDOW
VIEW
LINE (138, 0)-(719, 292), , B
VIEW (140, 2)-(717, 290)

WINDOW (xm1#, ym1#)-(xma#, yma#)

```

```

RETURN

```

```

plot:

```

```

FOR PX = dm% TO df% STEP 2
  x# = a%(PX): y# = a%(PX + 1)
  PSET (x#, y#)
NEXT

```

```

RETURN

```

```

best:

```

```

12 : PRINT " 1) Whole Screen  2) Portion"
    b = VAL(INPUT$(1))
    IF b = 1 THEN
      GOTO 13
    ELSEIF b = 2 THEN
      PRINT "  Set Point Range "
      GOSUB select
      GOTO 13
    ELSE GOTO menu
    END IF

```

```

13 : u# = 0: v# = 0: W# = 0: x2# = 0: y2# = 0
    FOR PX = dm% TO df% STEP 2
      x# = a%(PX): y# = a%(PX + 1)
      u# = u# + x# * y#: v# = v# + y#: W# = W# + x#: x2# = x2# + x# ^ 2: y2# = y2# + y# ^ 2
    NEXT
    m# = (np% * u# - W# * v#) / (np% * x2# - W# ^ 2)
    i# = (v# - m# * W#) / np%
    d# = SQR(ABS(np% * (y2# - i# * v# - m# * u#) / (np% * x2# - W# ^ 2) / (np% - 2)))

```

```

'plot best line
GOSUB findrange
FOR x# = xmi# TO xma# STEP (xma# - xmi#) / 580
  PSET (x#, a# + x# + 1#)
NEXT

PRINT : PRINT " 1) Plot Difference Data-Line  2) Main Menu"
b = VAL(INPUT$(1))
IF b = 1 THEN
  FOR PX = dmx TO dfx STEP 2
    a#(PX + 1) = a#(PX + 1) - (a#(PX) * a# + 1#)
  NEXT
  CLS :
  GOSUB findrange
  IF ymi# = 0 AND yma# = 0 THEN
    PRINT "=== EXACT MATCH ==="
    a# = INPUT$(1)
    GOTO menu
  ELSE
    GOSUB defwindow
    GOSUB plot
    GOTO menu
  END IF
ELSE GOTO menu
END IF

selct:

11 : PRINT : PRINT
    INPUT "Enter :  Ns, starting point  "; ns#
    INPUT "           Np, # of points    "; np#
    IF np# < 3 THEN GOTO 11
    dmx = 2 * ns# - 1: dfx = 2 * (ns# + np# - 1) - 1
    RETURN

format:

IF ex# <> 0 THEN GOSUB load
PRINT " 1) Y - ln X  2) ln Y - X  3) ln Y - ln X"
dp# = 0
b = VAL(INPUT$(1))
FOR PX = 1 TO nfx STEP 2
  x# = a#(PX): y# = a#(PX + 1)

  SELECT CASE b
    CASE 1
      IF x# < 1D-200 THEN dp# = dp# + 1: x# = 1: y# = 0
    CASE 2
      IF y# < 1D-200 THEN dp# = dp# + 1: y# = 1: x# = 0
    CASE 3
      IF x# < 1D-200 OR y# < 1D-200 THEN dp# = dp# + 1: y# = 1: x# = 1
  END SELECT

```

```

SELECT CASE b
CASE 1
  x# = LOG(x#): e% = 1
CASE 2
  y# = LOG(y#): e% = 2
CASE 3
  x# = LOG(x#): y# = LOG(y#): e% = 3
CASE ELSE
  GOTO menu
END SELECT
a$(PX) = x#: a$(PX + 1) = y#
NEXT
PRINT " 1) Continue    2) Save New Data"
b = VAL(INPUT$(1))
IF b = 1 THEN CLS 1: GOTO 3
IF b <> 2 THEN GOTO menu
INPUT "Enter File Name to Save "; s#
d# = "\MARK\bas\DATA2\"
MID$(d#, 17) = s#
OPEN d# FOR OUTPUT AS #1
WRITE #1, n%
FOR PX = 1 TO n% STEP 2
  WRITE #1, a$(PX), a$(PX + 1)
NEXT PX
CLOSE
GOTO menu

rd:
SCREEN 3: VIEW PRINT: CLS
PRINT "Data from file "; r#
OPEN d# FOR INPUT AS #1
INPUT #1, a
FOR PX = 1 TO n%
  INPUT #1, x#: INPUT #1, y#
  PRINT , , x#, y#
  IF PX / 20 = INT(PX / 20) THEN
    PRINT
    INPUT "Press <ENTER> to continue"; co#
    PRINT
  END IF
NEXT
CLOSE
VIEW PRINT 23 TO 24

menu:
PRINT " 1) Re-Plot Data  2) Best-Fit    3) Read Data    4) End    "
PRINT " 5) New Format    6) Original Data 8) Re-Start    ";
b = VAL(INPUT$(1))
SELECT CASE b
CASE 1
  GOSUB selct
  GOTO 3

```

```
CASE 2
  GOTO best

CASE 3
  GOTO rd

CASE 4
  END

CASE 5
  GOTO format

CASE 6
  GOTO 2

CASE 7
  GOTO menu

CASE 8
  CLEAR
  GOTO start

END SELECT

GOTO menu
```